The characterisation of genes from a genetic screen that promote invasion.

Louisa Taylor

September 2017

School of Life Sciences

Word Count: 33,222

Declaration

I confirm that the work presented in this dissertation is my own work except where stated in the text. I understand the nature of plagiarism and that it is a serious academic offence. I confirm that no material in this project has been plagiarised.

Name: ……………………………………………………………………………………………

Signed: ……………………………………………………………………………………………

Date: ……………………………………………………………………………………………

Abstract

Metastasis accounts for over 90% of cancer mortality. The first step of metastasis is the invasion of cancer cells into the tissue and vasculature surrounding the tumour. Despite its clinical importance, our understanding of invasion and its genetic determinants is limited. A large-scale, loss-of-function genetic screen in *Drosophila melanogaster* has recently been completed in the Georgiou Lab which identified a number of genes that may promote cellular invasion upon their depletion in the *Drosophila* epithelium. This project will focus on the characterisation of some of these hits.

Glioblastoma multiforme is the most frequent and invasive primary tumour of the central nervous system. Using the human U87 glioblastoma cell line, human orthologs of a number of the aforementioned invasive hits were studied in *in vitro* invasion assays. Knockdown of two of the tested genes, *TSNAX* and *JAG1*, reduced the invasive capacity of U87 glioblastoma cells and hence could represent targets for further research in glioblastoma invasion.

Gtp-bp is a gene implicated in co-translational protein targeting that was identified as possessing pro-invasive capabilities when depleted in the genetic screen. Prior to this study, a potential role for the gene in cell fate decisions was also revealed. In this project, the effect of *Gtp-bp* on cell fate decisions and cell specification was further explored using the *Drosophila* posterior midgut as a model system. Adult posterior midguts deficient for Gtp-bp show severe disruption of tissue homeostasis and a marked reduction in stem cell abundance. Further to this, depletion of Gtp-bp activity in the midgut results in an apparent reduction of the enterocyte population, likely due to defective differentiation. The results obtained here suggest that Gtp-bp plays an important role in intestinal stem cell maintenance and possibly differentiation, providing evidence for novel roles of co-translational protein targeting in tissue homeostasis and cell fate decisions.

Acknowledgments

I would like to thank my supervisor, Dr Marios Georgiou for his help and guidance throughout this project. I would also like to thank Dr Natalie Mack for her brilliant teaching and support. In addition, I would like to thank Dr Africa Couto, Zsuzsa Markus, Alexandra Rusu, Brenda Canales Coutino and Clare Martin for their help during my time in the lab. Finally, I also extend my thanks to Dr Ruman Rahman, Dr Maria Estevez Cebrero and Dr Jennifer Ward for their invaluable help and advice in cell culture.

Contents

Figures and Tables

Abbreviations

AJ	Adherens Junction
AJC	Apical Junctional Complex
aPKC	Atypical Protein Kinase
bHLH	Basic Helix-Loop-Helix
BSA	Bovine Serum Albumin
CNS	Central Nervous System
CO_2	Carbon Dioxide
C_T	Threshold Cycle
Dl	Delta
EB	Enteroblast
EC	Enterocyte
ECM	Extracellular Matrix
EE	Enteroendocrine
EGF	Epidermal Growth Factor
EGFR	Epidermal Growth Factor Receptor
EMT	Epithelial to Mesenchymal Transition
ER	Endoplasmic Reticulum
Flp	Flippase
GBM	Glioblastoma Multiforme
GFP	Green Fluorescent Protein
GPCR	G-protein Coupled Receptor
GTP	Guanosine Triphosphate

HBSS	Hanks Balanced Salt Solution
HS	Heat Shock
ISC	Intestinal Stem Cell
JAK/STAT	Janus Kinase/Signal Transducer and Activator of Transcription
JNK	C-Jun N-terminal Kinase
LGL	Lethal Giant Larvae
LOF	Loss of Function
MAPK	Mitogen-Activated Protein Kinase
MARCM	Mosaic Analysis with a Repressible Cell Marker
MET	Mesenchymal To Epithelial Transition
MMP	Matrix Metalloproteinase
N	Notch
NGS	Normal Goat Serum
p53	Tumour Protein 53
PBS	Phosphate Buffered Saline
PCR	Polymerase Chain Reaction
PFA	Paraformaldehyde
PM	Posterior Midgut
RFP	Red Fluorescent Protein
RNAi	RNA Interference
RT-PCR	Real Time PCR
siRNA	Small Interfering RNA
SOP	Sensory Organ Precursor Cell

SRP	Signal Recognition Particle
SRPR	Signal Recognition Particle Receptor
TF	Transcription Factor
TGF-β	Transforming Growth Factor β
TJ	Tight Junction
UAS	Upstream Activating Sequence
VEGF	Vascular Endothelial Growth Factor
WT	Wild Type

Chapter 1. Introduction

1.1 Cancer

Cancer is one of the leading causes of death worldwide. In 2014, 163,000 cancer deaths were recorded in the UK alone, equivalent to 450 deaths per day (Cancer Research UK, 2016).

Cancer is characterised by the presence of abnormal cells which divide without control and are able to invade other tissues. Due to the invasive nature of the disease, over 90% of cancer fatalities arise from secondary metastatic tumours (Mehlen and Puisieux, 2006), yet in spite of its clinical importance, relatively little is known about tumour progression and the biology that underlies the transition of a cancer cell to malignancy.

Recent advances in the diagnosis and treatment of cancer have seen survival rates improve significantly. In fact, in the last 40 years survival rates are reported to have doubled (Cancer Research UK, 2016). However, even with such substantial improvement, there remains a clear requirement for more effective treatment options for the disease.

1.2 Tumour Formation

Put simply, cancer is a genetic disease which arises from multiple dynamic changes to the genome (Vogelstein and Kinzler, 2004; Hanahan and Weinberg, 2000). Unlike many genetic diseases, no single mutation gives rise to cancer. Instead, multiple genetic alterations are required for the transformation of normal human cells into a malignant cancer.

Genetic alterations in three classes of genes are responsible for tumourigenesis: proto-oncogenes, tumour suppressor genes and maintenance genes (Vogelstein and Kinzler, 2004). Proto-oncogenes and tumour suppressor genes encode a range of proteins implicated in cell growth and proliferation. Proto-oncogenes are normal cellular genes that can be mutated into a cancer-promoting oncogene, often encoding growth promoting signalling molecules and their receptors, anti-apoptotic proteins and sometimes transcription factors. Activation of a proto-oncogene into an oncogene generally involves a dominant gain-of-function mutation rendering the gene product active under conditions the wild-type is not (Lodish et al., 2000; Vogelstein and Kinzler, 2004). Conversely tumour suppressor genes are negative regulators of the cell cycle – often transcription factors or regulators of transcription factors. Recessive loss-of-function mutations in tumour suppressor genes results in their inactivation, increasing the probability that a cell will undergo the neoplastic transformation to malignancy (Lodish et al., 2000).

From a genetic perspective, maintenance genes behave much like tumour suppressor genes, yet their mutation promotes tumourigenesis in a different way. Maintenance genes are required for both the detection and repair of damaged DNA and the inactivation and interception of mutagenic molecules (Hanahan and Weinberg, 2011). Their role is to keep genetic alterations to a minimum and hence inactivation can lead to DNA instability which in turn promotes greater levels of mutation in other genes (Vogelstein and Kinzler, 2004).

1.2.1 The Hallmarks of Cancer

Tumourigenesis is a complex, multi-step process involving multiple genetic alterations of cells and their physiological control mechanisms, resulting in the attainment of certain characteristics. These characteristics have been termed the "Hallmarks of Cancer" (Hanahan and Weinberg, 2000). They describe six essential biological capabilities thought to be shared by all types of human tumours which dictate malignant growth (Figure 1.1). They are: sustaining proliferative signalling, evading growth suppressors, resisting cell death, enabling replicative immortality, inducing angiogenesis and activating invasion and metastasis (Section 1.3 – Tumour Progression) (Hanahan and Weinberg, 2000). More recently, two further hallmarks have been proposed, referred to as "emerging" hallmarks. The first, evading immune response, describes how in order for a solid tumour to form, it must have either evaded the destructive elements of the immune system, or conversely avoided detection entirely (Hanahan and Weinberg 2011, Vinay et al., 2015). The second, reprogramming energy metabolism, describes the ability of tumour cells to limit their energy metabolism largely to glycolysis. Although less efficient than oxidative phosphorylation, this "metabolic switch" is more conducive to proliferation and via the diversion of glycolytic intermediates, allows the generation of various biosynthetic molecules required for the generation of new cells (Hanahan and Weinberg, 2011; Heiden et al., 2009). The attainment of a succession of these capabilities allows cancer cells to survive, proliferate and ultimately disseminate, evolving from a pre-malignant state to an invasive cancer.

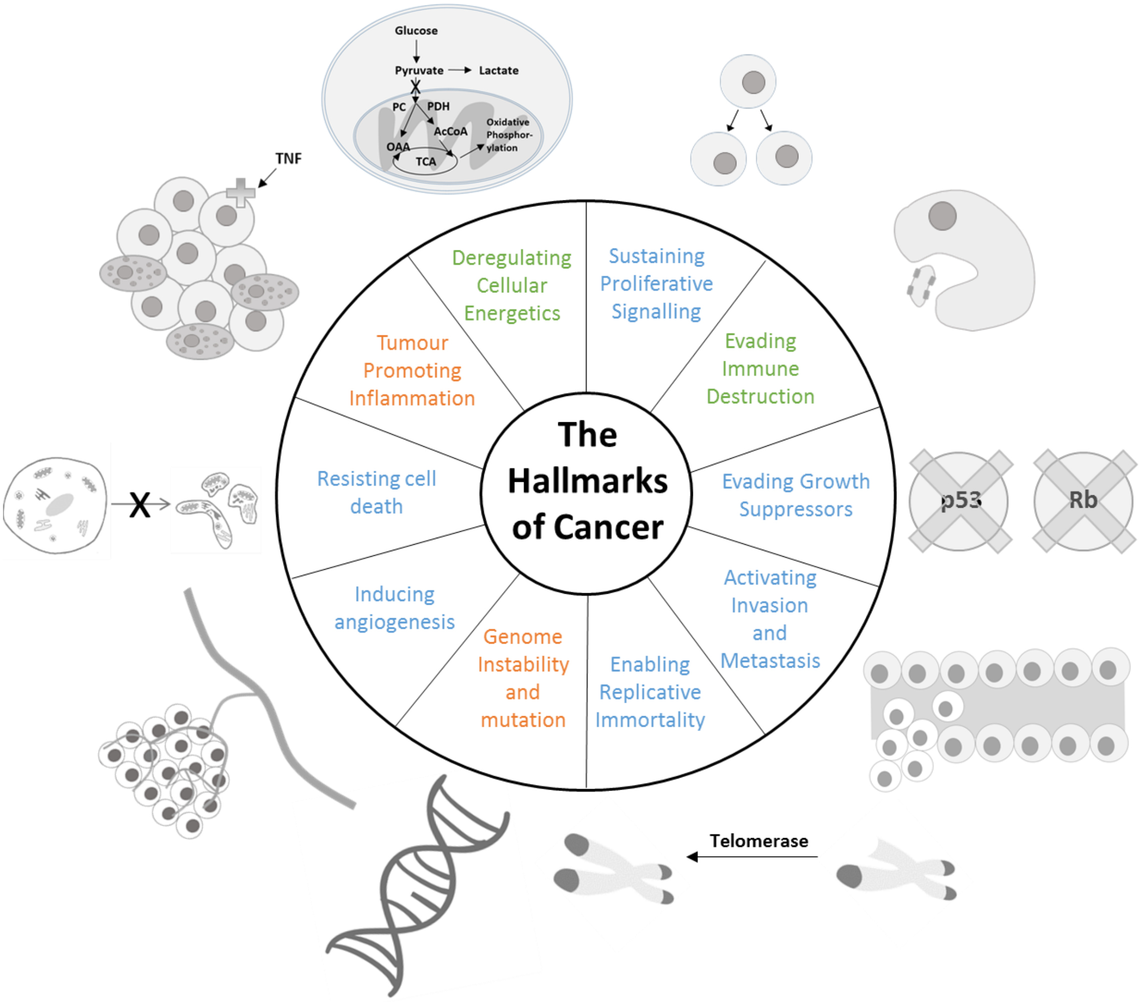

Figure 1.1. The Hallmarks of Cancer.
The Hallmarks of Cancer, as proposed by Hanahan and Weinberg, describe the six biological capabilities (blue text) possessed by all human tumours which are essential for malignant growth. Further to these are the "emerging hallmarks" (green text) and "enabling characteristics" (orange text).

Fundamental to the acquisition of these capabilities are two "enabling" characteristics, proposed by Hanahan and Weinberg in 2011. Genomic instability arises from the down-regulation of maintenance genes (Section 1.2 – Tumour Formation). Defective genome maintenance and repair accelerates the rate at which pre-malignant cells can accumulate mutations, resulting in the aberrant karyotypes responsible for hallmark acquisition. An inflammatory microenvironment is an essential component of all tumours (Grivennikov et al., 2010). Inflammation and the tumour-promoting effects of immune cells are thought to enable both hallmark attainment and function by supplying a variety of bio-active and actively mutagenic molecules to the tumour microenvironment, enhancing tumour progression (Hanahan and Weinberg, 2011; Pagés et al., 2010).

1.3 Tumour Progression

Metastasis is the leading cause of cancer mortality. In fact, at the point of diagnosis half of all cancer patients display clinically detectable metastatic disease. Metastasis is a complex process requiring a number of different events which can vary between cancer types, however common to all are changes in cell-cell and cell matrix adhesion, cell polarity and cytoskeletal organisation (Martin et al., 2013). Broadly, metastasis can be divided into two phases. The initial phase involves the spread of cancer cells to new tissues and organs, commonly by haematogenous and lymphatic routes. The second phase comprises local, intra-organ invasion resulting in tumour formation at a competent secondary focus (Cuddapah et al., 2014). This process is incredibly inefficient and it is estimated that just 0.01% of circulating cells are able to successfully colonise new tissue (Mack and Marshall, 2010).

It has been suggested that primary tumours may favour certain organs for metastatic colonisation, a theory first described almost 30 years ago by Stephen Paget with the “Seed and Soil Theory” (Paget, 1889). For example, breast carcinomas commonly metastasize to the lung, bone and brain, whereas colorectal and pancreatic carcinomas preferentially colonise the liver and lung. Interestingly, this trend is not mirrored by malignant gliomas, which although highly invasive and exceedingly adept at infiltrating organs, rarely colonise outside of the brain and instead invade locally into adjacent brain tissue (Cuppadah et al., 2014).

1.3.1 Epithelial Cell Polarity

Epithelial cells make up the most abundant cell type in multicellular organisms. They form highly organised layers and act as diffusion barriers, allowing vectorial transport from one side of the epithelium to the other (Chen and Zhang, 2013). Polarity is fundamental for epithelial cell physiology and function and is defined as the asymmetric distribution of proteins, lipids and other macromolecules in the cell (Lodish, 2000). Polarisation allows cells to elicit the appropriate response to cues from neighbouring cells and the surrounding microenvironment and hence when polarity is disrupted cells may become insensitive to signals promoting differentiation, apoptosis and senescence (Martin-Belmonte and Perez-Moreno, 2012). Correspondingly, disrupted cell polarity, tissue disorganisation and excessive cell growth are all features observed in cancer, with the loss of apical-basal polarity commonly linked to tumour progression (Royer and Lu, 2011).

Epithelial polarity mechanisms contribute to tumour suppression in a number of ways. First, apical-basal polarity is responsible for the regulation of asymmetric cell division, controlling the polarised localisation of cell fate determinants and the appropriate positioning of mitotic spindles (Royer and Lu, 2011). Additionally, the integrity of apical-basal polarity complexes is crucial for the maintenance of the apical junctional complex (AJC). The AJC comprises both adherens junctions and tight junctions (septate junctions in *Drosophila*) – highly organised structures located at the apex of the lateral membrane of polarised epithelial cells, which are required for the regulation of cell-cell adhesion, paracellular permeability and cell polarity (Vogelmann and Nelson, 2005).

The mechanisms of cell polarity are complex; however it is known that apical-basal polarity in epithelial cells is controlled by the interplay of certain polarity modules. Epithelial polarity complexes are highly evolutionarily conserved and were first identified in model organisms *C.elegans* and *Drosophila* (Martin-Belmonte and Perez-Moreno, 2012). Four main polarity complexes have now been identified, the apical complexes Crumbs and Par and the basolateral complexes Scribble and Yurt/Coracle (Figure 1.2). These complexes take part in mutually antagonistic interactions, which both restrict the activity of each module to a specific cortical domain and allow the correct positioning of adherens junctions (Humbert et al., 2008).

1.3.1.1 Apical Polarity Complexes

Both Par and Crumbs polarity complexes are responsible for promoting apical membrane identity in the cell. The Par complex has been shown to be vital in the establishment and maintenance of apical-basal polarity and apical domain development in epithelial cells (Royer and Lu, 2011). It is also implicated in cell division where it is required for the spatial restriction of the cytoskeleton and asymmetry of the spindle (Nance et al, 2003; Munro, 2006). The Par complex comprises PDZ domain-containing proteins Par6 and Par3 (Bazooka in *Drosophila*), the serine/threonine kinase atypical protein kinase (aPKC) and small GTPases such as Cdc42 (Aranda et al, 2008). Both Par3 and Par6 are multi-modular scaffold proteins, capable of binding to a range of cell polarity proteins and regulators. The interaction of Par3 with Nectin – a cellular adhesion molecule – is responsible for the initial targeting of the Par complex to the junctional region. Par3 also interacts with the Par6/aPKC heterodimer via its PDZ domain. Bound aPKC is then activated by binding of the GTP-bound GTPase Cdc42 to Par6, resulting in phosphorylation of Par3 and subsequent dissociation from Par6, a process whereby the Par complex is maintained at the apical lateral border (Chen and Zhang, 2013). Indeed, phosphorylation plays a key role in the maintenance of epithelial cell polarity and aPKC is capable of phosphorylating numerous polarity proteins. For example, aPKC-mediated phosphorylation of Lethal giant larvae (Lgl), a component of the Scribble complex, excludes the protein from the apical membrane, restricting it to the lateral domain.

aPKC-mediated phosphorylation is also required for maintaining the correct localisation of the Crumbs polarity complex. The Crumbs complex, vital for the establishment of adherens junctions and apical-basal polarity, is made up of the proteins crumbs, PALS (Stardust in *Drosophila*) and PATJ. The exact functions of the Crumbs complex are largely unknown, however it is understood that phosphorylation by aPKC and interaction with Par6 are both vital for the restriction of the Crumbs complex to the apical space (Aranda et al, 2008; Chen and Zhang, 2013; Bulgakova and Knust, 2009).

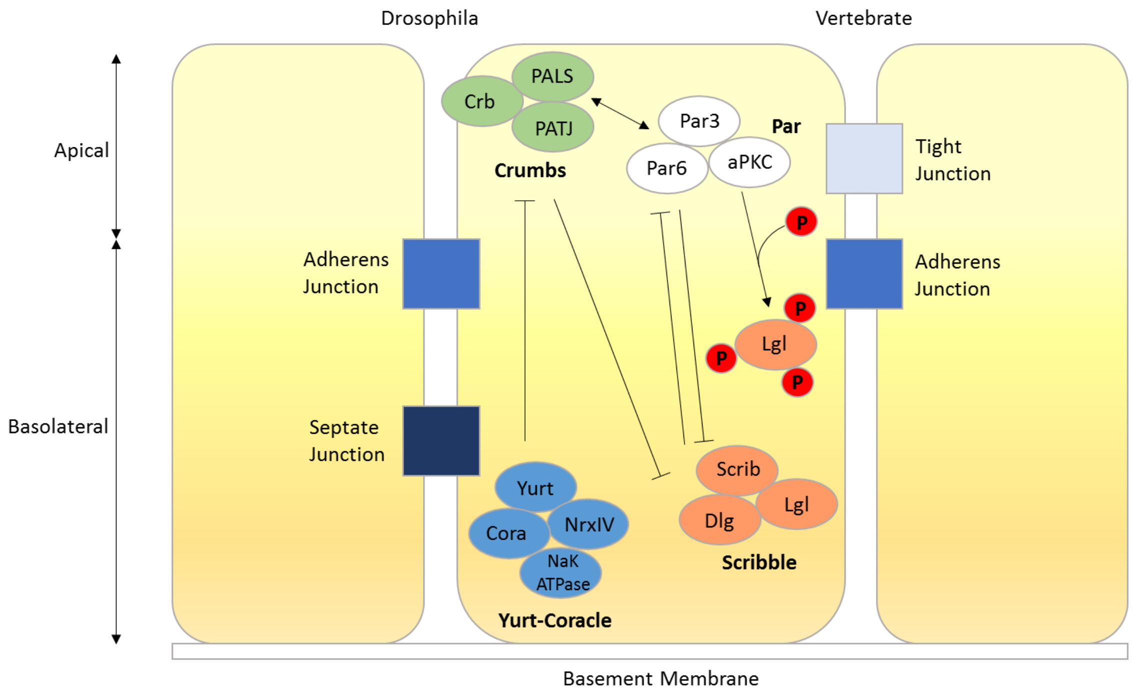

Figure 1.2. Epithelial cell apical-basal polarity is regulated by the interplay of four polarity modules. The basolateral Yurt-Coracle and Scribble complexes and apical Crumbs and Par complexes take part in mutually antagonistic interactions which define apical and basolateral domains in epithelial cells.

1.3.1.2 Basolateral Polarity Complexes

The Scribble and Yurt-Coracle polarity complexes function to define the basolateral domain by their antagonisation of apical polarity modules. The Scribble complex is comprised of Scribble (Scrib), Discs large (Dlg) and Lethal giant larvae (Lgl). It localises with adherens junctions in mammals and septate junctions in *Drosophila* to promote basolateral membrane identity. The Scribble complex acts to control the expansion of the apical domain through a number of antagonistic interactions. Lgl competes with Par3 and in doing so restricts the Par complex to the apical domain. The subsequent phosphorylation of Lgl by aPKC then restricts Lgl activity to the basal region of the cell thus promoting apical-basal polarity (Betshinger et al., 2003; Martin-Belmonte and Perez-Moreno, 2012).

In addition to their role in the maintenance of apical-basal polarity, the genes encoding the members of the Scribble polarity module – *scribble, lethal (2) giant larvae* and *discs large* – are also described as neoplastic tumour suppressor genes. Concurringly, all three members of the Scribble polarity complex are frequently mis-localised and/or aberrantly expressed in various human cancers including breast, colon, adenocarcinoma and prostate (Zhan et al., 2008; Gardiol et al., 2006; Lisovsky et al., 2011; Pearson et al., 2011). In *Drosophila* mutants of *scrib, dlg* or *lgl*, apical determinants become mis-localised to the basolateral regions of the cell, preventing the proper formation of adherens junctions (Bilder and Perrimon, 2000) and resulting in disruption of epithelial cell integrity and cell-cell communication. Furthermore, loss of the Scribble complex polarity proteins in *Drosophila* larval eye imaginal discs leads to neoplastic overgrowth and differentiation defects. It is, however, important to note that when generated in wild-type tissue the over-proliferative mutant cells are out-competed by wild-type tissue by way of c-Jun N-terminal kinase (JNK)-pathway mediated apoptosis (Brumby and Richardson 2003; Bilder and Perrimon, 2000).

Recent work in *Drosophila* has led to the discovery of novel regulators of polarity such as the Yurt-Coracle Group. The group is comprised of the *Drosophila* FERM proteins Yurt (Yrt) (EPB4115 in mammals) and Coracle (Cora), as well as the Na^+, K^+-ATPase and Neurexin IV (Nrx-IV). Like the Scribble polarity module, the Yurt/Coracle group also interacts antagonistically with the apical determinant Crumbs to promote basolateral membrane stability. The two groups however, do not seem to interact functionally and instead operate independently to counteract apical determinants at different time points during epithelial cell differentiation (Laprise and Ulrich, 2011; Laprise et al., 2009).

1.3.2 Invasion in Epithelial Cancers - The Epithelial To Mesenchymal Transition (EMT)

As previously described (Section 1.3 – Tumour Progression), metastasis (Figure 1.3) is the most life threatening event in patients suffering with cancer and remains one of the most cryptic aspects of the disease. The first step of metastasis is the invasion of tumour cells into the stroma. A developmental regulatory programme, defined as the "epithelial to mesenchymal transition" (EMT) is thought to be vital in the acquisition of characteristics that allow epithelial cells to invade, resist apoptosis and disseminate (Hanahan and Weinberg, 2010).

The EMT is a biological process whereby epithelial cells transdifferentiate into motile, fibroblast-like mesenchymal cells. Despite being prominently implicated in cancer cell invasion, this process is essential for embryonic development, gastrulation, wound healing and organ fibrosis (Tania et al., 2014). During EMT, polarised epithelial cells lose tight and adherens cell-cell junctions and the apical-basal polarity which defines their epithelial character. They also undergo cytoskeleton reorganisation, reprogram gene expression to promote invasive capabilities and elevate their resistance to apoptosis – all features which allow the development of an invasive mesenchymal phenotype (Lamouille et al., 2014; Tania et al., 2014).

As discussed previously (Section 1.3.1 – Epithelial Cell Polarity), epithelial cells form highly organised layers and are characterised by the distinct polarisation of their plasma membrane, evidenced by the presence of morphologically distinct, intercellular adhesive protein complexes such as tight junctions (TJs) and adherens junctions (AJs). The initial stages of the EMT involves the deconstruction of such junctions and disruption of cell polarity. The breakdown of the apically located TJs is promoted by decreases in the expression levels of TJ components occludin and claudin, as well as the diffusion of zonula occludens 1 (ZO1), impairing TJ stability (Huang et al., 2012; Lamouille et al, 2014).

A key event in the EMT is the loss of E-cadherin - the most abundant adhesion molecule in the AJs of epithelial cells – and the subsequent destabilisation of the AJs. Indeed, E-cadherin is known to be down-regulated in most, if not all cancers of epithelial cell origin (Cavallaro and Christofori, 2004; Martin, 2013). E-cadherin levels are diminished by various routes including transcriptional repression mediated by transcription factors such as Snail and Twist, as well as at a post-translational level where mature E-cadherin can be degraded by secreted matrix metalloproteinases (MMP) or released from the plasma membrane via endocytosis (Christofori and Yilmaz, 2009). Besides contributing to loss of cell-cell adhesion, recent evidence has suggested that the loss of E-cadherin function might also promote tumour progression by the activation of certain downstream signalling pathways. For example, a reduction in E-cadherin levels can result in the release of β-catenin – a protein usually sequestered by E-cadherin in AJ complexes. β-catenin is also a key component in the WNT-signalling pathway, a critical mediator of numerous developmental events and tissue homeostasis. Normally, non-sequestered β-catenin is rapidly phosphorylated by glycogen-synthetase kinase 3β (GSK-3β), which associates with adenomatous polyposis coli (APC) - a multi-functional tumour suppressor protein which regulates WNT signalling - in the APC– GSK-3β complex. The phosphorylated β-catenin is subsequently degraded. However, if APC is mutated and non-functional or the WNT pathway itself overactive, as is common in colon cancer, this is not the case and β-catenin accumulates in the cytoplasm. This results in the translocation of β-catenin to the nucleus where it can bind TCF/LEF-1 family transcription factors, thus activating the expression of TCF/LEF-1 target genes such as those important in tumour progression (Christofori and Semb, 1999).

A further characteristic of EMT is the re-organisation of the actin cytoskeleton into one conducive with directional motility, a feat that involves Rho signalling. RhoGTPase activation at the onset of EMT promotes actin re-arrangement and the formation of membrane protrusions. Specifically, RhoA promotes actin stress fibre formation, whereas Rac1 and Cdc42 are implicated in the formation of sheet-like protrusions known as lamellipodia and spike-like protrusions known as filopidia. Such re-organisation of the actin cytoskeleton is also responsible for the switch from the apical-basal polarity that is characteristic of epithelial cells, to the front-rear polarity which facilitates the directional movement of mesenchymal cells (Lamouille et al., 2014; Raftopoulou and Hall, 2004).

Perhaps the most noticeable hallmark of the EMT is the so-called “cadherin switch” – the replacement of E-cadherin expression with mesenchymal N-cadherin expression. In addition to the loss of cell-cell adhesion on account of E-cadherin loss, the gain of N-cadherin - usually expressed in vascular endothelial cells and nervous tissue - is thought to further promote cell migration and invasion (Christoferi and Yilmaz, 2009). These changes in cadherin expression are induced by EMT-transcription factors such as Twist and Snail, which act early in EMT and are described as master molecular switches. By recognising and binding E-box DNA sequences in the promoter region of E-cadherin, EMT-transcription factors recruit transcriptional co-factors and histone deacetylases, hence regulating and repressing E-cadherin expression (Tania et al., 2014).

In addition to the mesenchymal invasion regulated by EMT as described above, it should also be noted that two further modes of cancer cell invasion are known. “Collective invasion” describes the migration of cancer cells en masse into adjacent tissues and is common to cancers such as squamous cell carcinoma. Additionally, “amoeboid invasion” describes the movement of individual cancer cells which exhibit morphological plasticity, allowing them to slip through pre-existing spaces in the ECM (Hanahan and Weinberg, 2010).

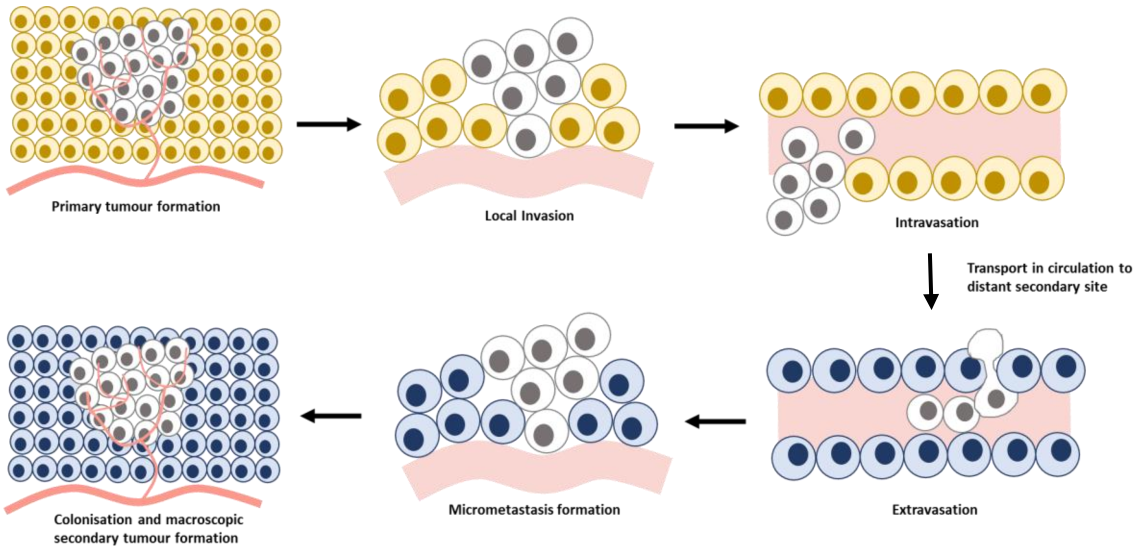

Figure 1.3. The invasion-metastasis cascade.
This diagram depicts a simplified version of the complex process of metastasis. Carcinoma cells must first invade locally at the site of the primary tumour. They then intravasate into the blood/lymphatic system where interaction with platelets, lymphocytes and other blood components facilitates their transport through the circulation to distant secondary sites. Upon entrapment in smaller blood vessels, the invading cells extravasate to from micrometastases. If successful in their adaptation to the new microenvironment, the cancer cells may eventually colonise the new tissue, enabling macrometastasis formation.

1.3.3 Intravastation and Extravastation

In the vast majority of cancers, the process of entering the bloodstream/lymphatic vessels, termed intravasation, is a crucial step in the development of distant metastases (Chiang et al., 2016). Intravasation is reliant on the access of tumour cells to the vasculature and hence angiogenesis plays a crucial role. A sufficient increase in tumour mass at the primary site of the tumour results in hypoxia and nutrient deprivation, inducing what is described as an “angiogenic switch”. Tumour cells release pro-angiogenic cytokines and growth factors, such as vascular endothelial growth factor (VEGF), which activate normal, quiescent vasculature to form new vessels which supply tumour cells with the required oxygen and nutrients, hence facilitating exponential tumour growth. (Hanahan and Weinberg, 2010; Cheresh and Weis, 2011; Bergers and Benjamin 2003). Despite its importance in tumour progression, the resultant neo-vasculature is structurally abnormal, leaky and tortuous (Deryugina and Quigley, 2015). Thus, the weak cell-cell junctions possessed by these novel vessels act as points through which cancer cells can migrate and enter the bloodstream.

After cancer cells have successfully intravasated into the lumen of a blood/lymphatic vessel, they must then survive both the hydrodynamic shear forces and circulating immune cells of the bloodstream before transport to distant sites (Weinberg, 2014). Cancer cells are ill-suited to migration through the circulatory system and due to their large size often arrest upon encountering capillaries and arterioles, hence inhibiting further transport. At this point, invading cancer cells must complete extravasation, a process whereby they adhere to the endothelial cell wall and undergo transendothelial migration into the parenchyma of target organs (Weinberg, 2014; Reymond et al., 2013).

After successful extravasation, cancer cells are faced with perhaps the most challenging step of the metastatic cascade – colonisation – where cells must both survive and proliferate in order to form macroscopic secondary tumours. In order to generate micrometastases, extravasated cancer cells first undergo a “mesenchymal to epithelial transition” (MET) whereby the pathology of the corresponding primary tumour is recapitulated. Challengingly, the foreign tissue environment of the secondary site is unfamiliar to the disseminated tumour cells and thus colonisation requires a number of complex adaptations and interactions with various components of the target organ microenvironment. Due to such restrictive forces, a number of disseminated cells will die, or instead remain in a state of proliferative dormancy for indefinite periods (Shibue and Weinberg, 2011). In order for eventual macroscopic tumour formation, metastasising cells must both be able to survive this period of dormancy and have the ability to commence tumour outgrowth when conditions become favourable (Nguyen et al, 2009).

1.4 Glioblastoma Multiforme

The treatment of malignant gliomas presents one of the biggest challenges facing cancer research to date. Gliomas comprise all primary central nervous system (CNS) tumours of glial cell origin. There are three types of glial cell: astrocytes, oligodendrocytes and microglial cells, the most numerous being the “star-shaped” astrocytes, which provide nutrition to the surrounding neurons and extracellular environment (Rao et al., 2003; Paw et al., 2015). Gliomas which develop from astrocytes are described as astrocytomas, and can be further graded I-IV based upon their degree of abnormality by criteria set by the World Health Organisation. Grades I and II describe low-grade, mostly non-malignant astrocytomas whereas grades III and IV encompass high-grade, rapidly growing malignant tumours. Grade IV astrocytomas, also referred to as glioblastoma multiforme (GBM), are the most malignant and deadliest of all gliomas (Paw et al., 2015). Unfortunately, together with being the most aggressive brain malignancy of the CNS, GBM is also the most common and accounts for over 51% of gliomas (Adamson et al., 2009). The prognosis for GBM remains incredibly poor and median survival after diagnosis stands at just 14 months (Adamson et al., 2009). GBM tumours are characterised histologically by wide regions of necrosis and vascular endothelial proliferation (Holland, 2000; Rao, 2003). The topographically diffuse nature of the disease renders complete surgical resection almost impossible, as tumour cells rapidly invade the surrounding regions of the brain. Furthermore, GBM tumours are amongst the most resistant to radiotherapy and chemotherapy (Cloughesey et al., 2014). It is clear that a deeper molecular understanding is required to develop more effective therapy options for this fatal disease.

1.4.1 Invasion in Malignant Gliomas

One of the main hallmarks, and conjointly one of the greatest challenges facing the treatment of malignant gliomas is the diffuse invasion of tumour cells into the surrounding brain. Even with current microsurgical techniques, gliomas frequently recur within 1-2 cm of the original tumour border due to tumour cell infiltration into surrounding normal brain tissue (Hou et al., 2006). While other aggressive solid cancers metastasise other organs, typically utilising the bloodstream and lymphatic systems (Section 1.3.2.2 Intravastation and Extravastation), it is estimated that less than 2% of gliomas actually metastasize outside of the brain (Beauchesne, 2011). Instead, invading glioma cells are thought to migrate through two pathways in the extracellular space of the brain: the perivascular space, which surrounds neuronal blood vessels, and the interstitial spaces of the brain parenchyma, which describes the narrow tortuous spaces lying between neurons and glial cells (Cuddapah et al., 2014; Paw et al., 2015).

The transition of glioma cells from a hyper-proliferative to an invasive phenotype is thought to be triggered by signals that cause cells to exit from the tumour mass, such as those activated by an acidic or hypoxic environment (Hoelzinger et al., 2007). Like other solid malignancies, the tumour microenvironment plays an active role in glioma invasion and glioma cells switch between proliferative and invasive phenotypes depending on the balance of cues from various microenvironmental factors and cell-cell interactions (Xie et al., 2014). Accordingly, although glioma cells do not rely on the circulatory system for transport to new sites, certain brain structures are critical to their invasion, such as nerve tracts and specifically blood vessels, where a continuous supply of oxygen, nutrients and growth factors are assured. Glioma cells are recruited to blood vessels by bradykinin, a signalling peptide which acts as a chemoattractant, directing glioma cells to blood vessels which themselves act as guides for glioma cell invasion. Binding of bradykinin to its G protein-coupled receptor (GPCR), bradykinin-2-receptor, then triggers a signalling cascade which results in an inositol-3,4,5-trisphosphate receptor 3-dependant increase in intracellular Ca^{2+} concentration. The oscillatory changes in Ca^{2+} level which result from prolonged bradykinin exposure in turn promotes the dramatic glioma cell shape and volume fluctuations necessary for invasion (Cuddapah et al., 2014; Montana and Sontheimer, 2011).

As in other malignant tumours, invasive glioma cells become morphologically polarised and develop membrane protrusions, allowing invading cells to anchor themselves to the extracellular matrix and effectively pull themselves forward. This transient attachment is mediated by interaction with various cell-cell and cell-matrix receptors including integrins, cadherins and neural cell adhesion molecules. Actin-myosin molecular motors generate the predominant contractile force for cell movement and myosin II has been suggested to be particularly important in glioma cell invasion (Cuddapah et al., 2014; Beadle et al., 2008). However, unlike other tumours, in order to move through the limited extracellular space of the brain, glioma cells are also able to dramatically alter their shape and volume by a mechanism described as the "Hydrodynamic Mode of Cell Invasion". 3D time-lapse imaging *in vivo* has shown that glioma cells are able to achieve decreases in cellular volume of 30-35%, a feat that requires cells to release essentially all unbound cytoplasmic water in a cascade of events involving ligand-induced activation of voltage gated Cl^- channels and Ca^{2+}-activated K^+ channels and the subsequent movement of K^+ and Cl^- ions and cytoplasmic water (Cuddapah et al., 2014; Watkins and Sontheimer, 2011).

Although interaction with the ECM molecules of the basement membrane is important for cell attachment, the ECM also presents a substantial physical barrier to the migration of glioma cells. To overcome this, invading glioma cells express a number of serine, cysteine and metalloproteinases which penetrate connective tissue barriers, breakdown normal brain tissue and promote vascular remodelling. A number of proteases have been reported to be upregulated in glioma cells compared to their normal cell counterparts, including matrix metalloproteinases (MMPs) (specifically MMP2 and MMP9) and cell surface proteases of the ADAMs (a disintegrin and metalloproteinase) family (Cuddapah et al., 2014; Rao et al., 2003). Additionally, glioma cells are also capable of recruiting stroma cells, including microglia, astrocytes and endothelial cells, to secrete proteases. Besides degrading the ECM, these proteases also play an important role in the liberation of auto- and paracrine growth factors bound to glioma/stroma cell surfaces and the ECM, further promoting glioma proliferation and migration (Mentlein et al., 2012).

1.5 *Drosophila Melanogaster* as a Model Organism

Drosophila melanogaster is a well-studied and highly tractable model organism, which over the past decade has become an important model system for cancer studies and the study of tumour progression. The fly was the first complex organism to have its genome fully sequenced (Adams et al., 2000) and the high level of conservation between the fly and human genome, which was sequenced a few years later (Human Genome Sequencing Consortium International, 2004), underscored the status of the fly as a useful model organism in the understanding of the mechanisms regulating cell growth, differentiation and development. Although overall identity at nucleotide and protein sequence level between fly and mammalian homologs is usually approximately 40%, it can be as high as 90% in conserved functional domains. Notably, 75% of disease causing genes in humans have functional homologs in *Drosophila,* making the fly an ideal tool for the study of disease related and developmental processes (Pandey and Nichols, 2001; Reiter et al., 2001).

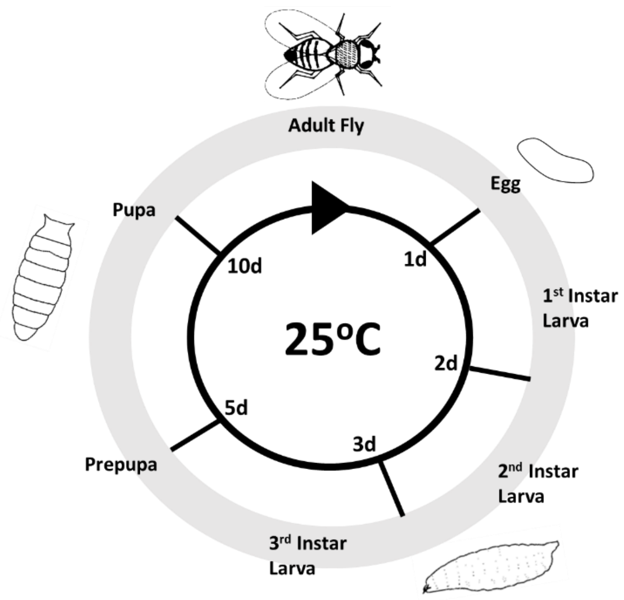

Figure 1.4. The life cycle of *Drosophila melanogaster.* The figure describes the stages and approximate time scale of the Drosophila life cycle at 25°C. The experiments described in the following research utilised *Drosophila* samples collected at the adult fly stage.

There are many features of *Drosophila* that make it a popular model for study. First, the fly is easy to manipulate genetically. The genome codes for 14,000 genes on just four chromosomes, of which only three carry the bulk of the genome. This, combined with the fact that the fly genome is also of low redundancy - namely one, or very few genes code for members of the same protein class – allows for far simpler analysis when studying the effects of genes on biological processes (Pandey and Nichols, 2001; Roote and Prokop, 2013). *Drosophila* also offer a wide range of powerful genetic tools and techniques allowing almost any gene to be the target of various genetic manipulations. The capacity to generate clones of mutant tissue in an otherwise phenotypically wild-type organism, as well as the existence of promoters which allow gene expression to be targeted to a specific tissue or switched on temporally (Miles et al., 2011) are just some of the unique benefits provided by *Drosophila* genetics which allow study of the mechanisms tumour development and the genes involved.

Practically, *Drosophila* offer numerous advantages over other model organisms. They are cheap, relatively simple to keep and can be kept in large quantities permitting high throughput experiments. *Drosophila* also have a rapid life cycle. A single fruit fly generation takes just 10 days at 25^{o}C, during which time many progeny are produced (Roote and Prokop, 2013), allowing for research to proceed quickly (Figure 1.4).

1.6 The *Drosophila* Intestinal Tract

The adult *Drosophila* gastrointestinal (GI) tract comprises a simple epithelium and is surrounded by visceral muscle, nerves and trachea. It is divided into three domains: the foregut, the midgut and the hindgut, each with a distinct function and different developmental origin. The foregut is ectodermal in origin and contains the pharynx, oesophagus and the crop – a temporary food storage pouch. Likewise, the hindgut is also of ectodermal origin and is the main site of water and ion reabsorption prior to waste excretion. Both the foregut and hindgut epithelium are lined apically by an impermeable cuticle. Contrastingly, the midgut epithelium is endodermal in origin and is the main site of digestion and nutrient absorption – the functional equivalent of the human small intestine. It is lined on the luminal side by the peritrophic matrix, a chitin-containing membrane which facilitates digestion and protects the midgut epithelium against bacterial infection. Malpighian tubes, a functional analogue of the mammalian kidneys, mark the midgut-hindgut boundary (Lemaitre and Michel-Aliaga, 2013; Buchon et al., 2013, Kuraishi 2011).

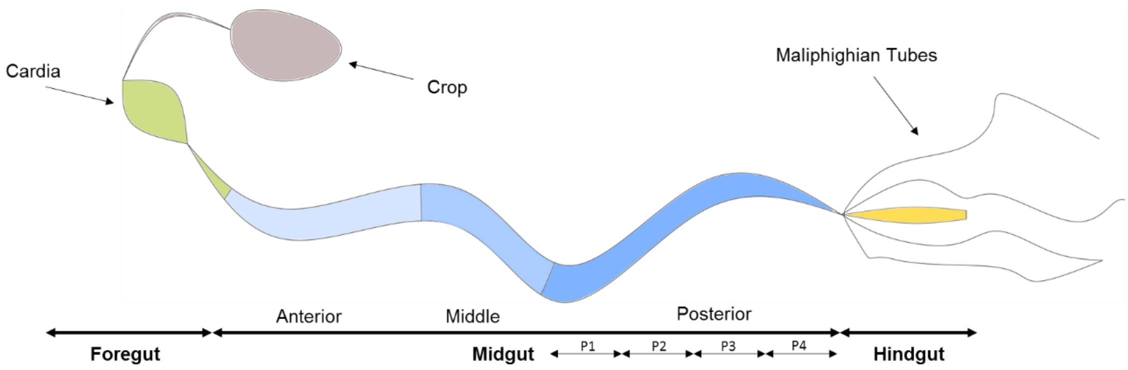

Figure 1.5. The *Drosophila* gastrointestinal tract.
A depiction of the different regions of the Drosophila intestine. The posterior midgut can be further sub-divided into four segments. P1-4 depict the segmentation pattern applied in this study.

The midgut exhibits further compartmentalisation along its anterior-posterior axis (Figure 1.5). Traditionally, it was divided into three histologically distinct regions: the anterior, middle and posterior midgut, however the existence of more complex regionalisation is now evident and the midgut is now considered as at least 10 sub-regions (Buchon et al., 2013; Maraines and Spradling, 2013). Gene expression has been shown to vary extensively between these regions. Similarly, each sub-region consists of cells with distinct structures and functions, reflecting the different roles played by each in digestion. Notably, the middle midgut contains an acidified region at the anterior-middle midgut axis thought to behave as a second stomach, which comprises morphologically distinct acid-secreting copper cells interspersed with specialised enterocytes (Section 1.5.1 – Cellular Organisation Of The Drosophila Midgut) known as interstitial cells. Posterior to this lies a domain with large, flat enterocytes, followed by an iron-region occupied by enterocytes enriched in ferritin. Varying gradients of pH can also be observed throughout the midgut lumen, with the aforementioned copper cells maintaining a strongly acidic region in the middle midgut, a neutral anterior midgut and an alkaline posterior region (Buchon et al., 2013; Mariannes and Spradling, 2013; Wanninger, 2015).

1.6.1 Cellular Organisation of the *Drosophila* Midgut

The adult midgut comprises two major types of differentiated epithelial cell, enterocytes (ECs) and enteroendocrine (EE) cells (Figure 1.6). Enterocytes – large, absorptive, polyploid cells – make up the majority of the epithelial monolayer. They exhibit apical-basal polarity and can be identified by distinct striation present on their luminal surface (Perrimon and Micchelli, 2006). ECs are interspersed with hormone-producing EE cells which make up just 10% of the differentiated epithelium and can be recognised by nuclear expression of the transcription factor (TF), Prospero (Ohlstein and Spradling, 2006).

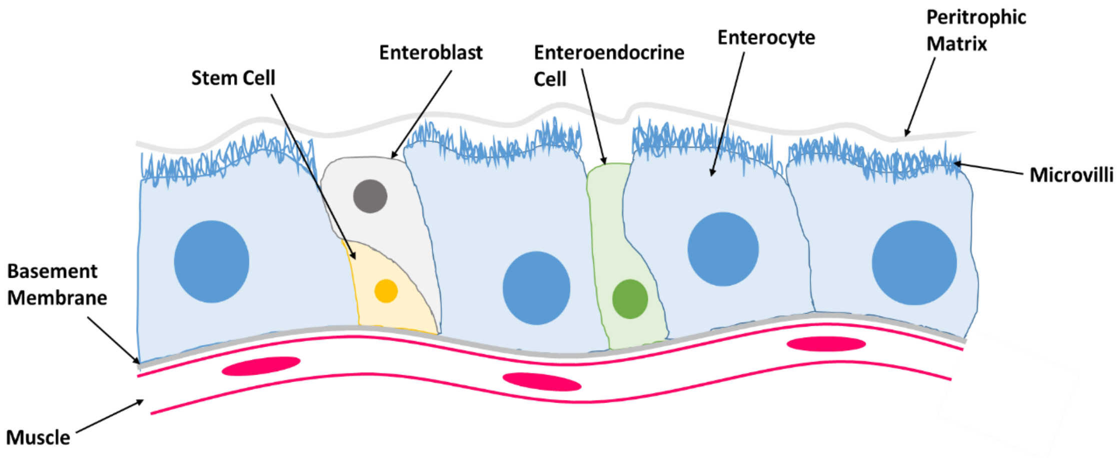

Figure 1.6. Cellular organisation of the *Drosophila* midgut.
The midgut comprises of a mono-layered epithelium surrounded by visceral muscle. The epithelium itself is made up of basally located intestinal stem cells, progenitor enteroblast cells and two main classes of differentiated cell - large polyploid enterocytes and small, nucleated enteroendocrine cells.

As in mammalian intestines, differentiated gut epithelial cells in *Drosophila* are maintained by a population of intestinal stem cells (ISCs). However, in contrast to mammals where stem cells lie in the base of intestinal crypts formed from a highly folded mucosa, *Drosophila* ISCs are scattered across the basement membrane. They can be identified by their small nuclear size, unique triangular shape and expression of the Notch ligand Delta (Marianes and Spradling, 2013). Midgut ISCs usually undergo asymmetric cell division, giving rise to enteroblast (EB) cells which gradually differentiate into ECs and less frequently into at least two types of EE cell (Figure 1.9) (Buchon et al., 2013; Ohlstein and Spradling, 2007). The midgut epithelium has a high turnover rate and is thought to be renewed every two weeks in females and monthly in males. Like other cell types in the *Drosophila* midgut, ISCs appear to be regionally distinctive. Notably, ISCs are most rapidly dividing in the posterior sub-regions of the midgut – the area upon which most research to date has focused - where they divide once daily. Contrastingly, ISC division is substantially slower in the middle region, a feature especially prominent in the acidic copper region where ISCs have been reported as both entirely quiescent (Strand and Micchellli, 2011) as well as dividing every 5 days (Marianes and Spradling, 2013).

1.7 The Notch Pathway

The Notch pathway is an evolutionarily conserved signalling pathway known to play a fundamental role in metazoan development. In addition to the well documented role of the Notch pathway in differentiation, it is also implicated in both apoptosis and proliferation. Despite the relatively simple molecular design of the pathway, Notch signalling affects multiple cell types at different steps of the cell lineage process and consequently, each step comprises a number of regulatory elements and features beyond that described hereafter (Andersson et al., 2011; Bray, 2016).

Mutations in Notch or components of the signalling pathway are associated with diseases in a wide-range of organs and tissues. Indeed, the Notch pathway has been repeatedly implicated in both tumourigenesis and cancer progression. A role for Notch in tumourigenesis was first identified in T-cell acute lymphoblastic leukaemia, where a chromosomal translocation giving rise to a constitutively active form of Notch protein 1 was detected (Ellisen et al., 1999). Further studies demonstrated that the constitutive activity of the Notch pathway that results drives the specification of an immature T-cell lineage which then progresses into a highly aggressive monoclonal T-cell acute lymphoblastic leukaemia (Radtke et al., 1999; Sethi and Kang, 2011). Since then, the Notch pathway has been implicated in the tumourigenesis of a range of solid malignancies including non-small cell lung cancer, melanoma, medulloblastoma and glioblastoma (Dang et al., 2000; Bedogni et al., 2008; Hallahan et al., 2004). Further to the well-documented oncogenic role of Notch signalling in cancer, recent evidence has also revealed that loss-of-function mutations in the Notch receptors promote the development of basal and squamous cell carcinomas, indicative of a tumour suppressive role (South et al., 2012; Wang et al., 2011). Thus, Notch signalling has a complex, bi-functional role in human cancer dependent on cellular context.

Beyond its role in cancer initiation, Notch signalling is also associated with cancer progression via its regulation of conserved signalling pathways, such as the EMT. It has been shown that, together with TGF-β, the Jag1-Notch pathway activates HEY1 –

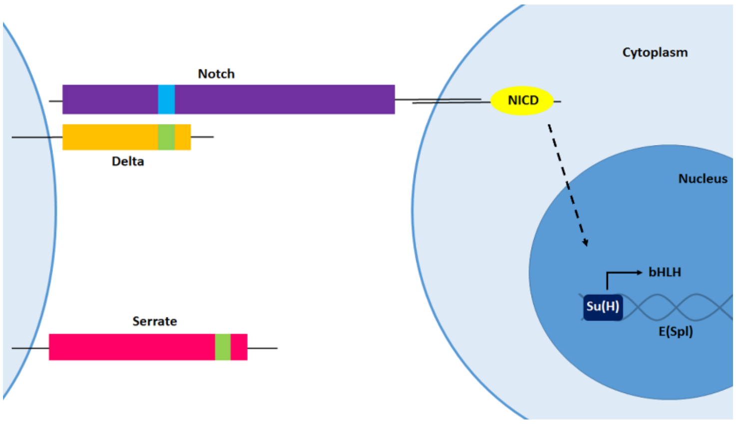

Figure 1.7. Delta/Notch signalling and lateral inhibition. Interaction of Notch with ligands Delta and Serrate, present on an adjacent cell, results in proteolytic cleavage of the Notch receptor and release of the NICD. The NICD translocates to the nucleus where it forms a complex with Su(H) protein which leads to the subsequent recruitment of a transcription activation complex , thereby inducing the transcription of Notch target genes.

a basic helix-loop-helix (bHLH)-type transcriptional repressor – to trigger EMT in tumours (Zavadi et al., 2004). Further to this, links between Notch signalling and the regulation of MMP-9, VEGF and nuclear factor-κB, proteins critically involved in the processes of tumour cell invasion and metastasis, have also been shown (Wang et al., 2006).

In brief, the Notch pathway is a short-range communication pathway which controls cell fate through local interactions, generally by the process of lateral inhibition, whereby a single cell is fated to differentiate upon the interaction of the Notch receptor with its ligand, present on an adjacent cell. The Notch gene encodes a single pass transmembrane receptor, shown to interact with Delta and Serrate transmembrane proteins (Delta and Jagged in vertebrates) (Gu et al., 1995; Greenwald, 1998). Following interaction of the extracellular domains of Notch with its respective ligand, the Notch receptor undergoes a multi-stage proteolytic cleavage releasing the soluble Notch intracellular domain (NICD). The NICD is then translocated to the nucleus, resulting in subsequent activation of the Suppressor of Hairless (Su(H)) transcription factor (CBF1/RLBk in mammals) which binds to Enhancer of Split (E(Spl)) complex genes, upregulating the expression of encoded bHLH proteins. It is these factors which can then affect regulation of downstream target genes (Bray, 2016; Artavanis-Tsakonas et al., 1999, Andersson et al., 2011). A simplified schematic of the Notch pathway is depicted in Figure 1.7.

1.7.1 The Role of the Notch Signalling Pathway in ISC Maintenance and Differentiation

Notch signalling plays a key role in the regulation of midgut ISC maintenance and differentiation, both promoting the asymmetric cell division of ISCs and controlling the fate of resultant EBs (Takashima and Hartenstein, 2012). In contrast to the mammalian intestine where Notch activation promotes ISC proliferation, Notch is absent in the *Drosophila* midgut ISC population and forced activation of Notch has been shown to promote ISC differentiation (Ohlstein and Spradling, 2006; Ohlstein and Spradling, 2007; Michelli and Perrimon, 2006).

ISC identity is maintained by the transcriptional repression of Notch target genes - namely those of the E(spl) complex - by Hairless. The bHLH transcriptional activator Daughterless (Da) is also thought to be essential for ISC maintenance, promoting the ability to self-renew and express the Notch ligand Delta. Following mitosis, asymmetric Delta expression can be observed between ISCs and their EB daughters, with only the ISC retaining punctate Delta expression (Ohlstein and Spradling, 2007). Delta then activates Notch signalling in the adjacent EB, relieving the suppression of Notch target genes by Hairless. These genes include bHLH transcriptional repressors which have been suggested to down-regulate Da-dependant bHLH activity, effectively “switching off” ISC identity and promoting differentiation (Figure 1.8). Fundamental to this process is tight adhesion between the ISC and daughter EB. In the absence of the cell adhesion protein E-cadherin, Delta signalling is ineffective, preventing Notch activity and hence inhibiting differentiation (Maeda et al., 2008).

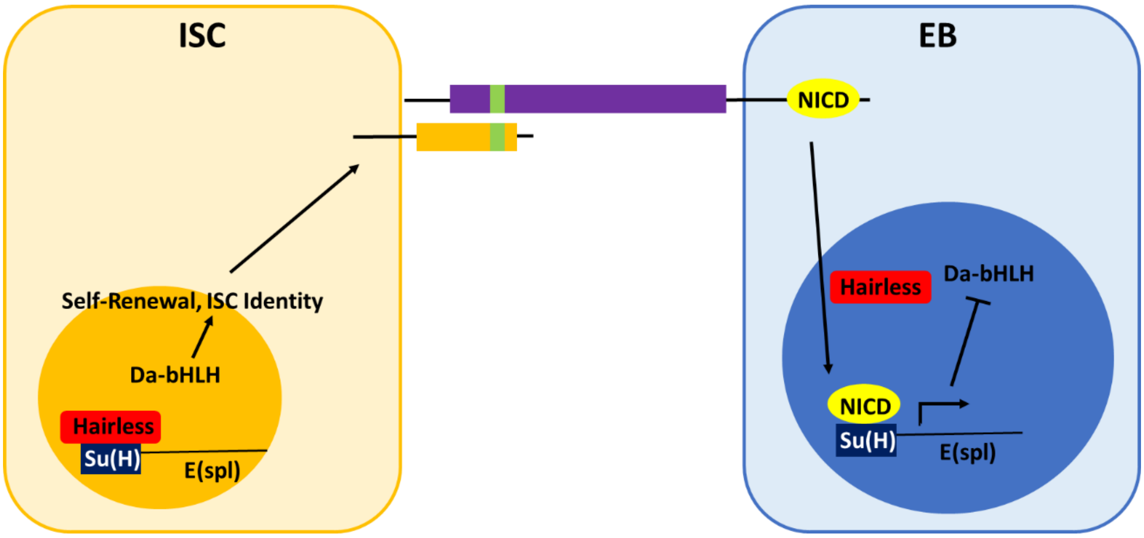

Figure 1.8. Delta/Notch signalling and ISC division.
Post-mitosis, the newly emerged ISC retains Delta expression. Delta binds to a Notch receptor on the neighbouring EB, resulting in the release of the NICD which competes with Hairless for Su(H) binding and in doing so activates expression of Notch target genes. The resultant down-regulation of Da-dependant bHLH activity promotes differentiation and switches off ISC identity within the EB cell.

A further layer of complexity arises from the additional role of Notch signalling in the determination of EB cell fate. Disruption of Notch signalling in the midgut has been shown to block EC cell production and instead lead to the expansion of ISC-like and EE cells, indicating that the determination of EE cell fate occurs in a Notch-independent manner (Ohlstein and Spradling, 2007; Michelli and Perrimon 2006). It has therefore been suggested that ISCs expressing high levels of cytoplasmic Delta stimulate high Notch activity within their EB daughters, inducing their differentiation towards ECs. In contrast, ISCs with low levels of Delta have the opposite effect, stimulating low Notch activity in their daughter EB, thus promoting the EE cell fate (Figure 1.9) (Ohlstein and Spradling, 2007).

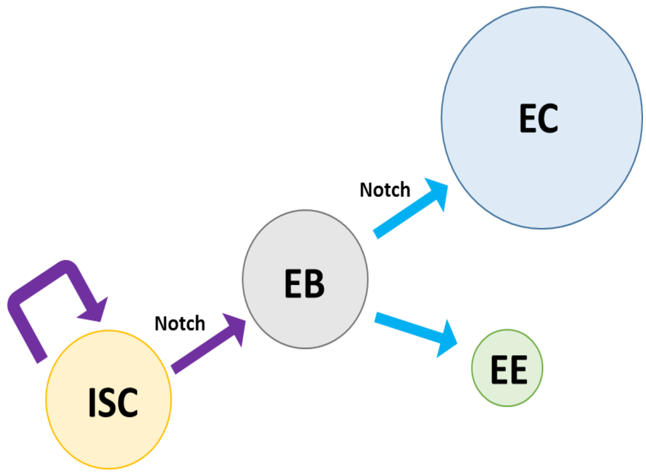

Figure 1.9. ISC cell lineage in the *Drosophila* midgut. Upon normal Delta expression and Notch pathway activation, ISCs divide asymmetrically giving rise to daughter EB cells which differentiate into EC cells, or less frequently EE cells in a manner dependant on Delta/Notch signalling. Purple arrows represent cell division, while blue arrows represent differentiation. Steps dependent on Notch signalling are indicated.

1.8 The Genetic Screen

The genes upon which the following report is based were identified in a large-scale loss-of-function genetic screen which took place in the Georgiou Lab between 2013 and 2017 (data unpublished).

Recent developments in sequencing, deep sequencing and microarray technologies have resulted in the analysis of a wide range of tumour types, the results of which have revealed many genes to be heavily mutated, or their expression levels altered, in certain tumours. In light of this, the genes studied in the aforementioned screen were selected on the basis that they have been shown to be frequently mutated, or their expression down-regulated in various cancers, although have not yet been well characterised. The aim of the screen was therefore to identify novel genes that promote or inhibit tumour progression using *Drosophila melanogaster* as a model system.

The screen used a novel *in vivo* system to generate neoplastic tumours within the epithelium of the fly. Complex *Drosophila* genetic techniques such as the MARCM system (Section 2.2.2.3 - Mosaic Analysis with a Repressible Cell Marker (MARCM) System) were utilised to allow the generation of homozygous mutant cells in wild type (WT) heterozygous tissue via mitotic recombination. Clones arising from transformed cells were homozygous mutant (-/-) for tumour suppressor gene *lgl* (Section 1.3.1.2 – Basolateral Polarity Complexes) while simultaneously expressing an RNA interference (RNAi) construct to knockdown a specific target gene. This system is highly advantageous in the fact that it is possible to knock down target gene function in a small subset of cells and examine the resulting phenotypes in an otherwise phenotypically wild-type organism. Crucially, mutant tissue also expresses a GFP reporter gene, hence permitting the detailed study of shape, behaviour and dynamics of transformed cells in high temporal and spatial resolution.

The screen is now complete and over 600 genes have been successfully screened. A number of phenotypes have been recorded, such as increased/decreased levels of clonal tissue coverage, epithelial multi-layering, the appearance of basal protrusions and the presence of invading cells. In order to identify specific genes that promote or inhibit tumour progression, the screen employed a qualitative scoring system whereby different phenotypes were given numerical scores based upon the strength of the phenotype, relative to that displayed by the *lgl* homozygous mutant. *Lgl-/-* clones display disrupted apical-basal polarity with slight multi-layering and increased levels of invasion (Figure 1.10) in contrast to WT clones, in which epithelial cells lie in highly organised layers with a characteristically polygonal apical shape (Section 1.3.1 – Epithelial Polarity). The subtle but visible phenotype presented by *lgl* -/- clones thus facilitates the detection of different phenotypic effects upon RNAi-mediated gene knockdown, with those most representative of that seen in *lgl -/-* animals awarded a score of 0 and positive and negative effects scored accordingly on a scale of -2 to 2.

***Drosophila* Gene**	**Average Score for Invasion**
Serrate (*Ser*)	1.0
I[[h]] channel (*Ih*)	1.3
Transilin-associated factor X (*Trax*)	1.5
GTP-binding protein (*Gtp-bp*)	0.9

Table 1.1. Chosen Genes
The table presents the genes selected for study in this project and the scores awarded for each for invasion by the scoring system utilised in the screen.

Genes that upon RNAi-mediated knockdown resulted in a pro-invasive phenotype, namely a high number of cells existing beneath the epithelium, were chosen for study in this project. Invasion was quantified in terms of the amount of invading cells; with none represented by a score of -2, few invading cells a score of -1, medium levels of invading cells a score of 0, lots of invading cells a score of 1 and extensive invading cells a score of 2. Over 70 genes were identified as presenting an invasive phenotype when depleted in combination with *lgl -/-* in the *Drosophila* epithelium. On account of the substantial increases in the number of invading cells observed, further research into the potential roles of these genes in tumourigenesis is warranted. As such, four of these pro-invasive hits were chosen as a basis for further study in this project (Section 1.9 – Aims), presented in Table 1.1.

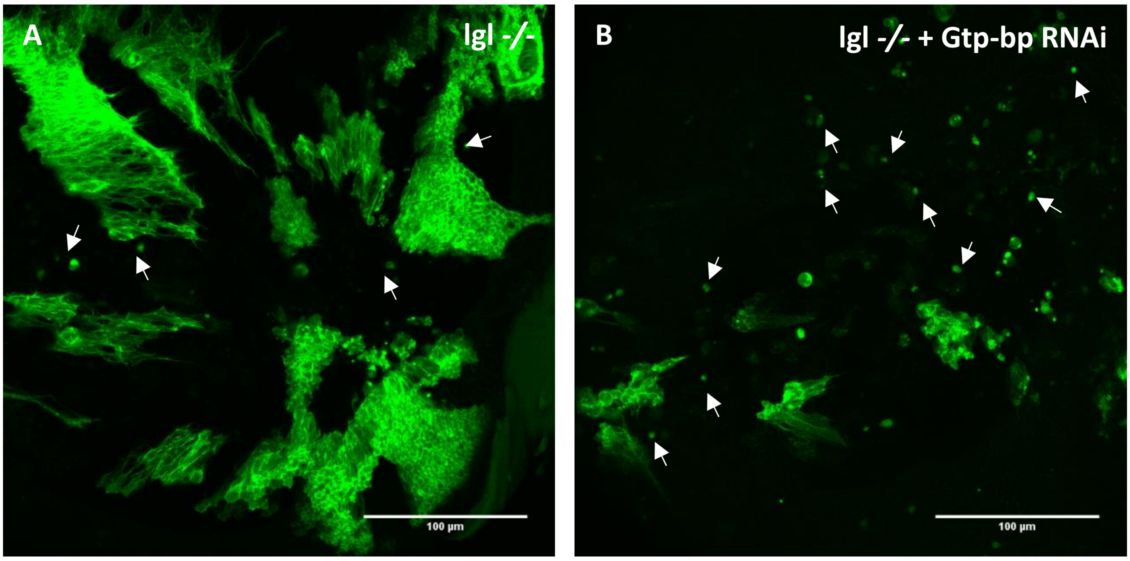

Figure 1.10 Depletion of *Gtp-bp* promotes invasion and reduces clonal tissue area in combination with *lgl -/-* in the *Drosophila* epithelium.
(A-B) Confocal images of mutant clones the *Drosophila* notum. Clones of GFP positive cells in the notum expressing homozygous mutant tumour suppressor gene *lgl* (A), or simultaneously expressing Gtp-bp RNAi in *lgl -/-* mutant clones (B). WT tissue is GFP-negative. Arrows indicate invading cells beneath the epithelium. A notable increase in the number of invading cells and decrease in GFP-marked clonal tissue is observed upon knockdown of *Gtp-bp.* Images are maximum intensity z-projections in x/y. Images courtesy of Georgiou lab.

One of these genes, *Gtp-bp,* gave a particularly interesting phenotype when depleted in combination with *lgl -/-* in the *Drosophila* epithelium. In addition to increased levels of invasion, clones also displayed drastically reduced clonal tissue size and increased multi-layering, where cells appear disorganised and appear in different planes, compared to the *lgl -/-* mutant (Figure 1.10). *Gtp-bp* encodes a component of the SRP-dependent protein targeting pathway, a universally conserved process which ensures correct targeting of nascent secretory and membrane proteins to the ER. The essential cellular role of this pathway makes this gene an especially interesting candidate for further research.

1.9 Aims

The progression of normal cells into a malignant invasive cancer is a complex process not yet fully understood. In recent years, a number of genes have been found to be mutated or aberrantly expressed in various cancers, yet for many, their biological role in tumour progression remains largely unknown. For this reason the characterisation and study of potential regulators of this process is an important area of research. As such, the main aim of this thesis was to begin characterisation of a number of genes identified as possessing pro-invasive capabilities when knocked down in the above-mentioned genetic screen.

In order to do this, this project was split into two parts. In the first, human orthologs of four of these pro-invasive hits (Table 1.1): signal recognition particle receptor alpha subunit (*SRPRA*), jagged 1 (*JAG1*), hyperpolarization activated cyclic nucleotide gated potassium channel 2 (*HCN2*) and translin associated factor X (*TSNAX*), were studied in *in vitro* invasion assays using the U87 human epithelial-like glioblastoma cell line. The objective of this work was to identify new potential targets for glioblastoma research, by testing whether genes that promote invasion in an *in vivo* *Drosophila* model could also mediate cellular invasion in human brain cancer cell line.

Previous research on the pro-invasive hit *Gtp-bp*, the fly ortholog of *SRPRA*, carried out in the Georgiou lab has suggested a further potential role of this gene in cell specification in the *Drosophila* notum. As such, the second aim of this project was to further examine the role of *Gtp-bp* in cell fate decisions in a different tissue. On account of the recent discovery of ISCs in the *Drosophila* GI tract (Micchelli and Perrimon, 2006; Ohlestein and Spradling, 2006), the posterior midgut (PM) is now considered as a new model system in which to study stem cell biology. To this end, my research aimed to establish and optimise this system in the lab and then go on to use the posterior midgut as a model system in which to examine the role of *Gtp-bp* in cell fate decisions and differentiation.

Chapter 2. Materials and Methods

2.1 Materials

2.1.1 *Drosophila* Stocks

Table 2.1 displays the fly strains utilised in this study. Stocks were maintained at 18°C on standard fly food media (Section 2.1.9 –Standard Fly Food Media).

Stock	Genotype	Source
M16	yw, FRT19A ; ; ; ;	Bloomington
M634	w, Gtp-bp^B, FRT19A / FM7 ; ; ; ;	Bloomington
M776	w, hsflp, ubi-nls-RFP, FRT19A ; ; ; ;	Bloomington
M42	w ; Ubi-p63-E-cad-GFP ; ; ;	DGRC Kyoto
M272	w, hsflp, FRT19A, tubGal80 ; ; MKRS / TM6b ;	Georgiou Lab
M22	w ; ; tubGal4/TM3 ;	Gift from Andrew Renault
M147	w ; ; ; ;	Bloomington
M225	w ; UAS-MoeGFP ; ; ;	Bloomington
M826	Gtp-bp^{B}FRT19A / FM7c, Kr-nls-GFP ; IF / CyoGFP ; ; ;	Georgiou Lab
M77	y, w, His2Av[GFP], hsFLP, FRT19A / FM7a ; ; ; ;	Bloomington
M21	w ; esg-Gal4, tubGal80ts, UAS-GFP; UAS-flp, Act>CD2>Gal4 (UAS-GFP) / TM6b ; ; ;	Gift from Julia Cordero
M191	; ; UAS-Ras 85D.V12 ; ;	Bloomington
M76	Esg-Gal4, tubGal80ts, GFP / Cyo ; + / TM6b ; ; ;	Georgiou Lab
14877	w ; P{GD6482}v14877 / TM3	VDRC

Table 2.1 *Drosophila* stocks

2.1.2 Balancer Chromosomes and Marker Mutations

The use of balancer chromosomes is vital for the maintenance of fly stocks. Balancer chromosomes both prevent meiotic recombination in females during mating schemes and additionally are often lethal in homozygosis, consequently abolishing genotypes that differ from the parental combination (Roote and Prokop, 2013). The use of balancer chromosomes and genetic markers also allows progeny of the desired genotype to be selected for throughout multiple genetic crosses. Those utilised in this study are displayed in Table 2.2.

Name	**Chromosome**	**Type**	**Phenotype**
FM7	1	Balancer	Kidney-Shaped Eyes
TM6b	3	Balancer	Tubby (rounded body), humeral (extra macrochaetes) and stubble (short bristles)
TM3	3	Balancer	Stubble
MKRS	3	Marker	Stubble
CyO	2	Balancer	Curled wings
IF (Irregular facets)	2	Marker	Slit-shaped, rough eyes

Table 2.2. Balancers and Genetic Markers

2.1.3 Transgenic Constructs

Genetic Construct	**Function**
hs-flp	Flippase (FLP) expression is under control of the heat shock (HS) promoter, allowing site specific mitotic recombination at equivalent FRT sites when flies are subjected to heat shock at 37^{o}C.
FRT19A	Flippase recognition target (FRT) site located at the 19A site on the 1st chromosome arm.

Kr-nls-GFP	GFP expression is driven by the Kruppel (Kr) promoter. Expression is limited to the nucleus due to the nuclear localisation sequence (nls).
Ubi-nls-RFP	RFP expression is driven by the ubiquitous (ubi) promoter and restricted to the nucleus on account of the nls.
His2Av-GFP	GFP expression is targeted to the nucleus due to Histone2AV (Variant Histone 2A).
Tub-Gal4	The tubulin (Tub) promoter ubiquitously drives expression of the transcriptional activator Gal4.
Esg-Gal4	Escargot (Esg) is expressed in both ISCs and EBs, allowing ISC/EB-specific genetic manipulation.
Tub-Gal80	The tubulin promoter drives expression of the Gal4 repressor protein GAL80.
UAS-Moe-GFP	Moesin (Moe) is tagged by GFP (under the control of the UAS promoter) via its actin binding domain and hence GFP localises to the actin cytoskeleton.
CyO-GFP	The Curley of Oyster (CyO) promoter drives GFP expression in the abdomen.

Table 2.3. Genetic Constructs

2.1.4 Primers for Real Time PCR (RT-PCR)

Gene Target	**Sequence**	**Source**
SRPRA (Forward)	CACCATTTTCTCCAAGGGCG	Sigma Aldrich
SRPRA (Reverse)	TGTTACCTCCCCGTTCCTGC	Sigma Aldrich
JAG1 (Forward)	CTGTCCATGCAGAACGTGAAC	Eurofins
JAG1 (Reverse)	AAGCAACGTATAGGACCTCGGC	Eurofins

TSNAX (Forward)	TCTTCACCCGTGATGTTGGC	Eurofins
TSNAX (Reverse)	CTTCCATATCAGGAGCACTTGT	Eurofins
HCN2 (Forward)	CCGCTACATCCATCAGTGGG	Eurofins
HCN2 (Reverse)	ACGAGTGGTTCACCATGCCA	Eurofins
GAPDH (Forward)	ATGTTCGTCATGGGTGTGAA	Sigma Aldrich
GAPDH (Reverse)	GTCTTCTGGGTGGCAGTGAT	Sigma Aldrich

Table 2.4. Primers used in RT-PCR.
All primers were designed with NCBI Primer Blast.

2.1.5 Small Interfering RNA (siRNA)

siRNA Target	**Sequence**	**Source**
SRPRA	GCGAGGAGUUCAUUCAGAA GAGCUUGAGUCGUGAAGAC UCAGACACCUCGGCUCAUU UGACGUGCAUCGGCUGUUU	Dharmacon
JAG1	GGGAUUUGGUUAAUGGUUA GGAACAUACUGCCAUGAAA UAACAUAGCCCGAAACAGU GAGCAACCCUUGUAGAAAC	Dharmacon
TSNAX	GUGAAACUUAGUCGGGAUA GGAGAAUUGAUGCGGAUGU GAGUCACACCUGUCGAUUA CCGUGAUGUUGGCCUUUAA	Dharmacon
HCN2	CCAGCGCGGUGAUGAGGAU CAGCUGACUUCCGCCAGAA GUAGGUAGCCGUAGUUGGA CGCAAUAAACGACAGCAUU	Dharmacon
Non-targeting Control		Dharmacon

Table 2.5. siRNA oligonucleotides utilised to knockdown target gene expression.
ON-TARGET plus siRNAs were used to reduce off-targets, ordered in the SMARTpool format – a mixture of four different siRNAs as a single reagent to promote specificity and potency.

2.1.6 Antibodies

Antibody	Cell Type Expression	Species	Dilution for IF	Source
Anti-Prospero	Enteroendocrine cells, nuclear.	Mouse	1:50	DSHB
Anti-Delta	Intestinal stem cells, cytoplasmic.	Mouse	1:100	DSHB
Anti-GFP	n/a	Rabbit	1:1000	Molecular Probes

Table 2.6. Primary antibodies.

Antibody	Dilution for IF	Source
Alexa Fluor ® 488 goat anti-rabbit	1:500	Molecular Probes
Alexa Fluor ® 647 goat anti-mouse	1:500*	Molecular Probes

Table 2.7. Secondary antibodies.

*For Delta staining a concentration of 1:1000 was utilised.

2.1.7 Cells

Cell Type	Description	Source
U87	Human adult glioblastoma cell line.	Gift from Dr Ruman Raman.

Table 2.8. Cancer cell lines utilised in this study.

The U87 cell line is derived from a malignant glioblastoma astrocytoma and possesses epithelial-like morphology.

2.1.8 Midgut Dissection and Immunostaining

Process	**Reagent**	**Description**
Fixation	4% Paraformaldehyde (PFA)	16% PFA diluted in 0.1% PBST
Permeabilisation	0.1 % PBST	Triton X-1000 diluted in Dulbecco's Phosphate-buffered saline (PBS)
Blocking	2% Normal Goat Serum (NGS)	100% NGS diluted in 0.1% PBST.

Table 2.9. Solutions utilised in midgut dissection and immunostaining.

2.1.9 Standard Fly Food Media

All flies in this study were cultured on standard cornmeal medium as described below.

<u>Cornmeal Medium (8L Batch)</u>

7340 mL H_20

565 mL Golden Syrup

536 g Cornmeal

127 g Yeast

73 g Soya Flour

42 g Agar

35.4 mL Propanoic Acid

2.2 Methods

2.2.1 *Drosophila* Husbandry

Flies were kept in vials containing standard cornmeal medium (Section 2.1.9 - Standard Fly Food Media) and maintained at either 18^{o}C or 25^{o}C through which generation time from egg to adult is approximately 21 and 10 days respectively (Dahmann, 2008). Flies were cultured by periodic mass transfer of adults to fresh food either weekly (18^{o}C) or bi-weekly (25^{o}C) (Parvathi et al., 2009). This process both minimises infections and maximises progeny (Roote and Prokop, 2013).

Flies were examined under both Leica M60 and Leica MZ10F fluorescence microscopes, which required prior anaesthetisation using CO_2 delivered via a porous polyethene gas diffuser and syringe. CO_2 exposure of over 20 minutes can result in lethality and hence prolonged exposure was limited (Stocker and Gallant, 2008). In order to perform genetic crosses females and males of the appropriate genotypes were selected by way of genetic markers and balancers. In each case 5-10 males were crossed with approximately 20 females. Males were distinguished from females by external genitalia. All crosses undertaken required virgin females. Males do not mate for 10 to 12 hours after emerging from the pupae (Parvathi et al., 2009) and hence to ensure controlled mating virgins were collected every 8 hours when maintained at 25^{o}C and every 16 hours when kept at 18^{o}C.

2.2.2 Genetic Manipulation

As previously described (Section 1.4 - *Drosophila melanogaster* as a Model Organism), the *Drosophila* genome, which was fully sequenced in 2000 (Adams et al., 2000), comprises ~14,000 genes across four chromosomes. *Drosophila* are diploid, namely having two homologous sets of chromosomes in which all genes exist in two copies and have one pair of sex chromosomes (heterosomes) and three pairs or autosomes. The fourth chromosome harbours very few genes and differs genetically from the other chromosomes and hence it is the X, second and third chromosomes which are the targets for genetic manipulation (Roote and Prokop, 2013; Dahmann, 2008).

A number of experiments described hereafter utilised genetic mosaic techniques to generate genetic manipulations in a subset of cells within a wild-type (WT) background. This system allows genetic changes to be studied that would be lethal if applied to an entire organism. By juxtaposing WT and genetically altered cells, genetic mosaic techniques also allow the effect of mutant cells alongside WT control cells to be examined (Blair, 2003). The genetic techniques utilised in this study are described below.

2.2.2.1 FLP/FRT System (and Negatively Marked Clones)

FLP/FRT is a site specific recombination system adapted from yeast. In a heterozygous parent cell, flippase (FLP) induces mitotic recombination between identically positioned flippase recognition target (FRT) sites on homologous chromosome arms to generate daughter cells which are either homozygous mutant or WT (Theodosiou and Xu, 1998) (Figure 2.1). Marking with cell-autonomous markers facilitates the identification of mutant clones and hence allows analysis of mutant cells. This site-specific recombination is random and only takes place in a small fraction of cells. Surrounding cells that did not undergo FLP-induced

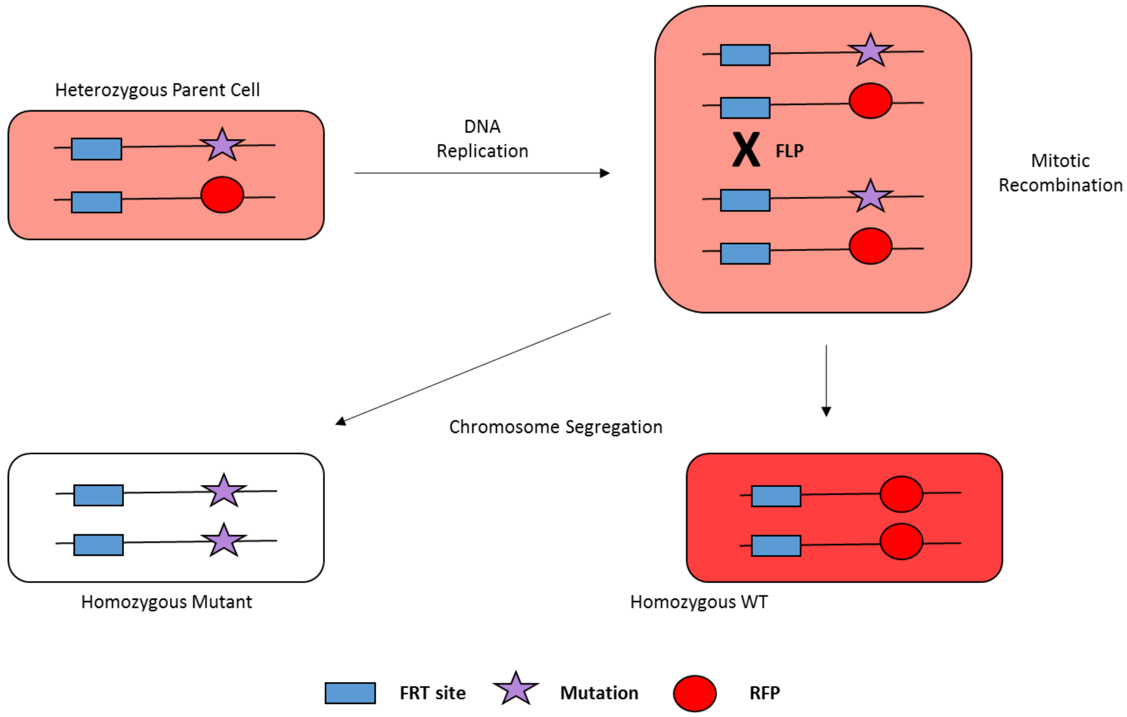

Figure 2.1. The FLP/FRT system.
One chromosome arm of the heterozygous parent cell contains the mutation of interest, FLP and the FRT site. The other contains an identical FRT site and a distal cell marker (in this case RFP). Following DNA replication, FLP-induced mitotic recombination occurs between FRT sites resulting in chromatid exchange between homologous chromosomes. Following chromosome segregation, one daughter cell will be homozygous mutant and RFP negative whilst the other will be homozygous WT and carry two copies of RFP.

recombination will remain heterozygous. The presence of a transgene expressing FLP under the control of a heat shock promoter allows induction of recombination between homologous FRT sites only when flies are exposed to a heat shock (which in this study took place at 37^{o}C).

2.2.2.2 Upstream Activating Sequence (UAS) / Gal4 System

The Gal4-UAS system is a versatile dual component system, again adapted from yeast, whereby flies carrying Gal4 expressing constructs are crossed with flies carrying UAS-constructs, allowing targeted gene expression in a temporal and spatial fashion (Figure 2.2). The transcription factor Gal4 binds to UAS enhancer elements located in the 5' UTR of genes, allowing activation of genes downstream from the UAS site. Numerous Gal4 lines exist which express Gal4 in specific tissues or cells at specific developmental stages by way of a tissue specific promoter (Roote and Prokop 2013; Duffy, 2002), for example the Esg-Gal4 line utilised in this study, which restricts

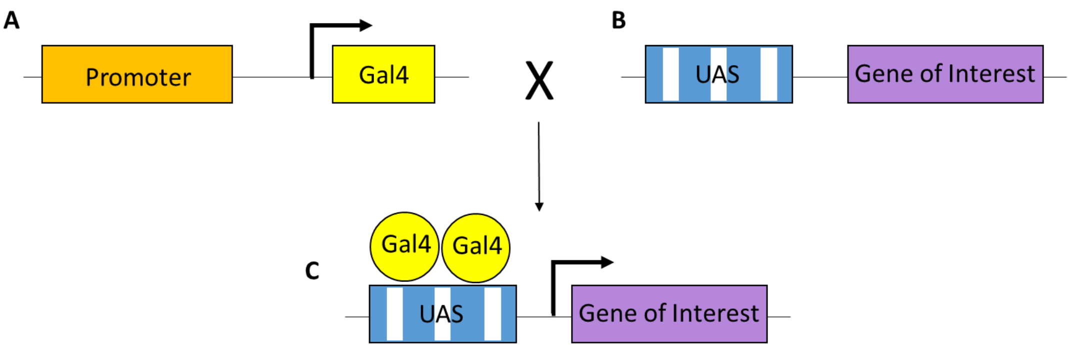

Figure 2.2. The Gal4-UAS System
A GAL4-expressing fly line (A) (expressing GAL4 under the control of a tissue specific promoter) is crossed to UAS construct fly line (B). Offspring will express the UAS-coupled gene in a tissue specific manner controlled by the GAL4 pattern of expression (C).

gene expression to the ISC and EB populations of the gut. This allows specific expression of the UAS-linked gene, including reporter gene constructs such as Moe-GFP, a construct used in this study.

2.2.2.3 Mosaic Analysis with a Repressible Cell Marker (MARCM) System

The MARCM system is a genetic mosaic system which combines both Gal4/UAS and FLP/FRT systems to allow the generation of positively marked clones (Lee and Luo, 1999). As well as using the Gal4/UAS and FLP/FRT techniques, the MARCM system also requires the introduction of a Gal4 repressor protein and hence the Tub-Gal80

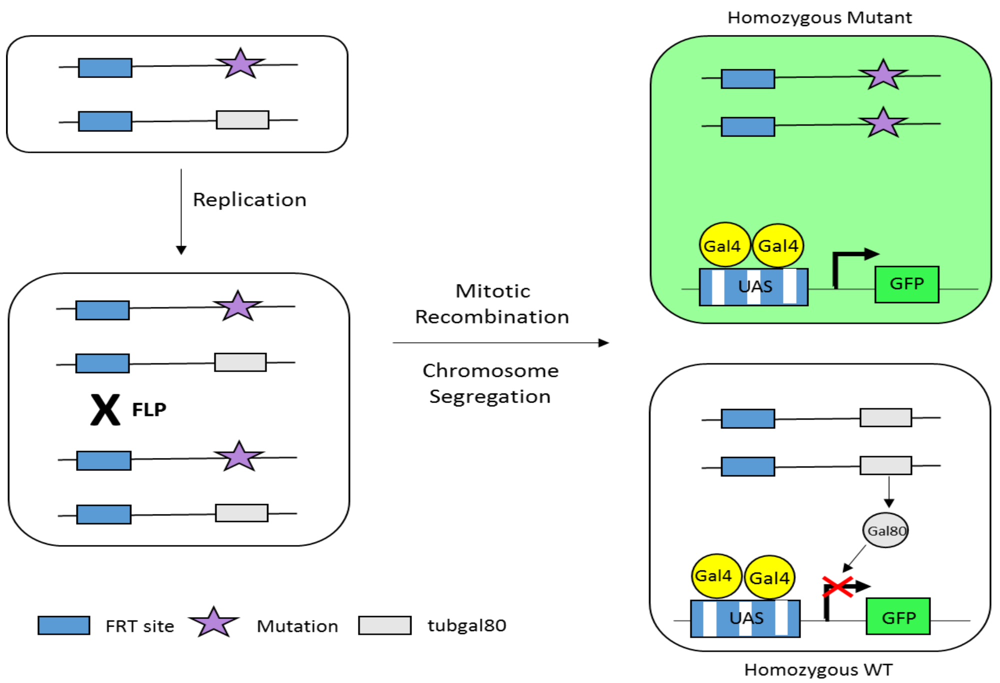

Figure 2.3. The MARCM System.
After site-specific recombination, a heterozygous parent cell can produce two daughter cells, one homozygous for the mutant gene and one homozygous wild type. When expressed, Gal80 inhibits expression of UAS-moesin-GFP, due to its repression of Gal4. Following mitotic recombination, the homozygous mutant daughter cell no longer expresses tubulin-Gal80, resulting in GAL4-mediated expression of the moesin-GFP marker gene.

transgene, encoding Gal80, a dominant repressor of the Gal4 transcription factor is placed downstream of the FRT site and *in trans* to the gene of interest (Lee and Luo, 1999). Following FLP/FRT-mediated recombination, the Tub-Gal80 is lost in one of the daughter cells, thus enabling Gal4 to drive expression of the UAS-linked transgene in this cell (Figure 2.3). The result is homozygous mutant cells able to express any GAL4-mediated transgene, hence allowing the specific labelling of mutant cells within WT tissue (Lee and Luo, 2001).

2.2.2.4 The FLPout System

The FLPout system (esg-Gal4, Gal80ts, UAS-FLP, Act > CD2 > Gal4, UAS-GFP) is a complex genetic technique which allows the analysis both midgut renewal and ISC lineage. The system uses the TARGET system (McGuire et al., 2004), which is a temperature-sensitive (ts) inducible Gal4 (esg-Gal4, Gal80ts) to express FLP recombinase in all intestinal progenitors of the midgut. Using this method, UAS-FLP is induced in ISC/EB cells by temperature shift, allowing FLP recombinase to excise the FRT-flanked CD2 cassette from the Act > CD2 > Gal4 construct, producing an active Gal4 driver which is heritably expressed under the ubiquitous actin promoter (Figure 2.4). This results in actin-Gal4 mediated activation of UAS-GFP, causing all ISCs and their progeny to inherit GFP expression, hence enabling ISC lineage tracking (Houtz and Buchon, 2014; Jiang et al, 2009).

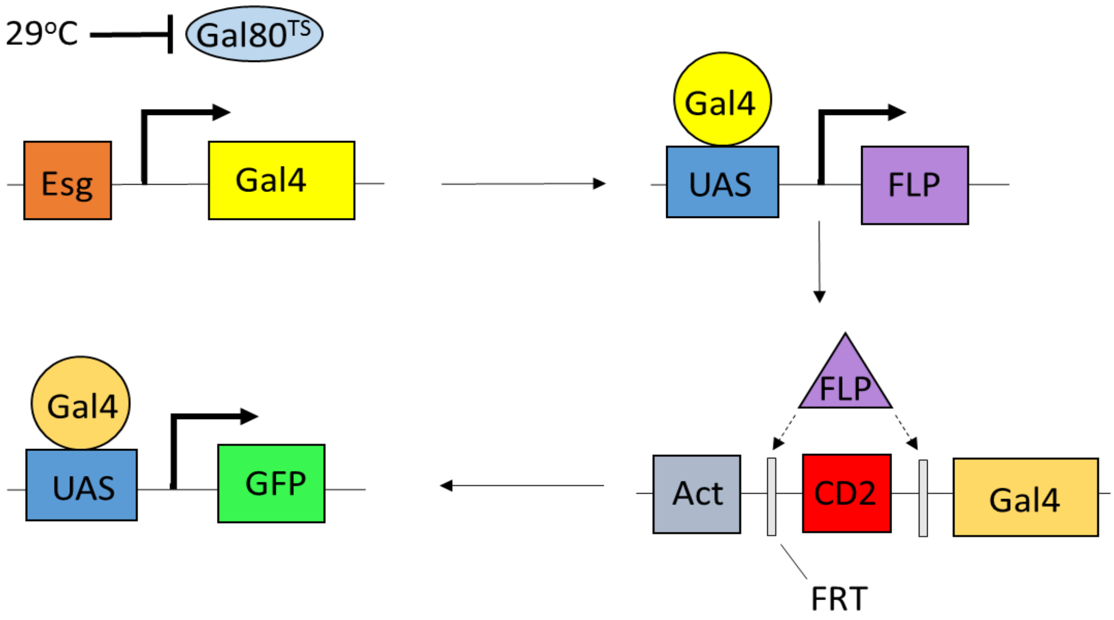

Figure 2.4. The FLPout System
Temperature sensitive expression of FLP recombinase in ISC and EB cells triggers the "flip out" of the CD2 cassette and subsequent activation of the Actin-Gal4 ubiquitous driver in ISC progeny, resulting in GFP expression.

2.2.3 *Drosophila* Genotypes Used in This Study

2.2.3.1 Using the FLP/FRT System to Generate RFP Negatively Marked Clones

To generate negatively marked clones, fly crosses were established and cultured at 25ºC. 3-5 day fertilised female flies were subjected to a 1 hr heat shock (HS) at 37ºC for clone induction. After heat shock flies were grown at 25ºC and transferred to fresh food every 2-3 days as to keep nutrition levels constant and maintain midgut homeostasis. Midguts were dissected and examined at 15-17 days ACI.

Flies expressing a mutant form of the *Gtp-bp* gene were utilised in number of experiments in this project. *Gtp-bp^B* contains a point mutation which is believed to lead to loss of protein activity.

M16, M634, M42 and M776 stocks were utilised. Genotype imaged for WT control: hs-flp, ubi-nls-RFP, FRT19A / FRT19A ; ubi-p63E-cad-GFP ; ; ;. *Gtp-bp*^{B} mutant: hs-flp, ubi-nls-RFP, FRT19A / Gtp-bp^{B}, FRT19A ; ubi-p63E-cad-GFP ; ; ;.

2.2.3.2 Using the FLP/FRT System to Generate GFP Negatively Marked Clones

GFP negatively marked clones were generated using the same method as employed for RFP negatively marked clone generation.

M16, M634 and M77 stocks were utilised. Genotype imaged for WT control: FRT19A / His-GFP, hs-flp, FRT19A ; ; ; ;. *Gtp-bp*^{B} mutant: Gtp-bp^{B}, FRT19A / His-GFP, hs-flp, FRT19A ; ; ; ;.

2.2.3.3 Using the MARCM System to Generate Positively Marked Clones

To generate MARCM clones, fly crosses were established and cultured at 25^{o}C. 3-5 day fertilised female flies were subjected to a 1 hr HS at 37^{o}C for clone induction. After HS flies were grown at 25^{o}C and transferred to fresh food every 2-3 days. Midguts were dissected and examined at 17-19 days ACI.

M272, M22, M16, M225, M634 and M826 stocks were utilised. Genotype imaged for WT control: hs-flp, FRT19A, Tub-Gal80 / FRT19A ; UAS-Moe-GFP / + ; Tub-Gal4 / +. *Gtp-bp*^{B} mutant: hs-flp, FRT19A, Tub-Gal80 / Gtp-bp^{B}, FRT19A ; UAS-Moe-GFP / + ; Tub-Gal4 / +.

2.2.3.4 Using an alternative MARCM System to Generate Positively Marked Clones

To generate positively marked clones, fly crosses were established and cultured at 25^{o}C. 3-5 day fertilised female flies were subjected to a 1 hr HS at 37^{o}C for clone induction. After HS flies were grown at 29^{o}C and transferred to fresh food every 2-3 days. Midguts were dissected and examined at 15-17 days ACI.

M272, M16, M634, M21 and M826 stocks were utilised. Genotype imaged for WT control: hs-flp, FRT19A, Tub-Gal80 / FRT19A ; Esg-Gal4, Tub-Gal80ts, GFP / + ; UAS-flp, Act>CD2>Gal4 (UAS-GFP) ; ;. *Gtp-bp^{B}* mutant: hs-flp, FRT19A, Tub-Gal80 / Gtp-bp^{B}, FRT19A ; Esg-Gal4, Tub-Gal80ts, GFP / + ; UAS-flp, Act>CD2>Gal4 (UAS-GFP) ; ;.

2.2.3.5 Using the Gal4/UAS System to Examine Effect *Gtp-bp* knockdown in a RasV12 Tumour Model

Fly crosses were established and cultured at 18^{o}C. 3-5 days post-eclosion, fertilised female flies were shifted to 29^{o}C to induce RNAi transgene expression. Flies were transferred to fresh food every 2-3 days and midguts examined at 3, 8 and 19 days after temperature shift.

M21, M76, M191 and 14877 stocks were utilised. Genotype imaged for *RasV12* alone: Esg-Gal4, Tub-Gal80ts, UAS-GFP / + ; UAS-RasV12 / + ; ; ;. *RasV12* + Gtp-bp RNAi: Esg-Gal4, Tub-Gal80ts, UAS-GFP / + ; UAS-RasV12 / UAS-Gtp-bpRNAi ; ; ;.

2.2.3.6 Using the Gal4/UAS System to Examine Effect *Gtp-bp* knockdown in ISC/EB Population

To drive Gtp-bp RNAi specifically in the ISC/EB population, the same methods were employed as previously described (Section 2.2.3.5).

M76, M147 and 14877 stocks were utilised. Genotype imaged for WT control: Esg-Gal4, Tub-Gal80ts, UAS-GFP / + ; ; ; ;. *Gtp-bp* RNAi: Esg-Gal4, Tub-Gal80ts, UAS-GFP / + ; UAS-Gtp-bpRNAi / + ; ; ;.

2.2.3.7 Using the FLPout System to study ISC/EB Differentiation

To drive Gtp-bp RNAi specifically in the ISC/EB population and mark subsequent progeny, crosses were established and cultured at 18^{o}C. 3-5 days post-eclosion, fertilised female flies were shifted to 29^{o}C to induce RNAi transgene expression. Flies were transferred to fresh food every 2-3 days and midguts examined at 19 days after temperature shift.

M147, 14877 and M21 stocks were utilised. Genotype imaged for WT control: Esg-Gal4, Tub-Gal80ts, UAS-GFP ; UAS-flp, Act>CD2>Gal4 (UAS-GFP) / + ; ; ;. Gtp-bp RNAi: Esg-Gal4, Tub-Gal80ts, UAS-GFP ; UAS-flp, Act>CD2>Gal4 (UAS-GFP) / UAS-Gtp-bp RNAi ; ; ;.

2.2.4 Dissection of the *Drosophila* Midgut

Fertilised female adult flies were anaesthetised using a CO_2 source and submerged in 95% ethanol for 30s before transfer to a silicon dissecting dish containing cold PBS. The entire GI tract was dissected using tungsten forceps under a Leica M60 Light Microscope. The reproductive organs, foregut and hindgut were then carefully removed to leave the midgut. Midguts were then immediately either mounted for live imaging (Section 2.2.4.1 - Live Imaging of the *Drosophila* Midgut), or transferred to a fixative for staining (Section 2.2.5.1 Immunostaining).

2.2.4.1 Live Imaging of the *Drosophila* Midgut

For live imaging, dissected midguts were carefully mounted on glass microscope slides in a single drop of M3 Insect Medium (Sigma Aldrich). Small glass coverslips (24 mm x 24 mm) were fixed at each end of the slide to form a bridge over which a long glass coverslip (50 mm x 50 mm) was placed, generating an interface between coverslip and midgut for imaging.

2.2.5 Cell Culture

2.2.5.1 Cell Maintenance

U87 cells were grown at 37^{o}C and 5% CO_2 using T75 cell culture flasks in DMEM containing 1% L-Glutamine and supplemented with 10% (v/v) FBS and 1% P/S. Cells were passaged twice weekly at 70-80% confluence as follows. Growth media was removed and cells washed in HBSS to remove protease inhibitors. Cells were detached by incubation for 5 minutes at 37^{o}C in 10x Trypsin-EDTA. After trypsinisation, an equal volume of pre-warmed medium was added to deactivate the trypsin and the solution centrifuged at 800 rpm for 5 min. The resultant pellet was re-suspended in growth medium and desired volumes of cells were seeded into new T75 flasks containing an appropriate volume of fresh media.

2.2.5.2 Cell Counting

For cell counting, cells were first washed and trypsinised (Section 2.2.5.1 - Cell Maintenance), after which cells were suspended in 1 mL growth media. Equal volumes of trypan blue and cell suspension were then gently mixed to form the cell counting solution. 10 µl of this solution was then applied to a haemocytometer BS 748 (Hawksley, UK). The number of viable cells (cells that do not take up the trypan blue solution and hence appear clear) in the four corner squares and one centre square of the haemocytometer grid were counted and the following equation utilised to calculate the number of cells per mL of cell suspension.

Cells / mL = number viable cells x (trypan dilution / number of squares counted) x 10^4

Where 10^4 represents the haemocytometer value.

2.2.5.3 Cell Storage

To freeze cells, cells were washed and trypsinised as previously described (Section - 2.2.5.1 - Cell Maintenance). The resulting pellet was re-suspended in 1 mL freezing medium comprising 90% FBS and 10% dimethlysulfoxide (DMSO) and counted (Section - 2.2.5.2 Cell Counting). Cells were then further diluted in freezing medium to give a final concentration of approximately 1 x 10^6 cells / mL. 1mL of cell suspension was then transferred to cryovials and placed in a Mr Frosty at -80^{o}C overnight, after which vials were transferred to liquid nitrogen for long term storage.

2.2.5.4 Culturing Cells From Frozen

To culture cells from frozen, cryovials containing stored cells were removed from the liquid nitrogen bank and immediately transferred to a water bath set at 37^{o}C to defrost. Meanwhile, an appropriate volume of pre-warmed media was added to a fresh T75 culture flask. Cells were then transferred from cryovial to flask by use of a plastic Pasteur pipette and incubated at 37^{o}C and 5% CO_2 overnight. After incubation for 24 hrs the media was replaced with an equal volume of fresh media and cells passaged when appropriate.

2.2.5.5 siRNA Transfection

Prior to transfection, cells were counted (Section 2.2.5.2 Cell Counting) and plated in an optimal density of 1 x 10^5 cells in 2 mL antibiotic-free complete medium per single well of a 6-well plate, after which the plate was incubated at 37^{o}C with 5% CO_2 overnight. A 5 µM siRNA solution was prepared in 1 x siRNA buffer and the solution further diluted 1:20 in serum-free phenol-red free medium. In a separate tube, DharmaFECT transfection reagent was diluted in serum-free phenol-red free medium to give a final concentration of 3 µL/well and both tubes incubated for 5 min at RT. Following this, the contents of each tube were mixed and the resultant transfection medium incubated for a further 30 min at RT. The transfection medium was then further diluted in antibiotic-free phenol-red free complete medium to give a final siRNA concentration of 25 nm. Culture medium was subsequently removed from each well of the 6-well plate and 2 mL of the appropriate transfection medium was added dropwise per well. The cells were then incubated at 37^{o}C in 5% CO_2 for 48 hrs. Post-transfection, cells were washed, trypsinised and the subsequent pellets harvested for downstream application (Section 2.2.5.6 – Invasion Assay or Section 2.2.6.5 – RT-PCR).

2.2.5.6 Invasion Assay

In order to perform the *in vitro* invasion assay, invasion chambers were prepared in single wells of a 24-well plate. Inserts containing an 8 µm pore size polycarbonate membrane were coated in High Concentration Matrigel Matrix (Corning) which was first diluted to 1 µg/µL in serum-free media. Utilising reverse pipetting to avoid air bubble formation, 50 µL matrix was added to each insert after which the plate was incubated for 1 hr at 37^{o}C. 48 hours post-siRNA transfection, cells were washed and trypsinised as previously described (Section 2.2.5.1 - Cell Maintenance) and the resultant pellet re-suspended in 1mL serum-free, phenol red-free medium containing 0.2% BSA (quenching medium). Cells were counted (Section 2.2.5.2 Cell Counting) and brought to a final volume of 2.4x10^5 cells/mL in quenching medium. 250 µL cell suspension was then added to each insert and 500 µL phenol red-free complete culture medium was added to the lower chamber. The plate was then incubated for 48 hrs at 37^{o}C with 5% CO_2. Post-incubation, cell suspension was removed from the upper chamber and the inserts placed into fresh wells

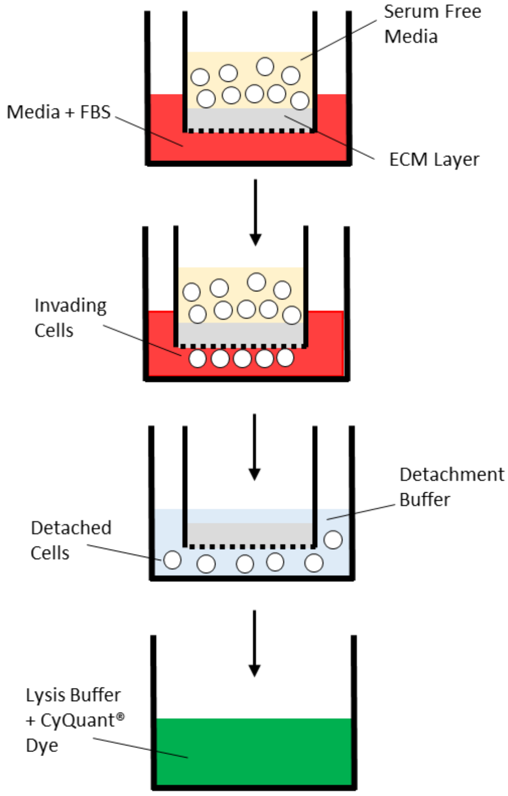

Figure 2.5. Invasion Assays
Invasion assays were performed in invasion chambers comprising of inserts coated in a thin layer of reconstituted basement membrane matrix. Invasive cells migrate through the ECM layer and cling to the bottom of the membrane, where they can be dissociated with cell detachment buffer, lysed and detected by CyQuant GR dye.

containing detachment solution (Merk Millipore). The plate was then incubated for 30 mins at room temperature, during which time it was gently shaken to aid cell detachment. CyQuant GR dye (Molecular Probes) was diluted 1:75 with lysis buffer (Merk Millipore) and 100 µL added to each well, after which the plate was incubated for a further 15 mins at RT. Samples were then transferred to a 96-well plate and read on a fluorescent plate reader with a 480/520 nm filter set and optimal gain. The assay is depicted in Figure 2.5.

2.2.6 Molecular Biology

2.2.6.1 Immunostaining of the *Drosophila* Midgut

For immunostaining, fertilised adult female intestinal tracts were first dissected (Section 2.2.4 – Dissection of the *Drosophila* Midgut) and transferred immediately to a glass dish containing 4% PFA for 15-20 min at room temperature (RT). The fixative was removed and midguts washed with PBS, after which they were transferred to 2% NGS blocking solution (Section 2.1.9 - Midgut Dissection and Immunostaining) and incubated for 1 hr at RT. After blocking, specimens were incubated with chosen primary antibodies at the aforementioned dilutions (Section 2.1.6 - Antibodies) at 4^{o}C overnight. Primary antibodies were rinsed twice with 0.1% PBST and washed twice for 15-20 min before the addition of appropriate secondary antibodies (Section 2.1.6 - Antibodies) for 1 hr at RT. Samples were then washed and rinsed as previously described. If DAPI staining was required, guts were rinsed in PBS before incubation in 1 μg/mL DAPI stain solution for 10 minutes at room temperature. After further rinsing with PBS, stained midguts were then mounted in FluoroGel mounting media (GeneTex) as described previously (2.2.4.1 Live Imaging of the *Drosophila* Midgut) and kept at 4^{o}C until imaging.

2.2.6.2 RNA Extraction

To extract RNA from U87 cell lines, a confluent flask of T75 cells was pelleted as previously described (Section 2.2.5.3) and 1mL Trizol reagent added, after which the sample was incubated for 5 min at room temperature (RT). Following the addition of

0.2 mL chloroform, the sample was shaken vigorously for 15s and incubated at room temperature for a further 2-3 min. The sample was then centrifuged for 15 min at 4^{o}C and 12,000 rpm to separate the organic and aqueous phases. Taking care not to disturb the protein-containing interphase layer, the upper aqueous upper layer was isolated and transferred to a nuclease-free Eppendorf tube. 0.5 mL 100% isopropanol was then added and the sample incubated for 10 min at RT. After centrifugation for a further 10 min at 12,000 rpm at 4^{o}C, the supernatant was removed to leave the RNA pellet, which was purified and concentrated using GeneJet RNA Purification columns (ThermoFischer Scientific) as per manufacturer's instructions.

The resultant RNA was then chilled on ice and either used immediately for downstream applications (Section 2.2.6.3 – cDNA Synthesis) or transferred to -80^{o}C for long-term storage. RNA concentration and absorbance was measured using a Nanodrop2000, and denaturing gel electrophoresis used to assess RNA quality.

2.2.6.3 cDNA Synthesis

cDNA synthesis was undertaken using RNA extracted from the U87 cell line (Section - 2.2.6.2 RNA Extraction). To a sterile nuclease-free tube, 1-2 µg template RNA and 1 µL Oligo $(dT)_{18}$ primer were added and the reaction mix made up to 12 µL with nuclease-free water. The tube was then incubated at 65^{o}C for 5 minutes in order to remove RNA secondary structure. Following chilling on ice, the following reaction components were added in the described order: 4 µL 5X Reaction buffer, 1 µL RiboLock RNase Inhibitor (20 U/µL), 2 µL 10mM dNTP Mix and 1 µL RevertAid Reverse Transcriptase (200 U/µL). The reaction mix was then incubated at 42 ^{o}C for 60 min and the reaction terminated by heating to 70 ^{o}C for 5 min. The resultant cDNA was either kept on ice for immediate use or stored at -20 ^{o}C.

2.2.6.4 Temperature Gradient Optimisation of Primers

In order to improve the efficiency of RT-PCR assays, temperature gradient PCR was employed. For each sample, 12.5 µL iQ SYBR master mix, 1 µM of each primer and 50 ng cDNA template was made up to a final volume of 25 µL in PCR tubes. The reaction was then run across a gradient of temperatures between the lowest and highest that would be appropriate for each primer pair in order identify the optimum annealing temperature. The PCR products were run on a 2% agarose gel and analysed to identify the annealing temperature that provided the highest specificity and yield.

2.2.6.5 RT-PCR

In order to assess relative gene expression levels following siRNA-mediated knockdown (Section 2.2.5.5 – siRNA Transfection), RT-PCR was implemented using SYBR-green chemistry in order to detect DNA amplification. Each reaction contained 10 ng cDNA, 5 µM forward and reverse primers and 12.5 µL of iQ SYBR Green Supermix, which was made up to a final reaction volume of 25 µL. A Bio-Rad C1000 CFX96 RT-PCR machine was utilised with the following conditions: 95^{o}C / 10 min; 40 cycles of: 95^{o}C / 15 sec, 60^{o}C / 1 min, 72^{o}C / 30 sec; 72^{o}C / 10 min.

Analysis was conducted using $\Delta\Delta C_T$ method outlined below, in which mRNA expression was normalised to endogenous reporter gene GAPDH.

ΔC_T sample = C_T (target) - C_T (GAPDH)

ΔC_T control = C_T (target) - C_T (GAPDH)

$\Delta\Delta C_T = \Delta C_T$ sample - ΔC_T control

Fold change = $2^{-\Delta\Delta CT}$

% Knockdown = $(1 - 2^{-\Delta\Delta CT}) * 100$

Where ΔC_T sample represents normalised gene expression value ΔC_T for the target (the gene being knocked down) in the experimental sample and ΔC_T control represent the equivalent ΔC_T for the non-targeting siRNA-treated sample.

2.2.7 Microscopy and Image Analysis

Live and fixed gut samples were imaged using either an inverted Leica SP2 confocal laser scanning microscope or a Zeiss LSM880C confocal microscope, with either a 10x immersion or 40x oil objective and 488 nm, 532 nm, 633 nm and 405 nm lasers. All images were taken at 1024x1024 pixel resolution as z-stacks with an appropriate step size. The resulting images were then viewed and analysed using Fiji (Image J) software. Where cell counting was required, CellProfiler analysis (Carpenter et al., 2006) of confocal reconstructions was undertaken.

2.2.8 Statistical Analysis

In order to carry out statistical analysis of collected data, Minitab Statistical Software was utilised. Where Student's t-tests were performed, statistical significance was accepted at $P < 0.05$ with *$P < 0.05$, **$P < 0.01$, ***$P < 0.001$ and ****$P < 0.0001$. Error bars plotted on graphs are presented as the mean ± standard error (SEM) unless otherwise indicated.

Chapter 3

In vitro invasion assays using the U87 glioblastoma cell line.

3.1 Introduction

Glioblastoma represents the most aggressive brain malignancy known. It is a cancer characterised by diffuse invasion into the surrounding tissue, which makes treatment almost impossible. Thus, research into glioblastoma invasion and the genes involved is a vital area of research.

In order to identify potential mediators of this process, genes were selected for study on account of the results obtained in the loss of function (LOF) RNAi-mediated genetic screen previously completed in the Georgiou Lab (Section 1.8 – The Genetic Screen). As described earlier, a number of genes in the screen were identified as presenting an invasive phenotype when depleted in combination with *lgl -/-* in the *Drosophila* epithelium. From these, four genes - *Gtp-bp, Ser, Ih* and *Trax* - were selected for further study due to their high scores for invasion in the screen and the reasonable % similarity and identity (Table 3.1) they shared with their closest human orthologs, *SRPRA*, *JAG1*, *HCN2* and *TSNAX* respectively. In addition, each gene had either never been linked to cancer invasion previously, or had been implicated in invasion however not in the context of glioblastoma. It would therefore be interesting to see whether, as in the screen, an invasive phenotype would be observed when the human ortholog of each gene was depleted in the U87 glioblastoma cell line (Section 2.1.7 – Cells) and invasion assays undertaken.

The assays utilised in this study (Section 2.2.5.5 – Invasion Assays), are based upon the widely used Boydon Chamber principle, with the addition of a reconstituted basement membrane layer. Such assays were chosen on account of their simple design and ease of use, which would allow the screening of multiple candidate genes.

Drosophila **Gene**	**Human Gene**	**Identity / %**	**Similarity / %**
Serrate (Ser)	Jagged 1 (*JAG1*)	33	46
I[[h]] channel (Ih)	Hyperpolarization-activated cyclic nucleotide-gated ion channel. (*HCN2*)	53	68
Transilin-associated factor X (Trax)	Transilin-associated factor X (*TSNAX*)	36	56
GTP-binding protein (Gtp-bp)	Signal recognition particle receptor alpha. (*SRPRA*)	52	69

Table 3.1 Pro-invasive hits chosen from the genetic screen.
The table shows the results obtained from pairwise alignments of orthologous proteins to assess their % similarity (% of amino acid residues with similar physiochemical properties) and % identity (% of identical residues).

3.1.1 *Gtp-bp/SRPRA*

Gtp-bp is a *Drosophila* gene that spans a 2056 bp region of the X chromosome. The gene codes for a 614 amino acid protein called GTP-binding protein (Gtp-bp). Together with signal recognition particle (SRP), Gtp-bp is a component of an essential, universally conserved protein targeting machine which couples synthesis of nascent proteins to their proper membrane localisation.

As previously described (Figure 1.10), in the genetic screen, a particularly striking phenotype was observed upon *Gtp-bp* depletion in the *Drosophila* epithelium. In addition to increased levels of invading cells, clonal tissue was drastically reduced in size and highly multi-layered, with cells losing polarised cell morphology and growing on top of one another. Table 3.2 displays the qualitative scores for key categories from the screen, scored as outlined earlier (Section 1.8 – The Genetic Screen) (See Appendix K for a full description of the scoring system utilised in the genetic screen).

	Dividing Cells	**Invading Cells**	**Clonal Tissue**	**Multi-layering**
Gtp-bp	-0.2	0.9	-1.0	1.2

Table 3.2 Qualitative scores for key phenotypes in *lgl* -/- ; Gtp-bp RNAi animals.
All scoring was relative to the phenotypes displayed by *lgl -/-*, with those most representative of that seen in *lgl -/-* animals awarded a score of 0.

The human ortholog of *Gtp-bp* is *SRPRA* (*SRPRA*), which is found on the long arm of chromosome 11 and encodes a 638 amino acid protein – signal recognition particle receptor alpha (SRPRA). Gtp-bp and SRPRA share a highly conserved N-terminal helical bundle domain and GTPase domain (NG domain) (Figure 3.1), which is also found in the 54 kDa SRP54 component of SRP. Both proteins also share an AAA-ATPase smart domain.

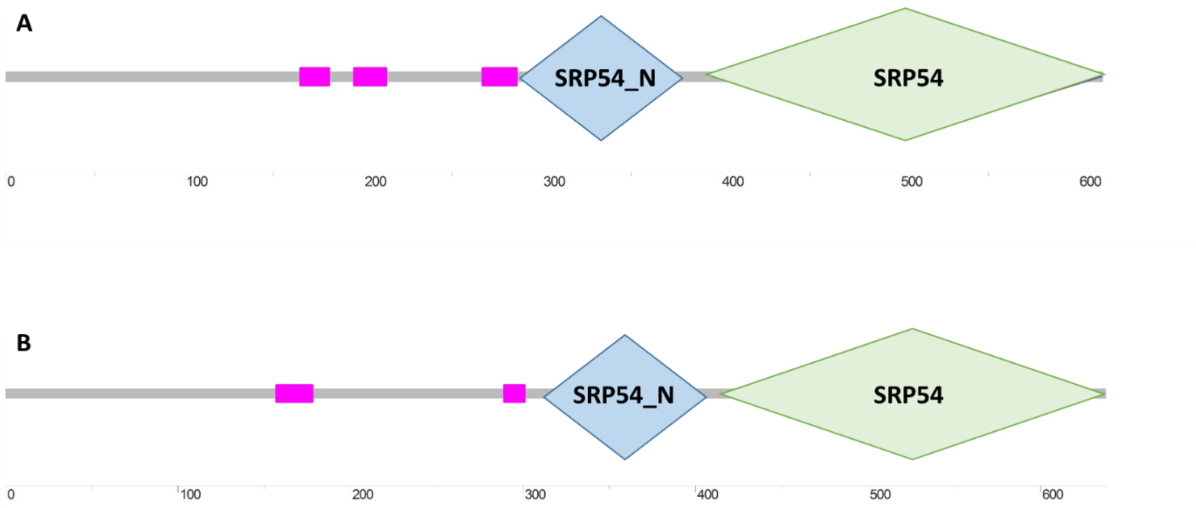

Figure 3.1. Conserved domains between Gtp-bp and SRPRA proteins.
The diagram shows highly conserved N-terminal helical bundle domains (SRP54_N) and GTPase domains (SRP54) in *Drosophila* Gtp-bp (A) and human SRPRA (B). The AAA-ATPase domain is not shown due to overlapping domains. Pink boxes represent low complexity regions. Adapted from (Schultz et al., 1998).

SRPRA, along with signal recognition particle receptor beta (SRPRB) make up the signal recognition particle receptor (SRPR), a membrane-bound receptor for the SRP. Collectively, SRPR and SRP comprise the major cellular machinery which mediates the co-translational transport of roughly 30% of the proteome from the ribosome to the endoplasmic reticulum (ER). This allows the proper localisation of proteins to their correct cellular destinations, a feat essential for the structure, organisation and function of all cells. The process begins upon the emergence of a nascent polypeptide, destined for either ER/plasma membrane targeting or secretion, from a translating ribosome. SRP recognises the N-terminal signalling sequence on the nascent polypeptide via its SRP54 domain, halting translation and allowing interaction with the SRPR. The SRPR then mediates targeting to the Sec61 translocon at the ER membrane, at which point translation resumes and the nascent chain is fed directly from the ribosome into the Sec61 translocon pore in the ER. This results in the dissociation of SRP from its receptor such that additional rounds of protein targeting can commence (Akopian et al., 2013; Saraogi et al., 2011).

In eukaryotes, the SRPR is a heterodimeric complex in which SRPRA, a 70 kDa peripheral membrane protein, dimerises with SRPRB, an integral membrane protein, via its N-terminal X-domain, localising the receptor to the ER membrane. Both subunits are GTPases. In fact, it is the multi-state GTPase activity possessed by both the SRPR subunits and SRP which provides the high temporal and spatial control required for efficient and precise SRP-dependent protein targeting (Shan et al., 2009; Jadhav et al., 2015; Zhang et al., 2008).

In recent years there has been an abundance of in-depth mechanistic investigations regarding SRPR and SRP-dependant protein targeting. However, in spite of this, relatively little is known about the consequences that defects or alterations within the pathway might have, especially within the context of disease. Furthermore, research has revealed that SRPR is the rate-limiting component of SRP-mediated protein targeting, suggesting that defects within this component have the potential to affect the entire pathway (Lakkaraju et al., 2008). For these reasons, the study of SRPRA/Gtp-bp and the potential effects of its depletion, especially within a cancer model, is particularly interesting and led to the selection of this gene to research further.

3.1.2 *Ser/JAG1*

Serrate is a well-characterised *Drosophila* gene located on the third chromosome. It encodes a 1407 amino acid protein with a universally conserved role in the Notch pathway (Section 1.6 – The Notch Pathway). Serrate is a single-pass, transmembrane protein with 14 EGF-like repeats in its extracellular domain. It plays an important role in wing imaginal disc morphogenesis, where its complex expression pattern has been shown to regulate position-specific cell proliferation (Speicher et al., 1994).

When *Ser* was depleted in combination with *lgl -/-* in the genetic screen, a strong phenotype was observed. Perhaps most striking was the substantial increase in multi-layering detected, where over half of all clonal tissue appeared dis-organised and multi-layered. Multi-layering is a trait frequently seen in conjunction with increased levels of invasion, as was detected upon *Ser* depletion in this system. Table 3.3 outlines the qualitative scores for *Ser* in key phenotypes analysed in the screen (See Appendix K for a description of the scoring system used).

	Dividing Cells	**Invading Cells**	**Clonal Tissue**	**Multi-layering**
Ser	0.2	1.0	-0.3	1.9

Table 3.3 Qualitative scores for key phenotypes in *lgl* -/- ; Ser RNAi animals.
All scoring was relative to the phenotypes displayed by *lgl -/-*, with those most representative of that seen in *lgl -/-* animals awarded a score of 0.

The human orthologs of *Serrate* are *JAG1* and *JAG2*, which are amongst the five canonical ligands for Notch receptors expressed by mammalian cells. The *JAG1* gene is located on the short arm of chromosome 20. Encompassing 26 exons, the gene encodes a 1218 amino acid protein, which is composed of a relatively small intracellular domain, a transmembrane domain and a large extracellular component. The extracellular domain of JAG1 is highly homologous to Serrate, with both proteins possessing a Delta/Serrate/Lag2 (DSL) domain (Figure 3.2) through which they interact with the Notch receptor and trigger Notch pathway activation. Downstream of the DSL domain lies 16 tandem EGF-like repeats, similar to those found in Serrate (Lindsell et al., 1995; Cordle et al., 2008).

In addition to its role in Notch signalling, *JAG1* is frequently mutated in Alagille syndrome, an autosomal dominant disorder characterised by multi-organ developmental abnormalities. 94% of Alagille cases arise from mutations in the *JAG1* gene, commonly resulting in a truncated JAG1 protein lacking a transmembrane domain (Grochowski et al, 2016).

JAG1 has also been implicated in multiple aspects of cancer biology, such as tumour angiogenesis, neoplastic cell growth, the EMT and resistance to therapy (Li et al., 2014). In glioblastoma, *JAG1* has been shown to be directly implicated in tumour development and proliferation and as such, it is considered a poor prognosis factor for the disease (Qiu et al., 2015; Purow et al., 2005). However, the role of *JAG1* in glioblastoma invasion has not been widely studied and hence it would be interesting to investigate its potential role in invasion in a glioblastoma cell line.

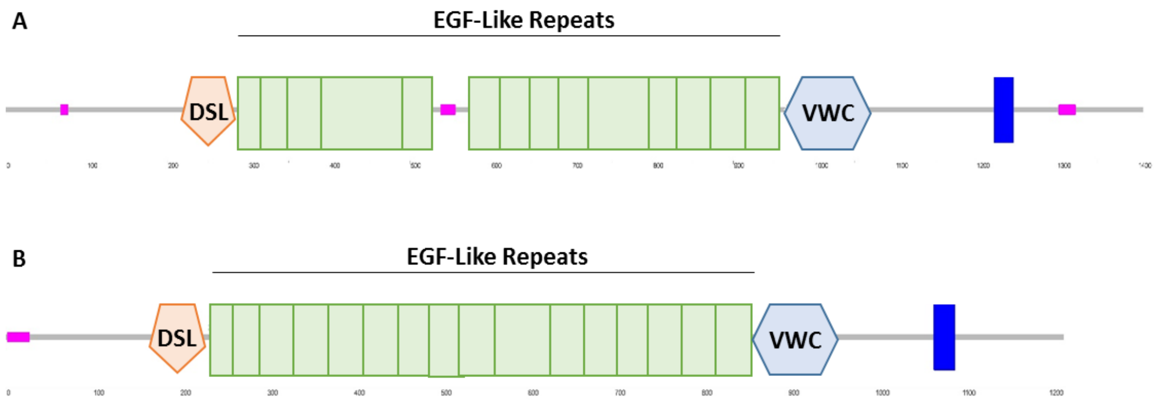

Figure 3.2. Conserved domains between Serrate and JAG1 proteins.
The diagram shows the conserved DSL domains and EGF-like repeats between Serrate (A) and JAG1 (B). Blue boxes represent the transmembrane domain while VWC is a von Willebrand factor (vWF) type C protein binding domain. Pink boxes represent low complexity regions. Adapted from (Schultz et al., 1998).

3.1.3 *Ih/HCN2*

Ih is a *Drosophila* gene located on the second chromosome that encodes a 618 amino acid protein which functions as a hyperpolarisation-activated cyclic nucleotide-gated channel (HCN). HCN channels are responsible for the hyperpolarisation-activated (Ih) current, an important regulator of excitability and rhythmicity through control of basic membrane properties. Despite having multiple important roles in mammals, the physiological role of HCN channels in invertebrates is less clear. *Drosophila* mutant for *Ih* display altered circadian rhythms and behavioural defects, and it has been suggested that Ih current is required for the maintenance of normal dopamine fluctuations (Gonzalo-Gomez at al., 2012; Chen and Wang, 2011).

In the genetic screen, RNAi-mediated knockdown of *Ih* resulted in a highly invasive phenotype. Extremely high levels of epithelial cells were identified beneath the plane of the epithelium, accompanied by an increase in the amount of multi-layered tissue compared to *lgl -/-* alone. The average scores for *Ih* in key categories studied in the screen are summarised in Table 3.4.

	Dividing Cells	**Invading Cells**	**Clonal Tissue**	**Multi-layering**
Ih	-0.3	1.3	-0.4	0.6

Table 3.4 Qualitative scores for key phenotypes in *lgl* -/- ; Ih RNAi animals.
All scoring was relative to the phenotypes displayed by *lgl -/-*, with those most representative of that seen in *lgl -/-* animals awarded a score of 0.

The human orthologs of *Ih* are *HCN1-4* of which *HCN2* is most similar. *HCN2* is located on the short arm of chromosome 19 and encodes an 889 amino acid protein. Both *Ih* and *HCN2* share a C-terminal cytoplasmic cyclic nucleotide binding domain, conferring sensitivity to cyclic adenosine monophosphate (cAMP) which modulates HCN activity (Figure 3.3). HCN channels are pore loop channels that assemble into homo- or heterotetrameric complexes found in a number of excitable and non-excitable cell types. They are responsible for the pacemaker currents in neurons and cardiac cells and for this reason have become prominent targets for the treatment of cardiac rhythm disorders. In addition to cardiac dysfunction, recent studies have also shown HCN channels to be associated with certain neurological disorders such as epilepsy and pain (Lewis and Chetkovich, 2011). Indeed, in 2011 *HCN2* was identified as the gene responsible for chronic and neuropathic pain (Emery et al., 2011).

As of yet, *HCN2* has not been implicated in cancer. On account of this, and the fact that *HCN2* is highly expressed in brain tissue, the study of this gene in invasion using a brain cancer cell line would be interesting and could contribute to our understanding of the potential role of this gene in disease.

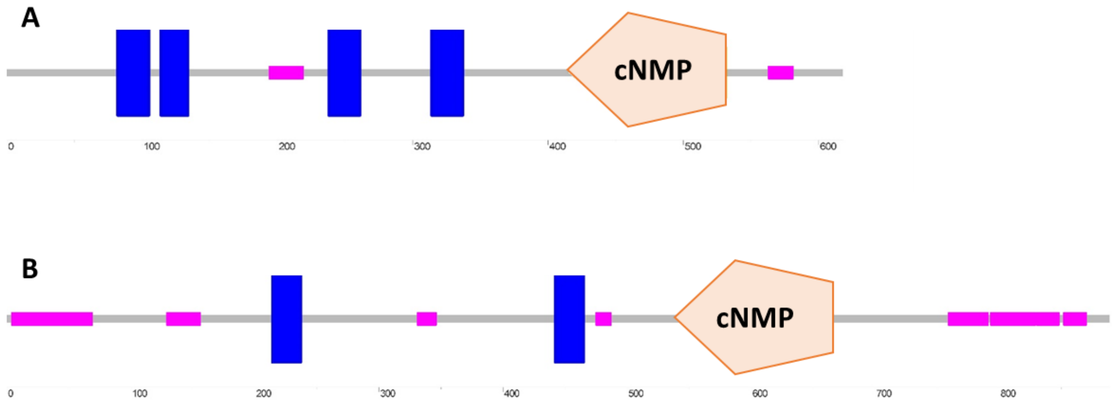

Figure 3.3. Conserved domains between Ih and HCN2 proteins.
The diagram shows the conserved cyclic nucleotide binding domain (cNMP) between Ih (A) and HCN2 (B). Blue boxes represent transmembrane domains while pink boxes represent low complexity regions. Adapted from (Schultz et al., 1998).

3.1.4 *Trax/TSNAX*

Trax is a *Drosophila* gene located on the third chromosome. Upon *Trax* knockdown in combination with *lgl -/-* in the genetic screen, an interesting phenotype was observed. In addition to extremely high levels of invading cells, mutant tissue also contained substantially fewer dividing cells than that seen in the *lgl -/-* mutant alone. A summary of the average scores given for key categories during the genetic screen is presented in Table 3.5 (See Appendix K for a description of the scoring system used).

	Dividing Cells	Invading Cells	Clonal Tissue	Multi-layering
Trax	-0.9	1.5	-0.2	0.4

Table 3.5 Qualitative scores for key phenotypes in *lgl* -/- ; Trax RNAi animals.
All scoring was relative to the phenotypes displayed by *lgl -/-*, with those most representative of that seen in *lgl -/-* animals awarded a score of 0.

Trax is orthologous to a single human gene, *TSNAX*, which is located on the long arm of chromosome one in humans. Both *Drosophila* and human genes encode relatively small proteins of 298 and 290 amino acids respectively. TSNAX was identified in a yeast two-hybrid screen for proteins that interact with Transilin, a single-stranded DNA (ssDNA) and RNA binding protein. TSNAX shares conserved sequence similarities with transilin and appears to depend on translin interaction for stability (Yang et al., 2004; Claussen et al., 2006). Due to its ability to bind ssDNA and RNA, the transilin-TSNAX complex has been implicated in a number of cellular functions such as DNA repair (Kasai et al., 1997), RNA trafficking and processing (Chiaruttini et al., 2009) and the regulation of cellular proliferation (Yang et al., 2004; Yang and Hecht., 2004).

Both *transilin* and *TSNAX* have also been implicated in a disease context. It has been suggested that transilin may play a role in reciprocal chromosomal translocations and has been shown to bind consensus sequences within recombination hotspot regions in both lymphoid (Aoki et al., 1997) and solid malignancies (Hosaka et al., 2000). Furthermore, *TSANX* is significantly involved in major psychiatric disorders in certain populations via its intergenic splicing with *disrupted-in-schizophrenia 1* (*DISC1*), a gene located immediately downstream of *TSNAX.* This genomic region has been closely related to susceptibility for bipolar disorder and associated with schizophrenia (Okuda et al., 2010).

There are currently no studies which implicate *TSNAX*, either independently or within the transilin-TSNAX complex, to cancer invasion. On account of both this and a number of the suggested cellular functions of this gene, it would be interesting to further explore the effect that depletion of TSNAX might have on the ability of cancer cells to invade.

3.2 Results

3.2.1 siRNA-mediated knockdown of *SRPRA, JAG1, HCN2* and *TSNAX*

Depletion of *Gtp-bp, Ser, Ih* and *Trax* in a *Drosophila* epithelial model promotes the invasive capabilities of transformed cells. To see whether the human orthologs of each of these genes – *SRPRA*, *JAG1*, *HCN2* and *TSNAX* respectively – may also act as mediators of invasion when knocked down in a human malignant brain cancer model, *in vitro* invasion assays were performed.

In order to ensure adequate expression levels of each gene in the U87 glioblastoma cell line prior to gene knockdown, RT-PCR (Section 2.2.6.5 – RT-PCR) was first performed and expression levels measured relative to endogenous reference gene *GAPDH*. Prior to RT-PCR reactions, temperature gradient optimisation of PCR primers was undertaken to validate optimum primer annealing temperatures (Appendix A and B). All four genes were found to be strongly expressed in the U87 glioblastoma cell line and C_T values indicative of abundant target nucleic acid were recorded (Appendix C-F).

Accordingly, U87 cells were transfected with non-targeting control siRNA and siRNA targeting either *SRPRA, JAG1, HCN2* or *TSNAX* (Section 2.2.5.5 – siRNA Transfection). 48 hours post-transfection, RT-PCR was undertaken (Figure 3.4) (Appendix G-J) and % knockdown calculated using the ΔΔCT method normalised to *GAPDH*. For all four genes, average % knockdown was calculated to be between 97-98.6% (Table 3.6), indicative of consistent gene knockdown between independent assays.

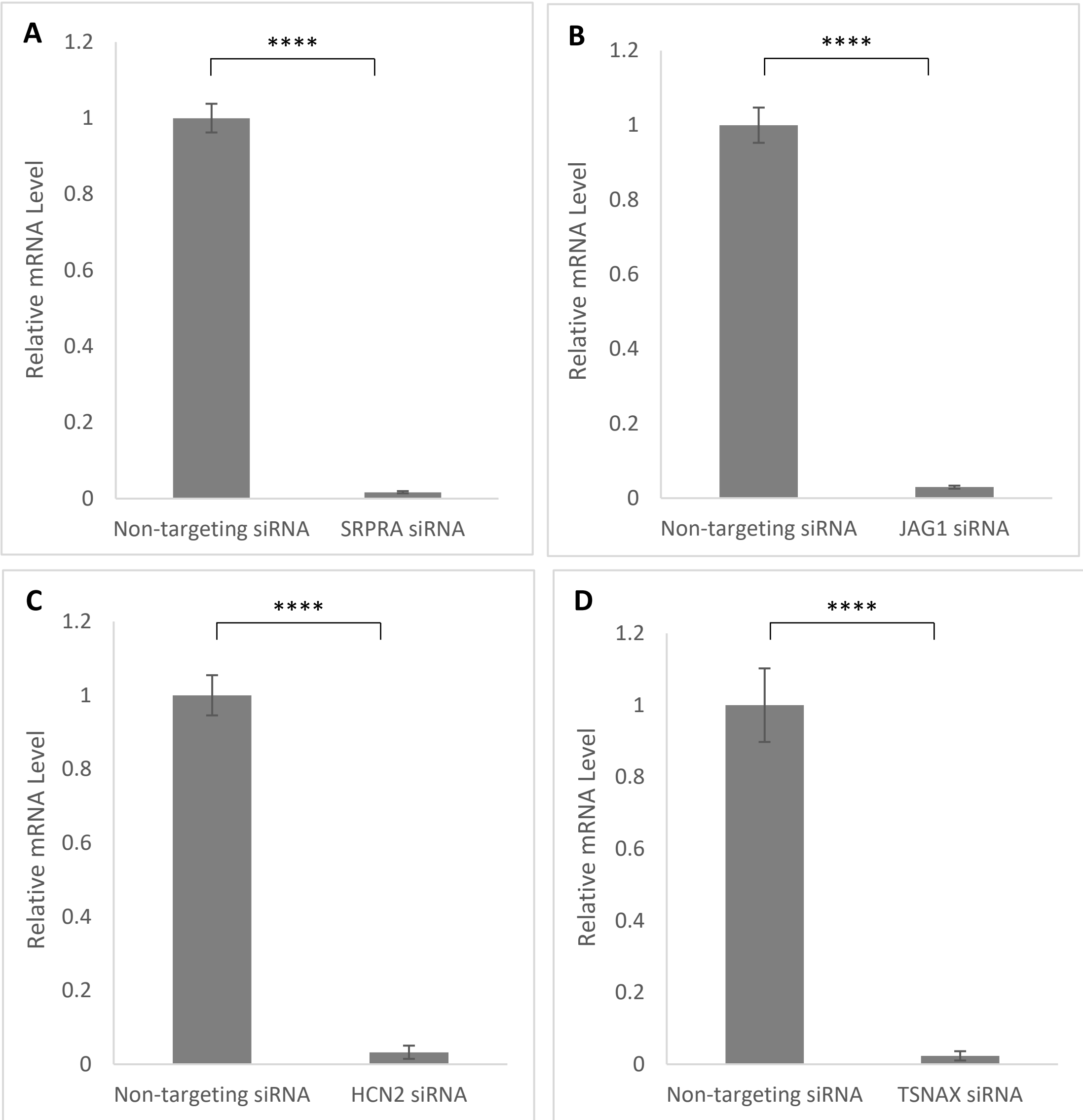

Figure 3.4. RT-PCR to analyse gene expression post-siRNA transfection.

To assess effectiveness of siRNA knockdown, U87 cells were transfected with non-targeting control siRNA and siRNA targeting *SRPRA*, *JAG1*, *HCN2* or *TSNAX*. 48 hr post-transfection, cDNA was harvested and analysed by RT-PCR for *SRPRA* (A), *JAG1* (B), *HCN2* (C) or *TSNAX* (D) expression levels. Data was normalised to GAPDH and is presented relative to expression levels in the non-targeting siRNA control sample. RT-PCR was performed in triplicate. Mean ± SD plotted; data was analysed by Student's t-test and statistical significance set at $P < 0.05$; n=3; ****$P < 0.0001$.

Gene	Average Expression Fold Change / $2^{-\Delta\Delta CT}$	Average Knockdown / %
SRPRA	0.0140	98.6
JAG1	0.0294	97.1
HCN2	0.0267	97.3
TSNAX	0.0148	98.5

Table 3.6 Average % Knockdown

Expression fold change was calculated using the ΔΔCT method, in which mRNA expression was normalised to endogenous reporter gene *GAPDH* and the non-targeting control. The average fold change was then used to estimate % knockdown.

3.2.2 Depletion of *JAG1* and *TSNAX* in a human glioblastoma cell line suppresses invasion

Quantitative *in vitro* invasion assays, in which tumour cell invasion was analysed through a basement membrane model (Section 2.2.5.6 – Invasion Assay), were performed with transfected glioblastoma-derived U87 cells (Figure 3.5). Notably, knockdown of *JAG1* resulted in a 55% reduction in the number of invading U87 cells, suggesting that loss of JAG1 function partly suppresses the invasive capabilities of U87 glioblastoma cells. Likewise, depletion of *TSNAX* in U87 cells resulted in a 42% reduction in the levels of cell invasion, again implying that *TSNAX* knockdown has a repressive effect on the invasive properties of this cell line. Interestingly, these results differ from the highly invasive phenotype observed upon knockdown of *Ser* and *Trax* in the *Drosophila* genetic screen, suggesting that *JAG1* and *TSNAX* may play different roles in cancer cell invasion in a human malignant brain cancer model than they do in an epithelial *Drosophila* model.

Knockdown of both *SRPR* and *HCN2* did not significantly change the invasive capabilities of U87 cells, although it must be noted that there was some variability between independent assay repeats. As such, it must be concluded that *SRPR* and *HCN2* do not appear to mediate cellular invasion in the U87 glioblastoma cell line. These results do not, however, discount the possibility that these genes may have a role in U87 cell migration that precedes invasion.

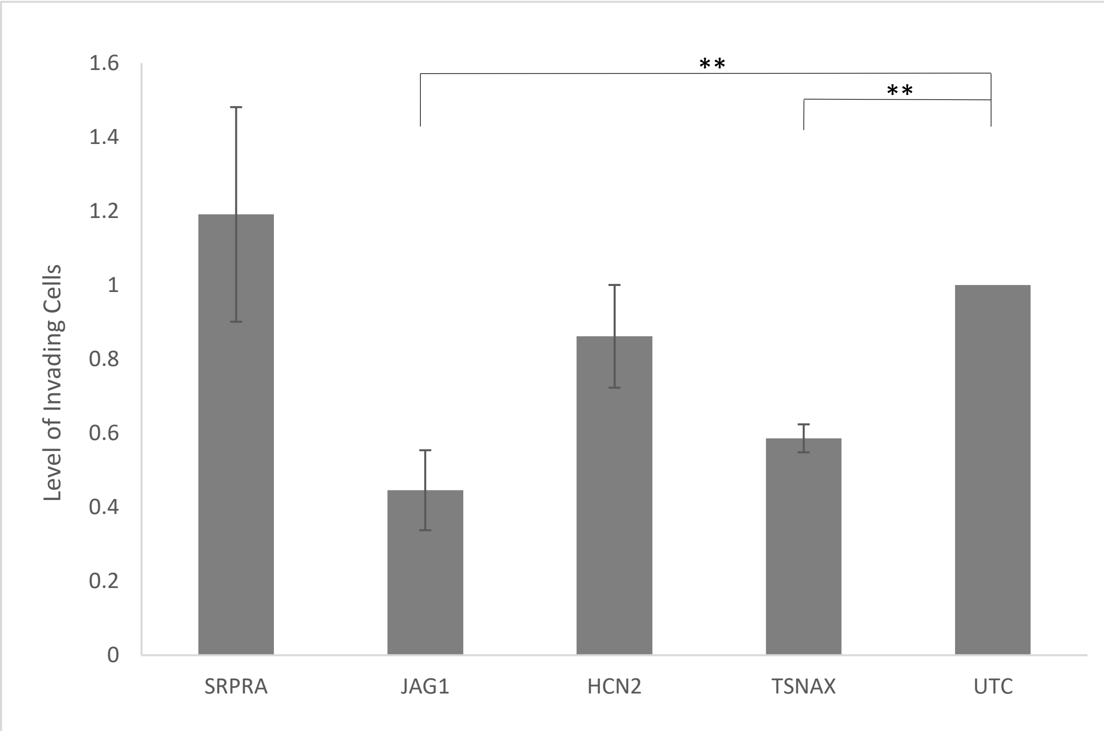

Figure 3.5 Depletion of *JAG1* and *TSNAX* results in a significant decrease in invasion of U87 cells. Invasion assays were performed using the U87 glioblastoma cell line transfected with siRNA targeting the expression of human *SRPRA, JAG1, HCN2* and *TSNAX* genes. The graph displays the effect of each gene knockdown on U87 cell invasion relative to the invasion of un-transfected U87 cells (UTC). Assays were performed in triplicate. Data was analysed by Student's t-test and statistical significance set at $P < 0.05$. Mean ± SEM plotted; $n = 3$; ** $P < 0.01$.

Chapter 4

Further characterisation of *Gtp-bp*

4.1 Introduction

The *Drosophila* gene *Gtp-bp* encodes the alpha component of the signal recognition particle receptor, a protein vital for SRP-dependent co-translational protein targeting to the ER membrane (Section 3.1.1 – *Gtp-bp* and *SRPRA*). As previously discussed, *Gtp-bp* was identified in the genetic screen due to the invasive phenotype presented upon its knockdown in *lgl* -/- mutant cells in the *Drosophila* notum epithelium. Consequently, additional research into the potential roles of this gene in tumourigenesis is warranted.

As such, prior to this project numerous further experiments had revealed many interesting findings. Firstly, generation of *Gtp-bp* loss of function (LOF) clones in a WT background results in increased delamination and decreased clonal tissue area compared to WT clones. Secondly, labelling of sensory organ precursor (SOP) cells within *Gtp-bp* mutant clones in the *Drosophila* notum, by way of the *neuralized* promoter to drive GFP expression, showed expansion of the SOP cell population. SOP cells are usually evenly spaced cells present within the notum that give rise to the external sensory organs, a process in which Delta-Notch signalling plays a pivotal role. *Neuralized* (*neur*) is a gene expressed in SOP cells that will give rise to macro- and microchaetae (bristles). The clumps of SOP cells and perturbed bristle formation that resulted from loss of Gtp-bp activity in the clones are suggestive of both defective Delta-Notch signalling and cell fate decisions. Further to this, expression of a live Notch reporter in *Gtp-bp* mutant clones in the notum revealed disrupted Delta-Notch signalling within the clones. Taken together, these experiments suggest that loss of

Gtp-bp function in the *Drosophila* notum results in a cell specification defect influencing cell fate decisions (Data un-published).

As a result, further examination of the role of *Gtp-bp* in cell fate decisions was required. To do this, the *Drosophila* midgut was chosen as a model system (Section 1.5 – The *Drosophila* Intestinal Tract). The midgut epithelium is maintained by a population of intestinal stem cells (ISCs) (Section 1.5.1 – Cellular Organisation of the *Drosophila* Midgut) which, like their mammalian counterparts, require multiple signals to maintain their proper function, primarily Notch, Janus Kinase-Signal Transducer and Activator of Transcription (JAK/STAT) and epidermal growth factor receptor (EGFR). The role of the Notch pathway in cell fate choice and differentiation is particularly well-researched and this, combined with the simplicity of the midgut cell lineage and its high rate of epithelial turnover were reasons why the midgut was chosen to use in this study.

4.2 Results

4.2.1 Loss of Gtp-bp activity in RFP negatively marked clones inhibits clonal expansion.

Previous experiments showed that loss of *Gtp-bp* expression in clones generated within the notum resulted in a decreased clonal area when compared to WT clones. In order to see whether the same phenotype would be observed in the midgut, negatively marked clones expressing a mutant *Gtp-bp* (*Gtp-bp*^{B}) (Section - 2.2.3.1 Using the FLP/FRT System to Generate RFP Negatively Marked Clones) were generated using the FLP/FRT system.

As anticipated, single cell and multi-cell clones were detected for both *Gtp-bp*^{B} mutant and WT control genotypes (Figure 4.1 A-B'). *Gtp-bp*^{B} clones were smaller than WT control clones at 15–17 days ACI, with the majority being just single cells. In addition, the *Gtp-bp*^{B} multi-cell clones that did form failed to reach the larger clone sizes of those found in the WT control. *Gtp-bp*^{B} multi-cell clones were predominantly made up of just two cells, with only 8% of clones reaching a size of 5 cells or greater, in comparison to 37% of WT clones reaching this larger size (Figure 4.1 C).

It was also observed that individual cells were generally smaller within *Gtp-bp*^{B} mutant clones than WT clones. This was particularly noticeable amongst the single cell clone population, in which cell area was found to be significantly reduced upon *Gtp-bp*^{B} expression (Figure 4.1.D). This could perhaps be representative of a different cell type in each genotype constituting the majority of clones this size.

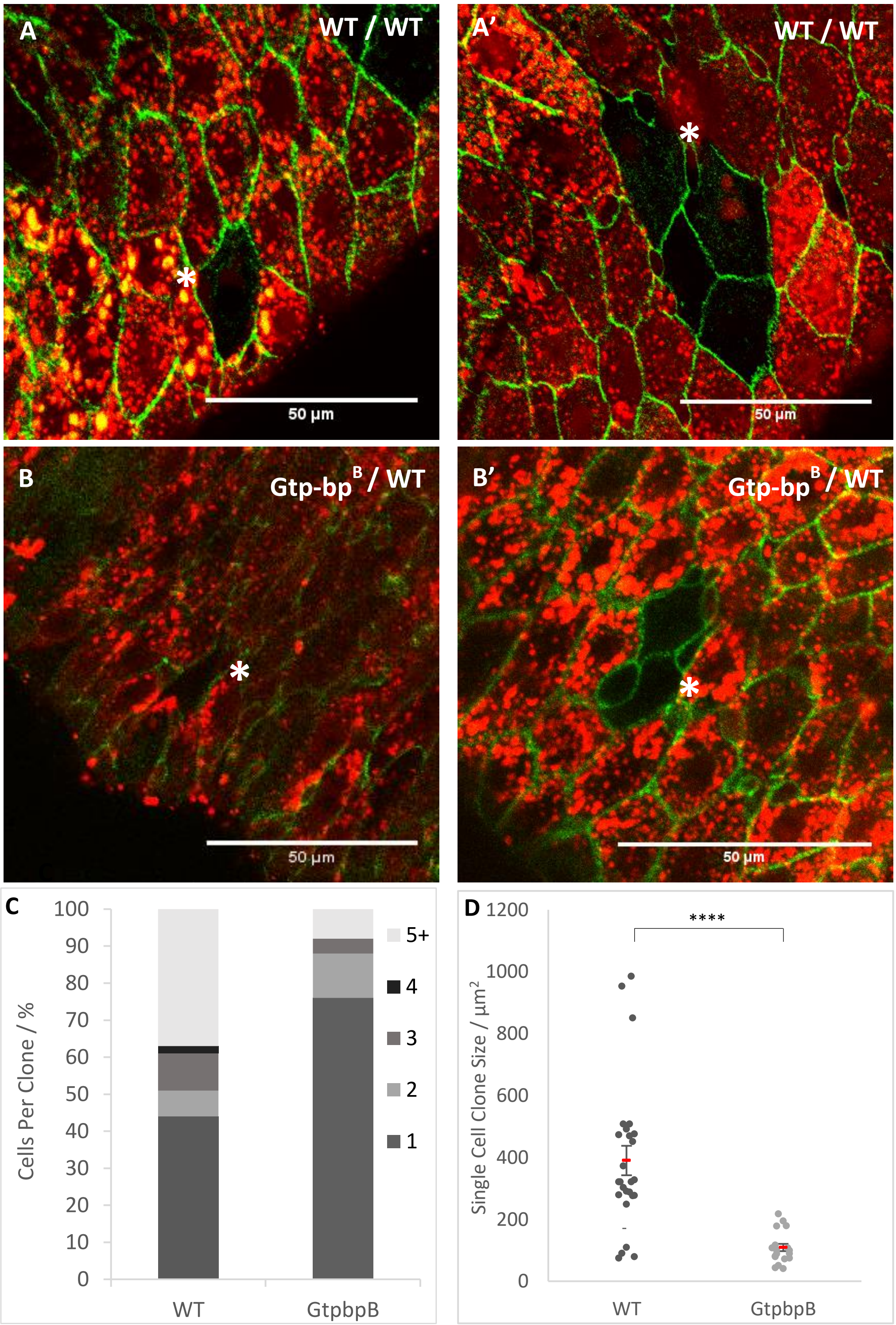

Figure 4.1. *Gtp-bp* mutation inhibits clonal expansion.

Posterior midguts harbouring control (A and A') or *Gtp-bp*^{B} mutant (B and B') clones, marked by the absence of RFP (labelled with asterisk). Guts were analysed at 15-17 days ACI and cells identified and counted by means of E-cadherin-GFP expression (green). A and B show examples of single cell clones, while A' and B' show examples of multi-cell clones. The graph in (C) shows the distribution of clone size observed. WT: n = 59 clones from 14 midguts; *Gtp-bp*^{B}: n = 25 clones from 8 midguts. The graph in (D) shows quantification of single cell clone area. Data was analysed by Student's t-test and statistical significance set at P < 0.05. Mean ± SEM plotted; ****P < 0.0001; WT n = 26; *Gtp-bp*^{B} = 19.

4.2.2 Loss of Gtp-bp function in GFP negatively marked clones both suppresses clone size and decreases EC population

In order to further examine the phenotypes recorded in the RFP negatively marked clones experiment, it would be important to analyse whether there are any differences in differentiated cell type and number between WT and *Gtp-bp*^{B} mutant clones. Due to the inability of RFP expressed in the midgut to maintain fluorescence after fixation and lack of an RFP antibody, a new negatively marked system was designed, again using the FLP/FRT system but this time with histone-GFP to label cell nuclei.

Consistent with the RFP system, the majority of *Gtp-bp*^{B} clones were single cells, with fewer multi-cell clones than the WT control at 15-17 days after clone induction (ACI) (Figure 4.2 E). However, more single cell WT clones were detected in the GFP system. Again, *Gtp-bp*^{B} multi-cell clones that did form tended to contain less cells than WT multi-cell clones, with only 6% of *Gtp-bp*^{B} clones reaching a size of 5 cells or greater in comparison to 20% of WT clones which were of this larger size. These results further confirm that *Gtp-bp* mutation impacts clonal expansion, potentially suggestive of defective ISC proliferation upon loss of Gtp-bp activity.

In addition, on average, fewer *Gtp-bp*^{B} clones in total were detected per posterior midgut than WT clones (Figure 4.2 F). Upon statistical analysis, this result was not quite significant ($p = 0.06$), likely due to the small sample size imaged and varying levels of clone induction detected between animals, perhaps as a result of the heat shock technique used.

On account of the smaller cell sizes observed in *Gtp-bp*^{B} clones in the RFP system, the possibility that cell types within WT and *Gtp-bp*^{B} mutant clones may differ was addressed. In order to identify enteroendocrine (EE) cells, posterior midguts were stained for Prospero, a transcription factor specific to the EE population. Enterocyte (EC) cells were identified by their large size and defined as possessing a nuclear diameter of 7 µm or greater (Bardin et al., 2010; Tauc et al., 2017). In the few expanded *Gtp-bp*^{B} clones, it was possible to identify both EE and EC cells, indicating that ISCs are still able to divide and differentiate in the absence of proper Gtp-bp function. No significant difference was observed between the percentage of WT and *Gtp-bp*^{B} clones possessing at least one Prospero positive cell (Figure 4.2 B). However, large variation between posterior midgut samples was found, again likely to be attributable to varying levels of clone induction following HS.

In contrast, approximately half as many *Gtp-bp*^{B} clones contained an EC cell than WT clones. The fact that the EE population appears unaffected upon Gtp-bp loss and yet the EC population is significantly depleted from the same midguts is an interesting finding and could be representative of a differentiation defect towards the EC cell lineage upon loss of Gtp-bp.

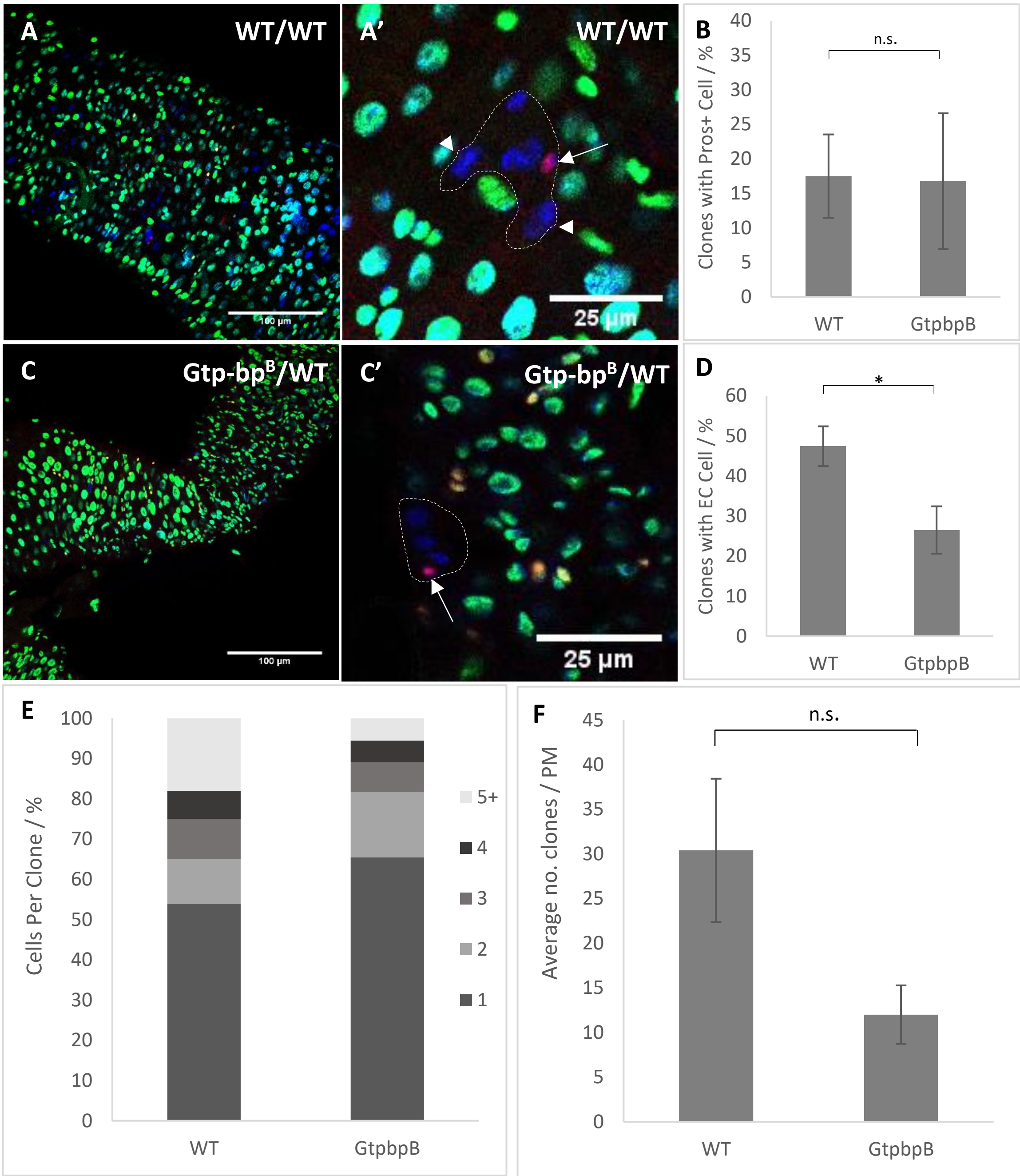

Figure 4.2. *Gtp-bp* mutation reduces both enterocyte population and clonal growth.

Posterior midguts harbouring control (A, A') or *Gtp-bp^B* mutant (C, C') clones, were dissected at 15-17 days ACI. Clones were marked by the absence of GFP and DAPI (blue) used to identify cells in GFP-negative spaces. Prospero (red, nuclear) was used to identify EE cells (arrows), while nuclei with diameters >7 µm were classed as EC cells (arrowhead). The percentage of clones harbouring one or more EE cells or EC cells are displayed in graphs (B) and (D) respectively. Data was analysed by Student's t-test and statistical significance set at P < 0.05. Mean ± SEM plotted; *P < 0.05; WT n = 4 (B) and 5 (D); *Gtp-bp^B* n = 4 (B) and 8 (D). Graph (E) shows the distribution of clone size observed and (F) shows the average number of clones detected per posterior midgut (PM). WT n = 5; *Gtp-bp^B* n = 6; mean ± SEM plotted.

4.2.3 Positively marked clones in the *Drosophila* midgut

In order to further examine the effect of Gtp-bp loss of function on clone size and composition, as well as to examine cell morphology, the MARCM system was chosen in order to generate clones of marked cells homozygous for *Gtp-bp*^{B}. Generating positively marked clones in the posterior midgut proved difficult throughout this study. As a result, it was not possible to obtain a full set of results from either of the MARCM systems attempted. Preliminary data obtained, as well as problems encountered using these systems are displayed hereafter.

4.2.3.1 MARCM labelling system chosen is ineffective at long time points

In the first MARCM system attempted, the GFP fusion protein, Moesin-GFP was utilised in order to mark the actin cytoskeleton of transformed cells and allow detailed analysis of midgut cell morphology.

Upon analysis of WT posterior midguts, huge variability between samples was detected. Both clone size and number of clones detected per midgut were inconsistent and a high proportion of both WT and *Gtp-bp*^{B} midguts did not contain any clones. Quantification of images collected yielded unexpected results, with larger *Gtp-bp*^{B} clones detected than WT clones, a finding in disagreement with previous results obtained from the midgut and the nota (Figure 4.3 A). Controls carried out alongside the experimental samples also produced strange results. To test the constructs used in this experiment to label transformed cells, UAS-MoeGFP expressing flies were crossed with flies expressing a Tubulin-Gal4 construct (Section 2.2.2.2 – The Gal4/UAS System). It was anticipated that the resultant progeny would express Moesin-GFP ubiquitously on account of the Tubulin-Gal4 driver. At short time periods post-heat shock, this was indeed the case and the entire midgut was appropriately labelled with GFP (Figure 4.3 B). However, at the longer time periods required for this experiment, this labelling mechanism was neither consistent nor effective and only a small number of cells appeared to retain Moe-GFP expression (Figure 4.3 C). Thus, it is likely that the discrepancies in this labelling system are responsible for the variable results obtained in this experiment.

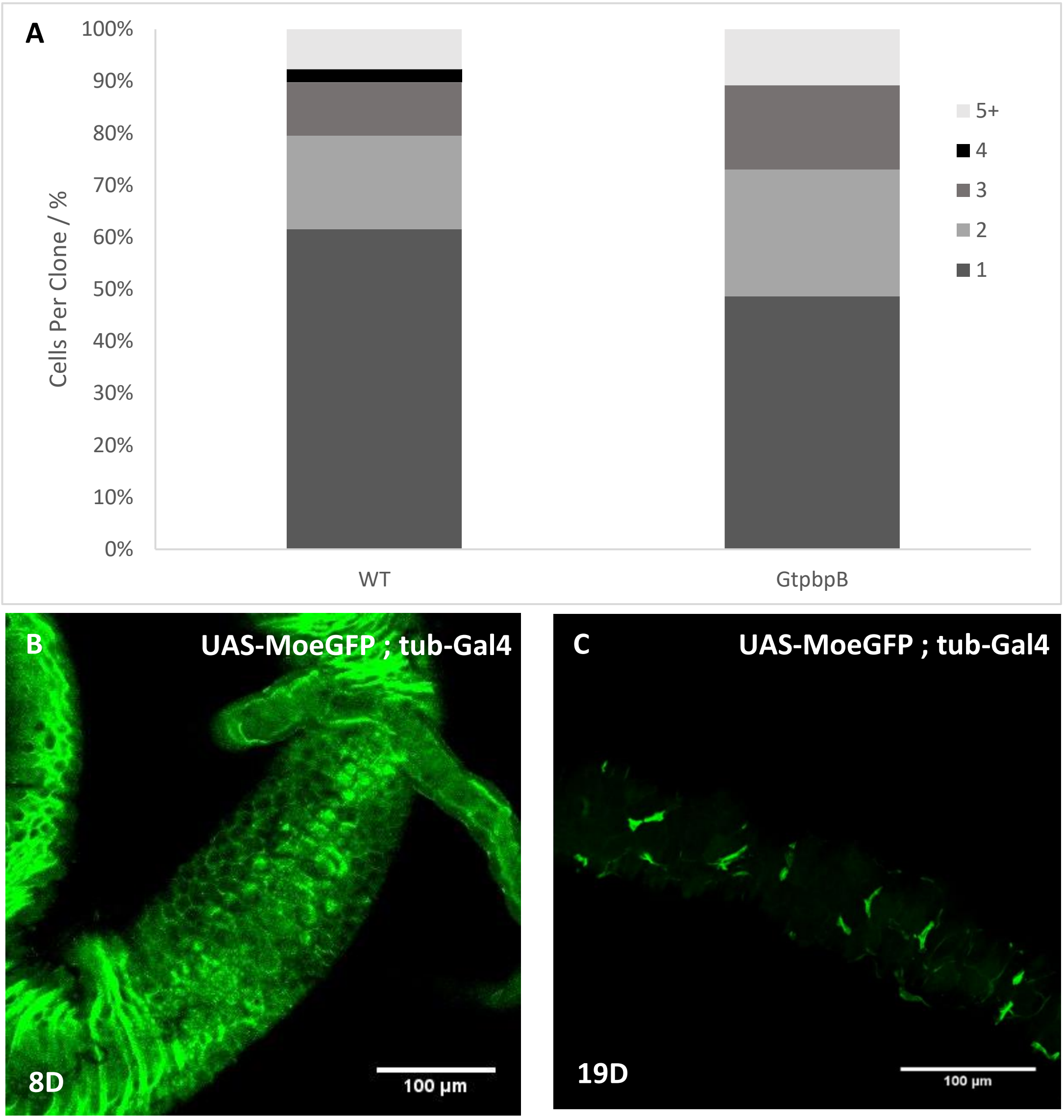

Figure 4.3. The Gal4-UAS system utilised to label MARCM clones is not effective at late time points post-heat shock.

The graph in (A) shows the distribution of clone size observed using the MARCM system to generate positively marked *Gtp-bp*^{B} mutant or WT clones in WT tissue. WT: n = 78 clones in 29 midguts; *Gtp-bp*^{B}: n = 37 clones in 17 midguts. (B) and (C) are posterior midgut regions presented as maximum intensity z-projections of multiple z-sections in x/y. Flies expressing a UAS-Moesin-GFP transgene under the control of Tub-Gal4 were subjected to a 1 hr HS at 37^{o}C and dissected at the time points specified. (B) shows Moesin-GFP expression at 8D post-heat shock while (C) represents the depleted Moesin-GFP expression observed at 19D post-heat shock.

4.2.3.2 Alternative MARCM scheme

A new MARCM system was then designed which employed TARGET (esg-Gal4ts) and FLPout systems in order to generate positively marked clones labelled with GFP.

Again, this system presented some problems. Substantial GFP background was detected in all samples, which made clonal analysis difficult. This is likely to be due to background signal from the Gal4/UAS system. Such elevated background levels of GFP meant that, although identification of large EC-like cells was simple, detecting smaller cells was problematic. As such, fewer small cells than expected were found in WT clones, a factor potentially owing to the difficulties of clone identification in this system. Interesting however, was that the large EC-like cells which were easily detectable and made up almost every WT clone identified (Figure 4.4 A) were rarely found *in Gtp-bp*^{B} clones, which were generally small, single cells (Figure 4.4 B).

Surprisingly, very few large multi-cell WT control clones were detected in this system. Instead, clones existed in large clusters of smaller, one- or two-cell clones and independent clones were rare (Figure 4.4 A). Nevertheless, in agreement with previous research (Figure 4.1, 4.2), more single cell clones and fewer multi-cell clones were detected upon *Gtp-bp*^{B} expression than in WT clones and the *Gtp-bp*^{B} multi-cell clones that did form were smaller (Figure 4.4 C). Additionally, significantly fewer *Gtp-bp*^{B} clones were recorded per posterior midgut than WT clones (Figure 4.4 D), in support of trends identified earlier (Figure 4.2).

The results obtained from the second MARCM system tested appear less variable than the first and there were fewer animals in which no clones were detected. However, this data must be considered as merely preliminary and further optimisation of this system is required. It will be especially important to validate that the labelling system in this MARCM scheme is retained in old flies before it can be used reliably.

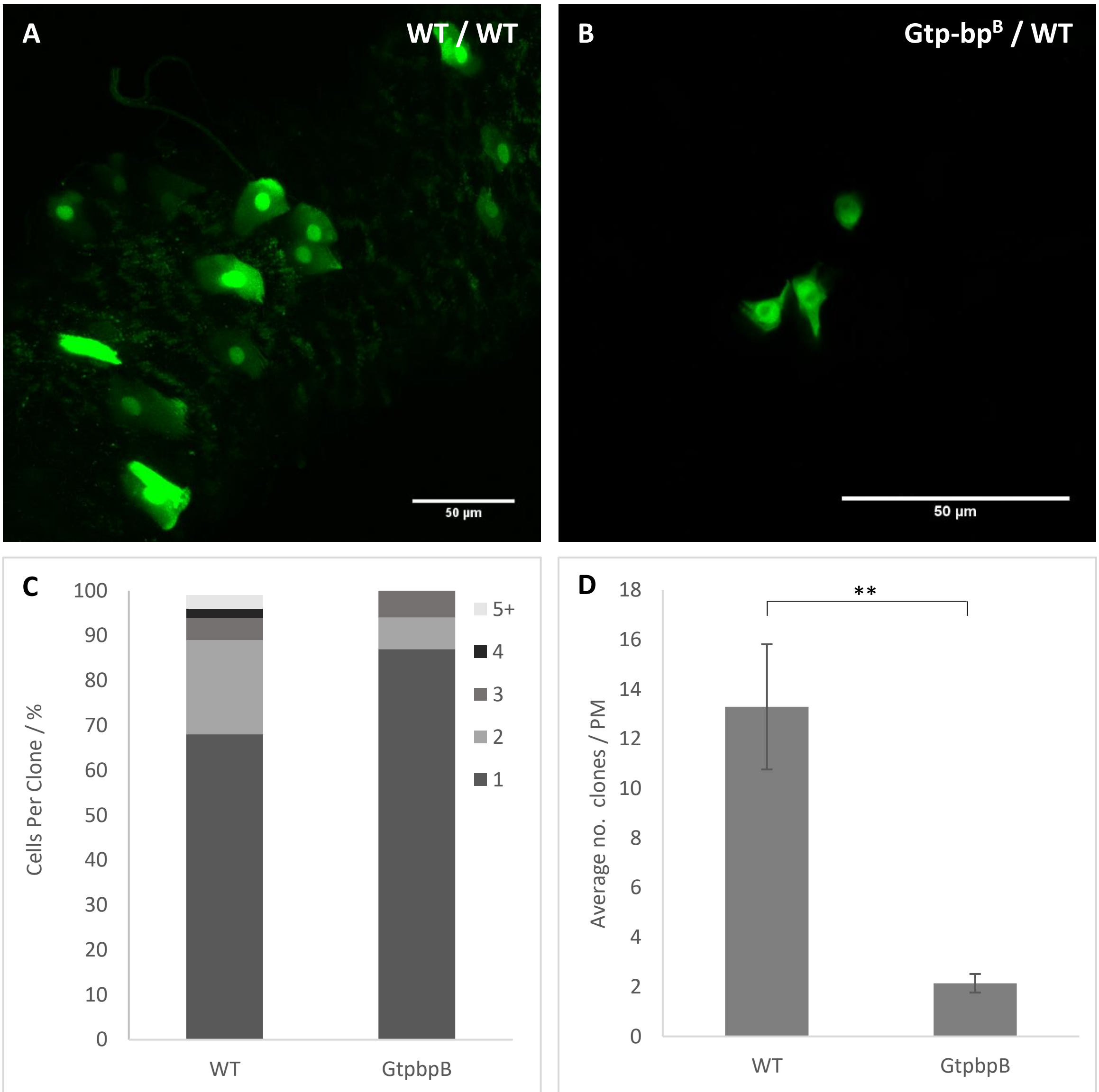

Figure 4.4. Loss of Gtp-bp function may reduce clone number in posterior midguts.
Posterior midguts harbouring control (A) or *Gtp-bp*^{B} mutant (B) clones, marked by the expression of GFP. Guts were analysed at 15-17 days ACI. Images are maximum intensity z-projections of multiple z-sections in x/y. The graph in (C) shows the distribution of clone size observed. WT: n = 92 clones in 7 PMs; *Gtp-bp*^{B}: n = 15 clones in 7 PMs. The graph in (D) shows quantification of the number of clones per PM. Data was analysed by Student's t-test and statistical significance set at $P < 0.05$. Mean ± SEM plotted; $^{**}P < 0.01$; WT n = 7; *Gtp-bp*^{B} = 7.

4.2.4 Loss of Gtp-bp function influences ISC/EB maintenance

Results from the negatively marked clone experiments suggested that *Gtp-bp* may have a role in ISC proliferation and cell fate in the posterior midgut. To explore this further, *Gtp-bp* loss in the progenitor populations (ISC/EB) was examined using the driver esg-Gal4ts (TARGET system), which is strongly expressed in ISCs and EBs, to both drive Gtp-bp RNAi in ISCs/EBs and mark them with GFP.

Midguts containing ISCs/EBs expressing the Gtp-bp RNAi transgene displayed no significant difference in the abundance of ISC/EB cells in the midguts of flies aged to 3 and 8 days (post-temperature shift to 29^{o}C to induce RNAi expression). However, when midguts were examined at a later time point of 19 days post-temperature shift, a dramatic and significant reduction in the number of GFP+ cells compared to the control was recorded (Figure 4.5), showing that the ISC/EB population is greatly reduced.

In order to directly quantify the nature of the remaining GFP+ cells at 19 days, WT and Gtp-bp RNAi-expressing midguts were stained for Delta (Dl), which is specific for ISCs (although newly divided EB cells may also retain some Delta expression). Although the number of Dl+ GFP+ cells were drastically reduced in midguts expressing Gtp-bp RNAi (Figure 4.6 C), the proportion of the GFP+ population that were Dl+ remained similar in both control and Gtp-bp RNAi midguts, suggesting that loss of Gtp-bp results in the depression of both the ISC and EB populations (Figure 4.6 D). It can therefore be concluded that the loss of Gtp-bp activity severely affects ISC maintenance in older flies, however whether the ISC loss phenotype observed is due to cell death, differentiation or an ISC proliferation defect requires further investigation.

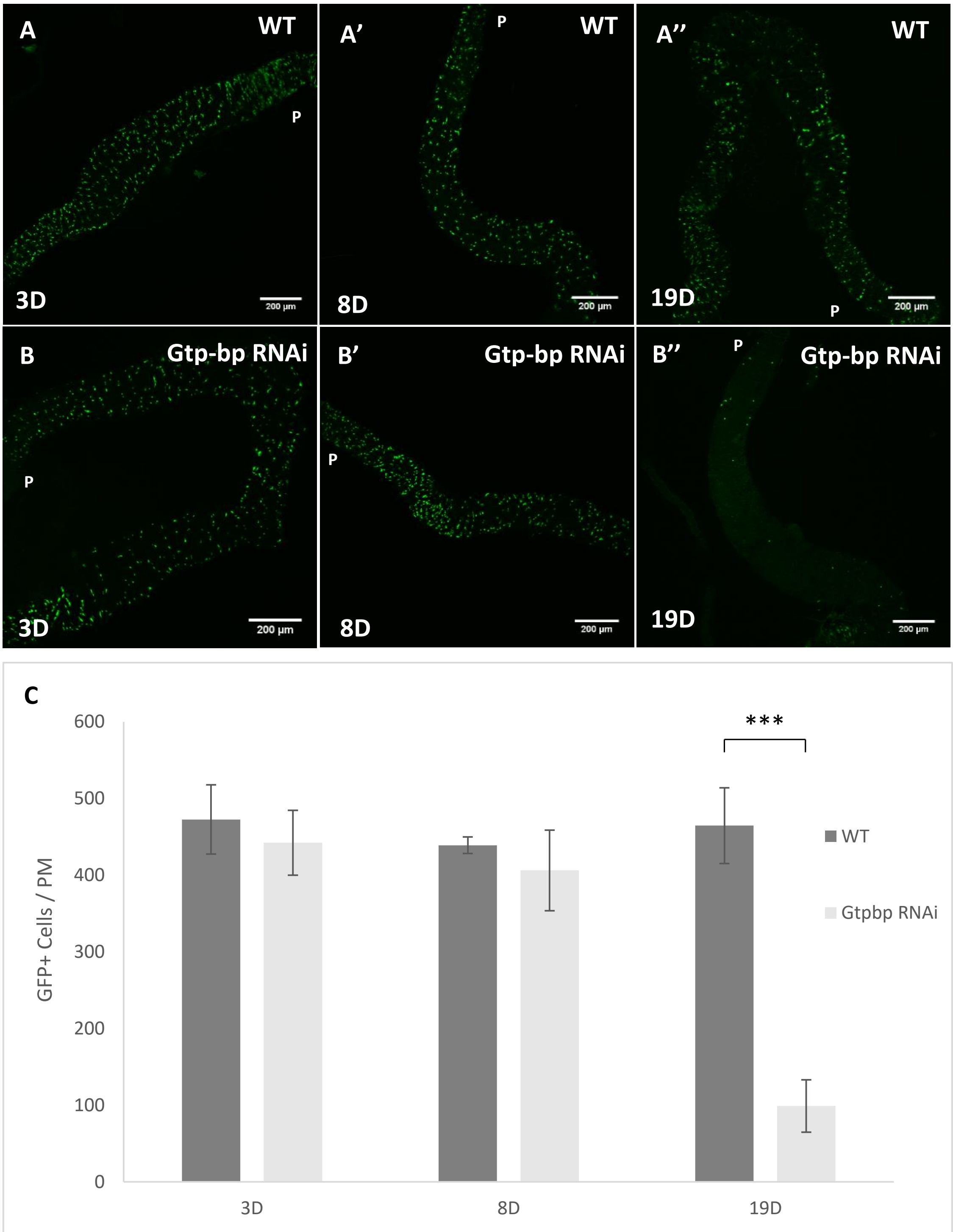

Figure 4.5. Driving Gtp-bp RNAi expression in ISC and EB populations affects ISC/EB maintenance at late time points.

Confocal images (top panel) depict GFP fluorescence (marking ISC and enteroblast populations) of either control posterior midguts (A-A'') or posterior midguts expressing a Gtp-bp RNAi transgene (B-B'') driven by esg-Gal4 at 3, 8 and 19 days after shifting to 29^{o}C induce transgene expression. Images are maximum intensity z-projections of all z-sections in x/y. P represents the posterior most end of the posterior midgut (P4). The graph in (C) shows quantification of the effect of *Gtp-bp* knockdown on GFP-positive cells in the posterior midgut region at increasing time points. Data was analysed by Student's t-test and statistical significance set at $P < 0.05$. Mean ± SEM plotted; ***$P < 0.001$; WT 3d n = 6; WT 8d n = 3; WT 19d n = 5; Gtp-bp RNAi 3d n = 10; Gtp-bp RNAi 8d n = 7; Gtp-bp RNAi 19d n = 8.

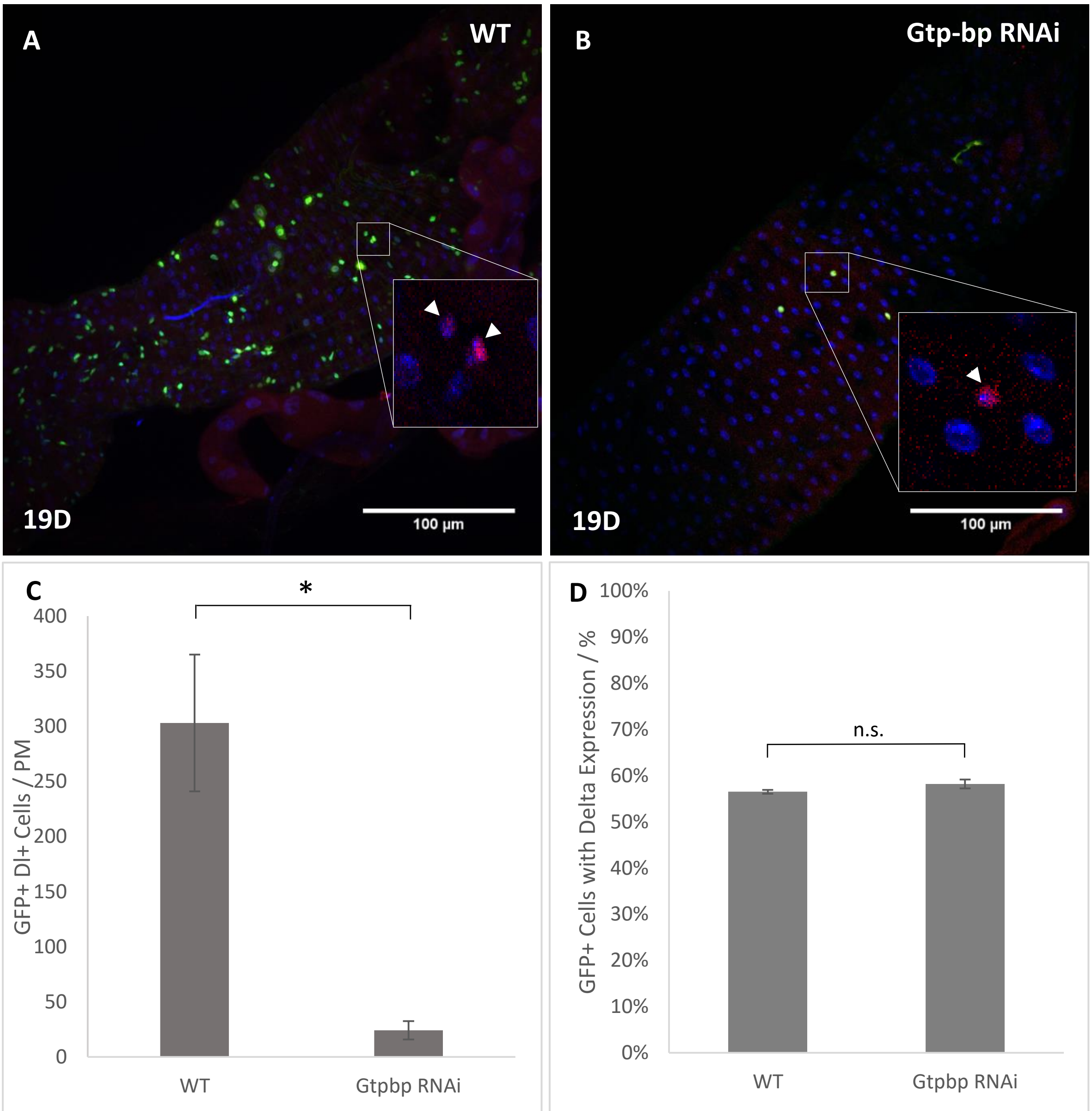

Figure 4.6. *Gtp-bp* knockdown causes a dramatic decrease in GFP+ ISC and EB cell numbers, but does not affect the proportion of GFP+ cells expressing Dl.

Flies expressing esg-Gal4ts-GFP with (B) and without (A) UAS-Gtp-bp RNAi were collected at 19 days post-RNAi induction and posterior midguts immunostained with GFP antibody (green) to mark ISC and EB populations, DAPI (blue) to identify cell nuclei and Delta antibody (red) to detect ISCs (and newly formed EB cells). Images are presented as maximum intensity z-projections of multiple z-sections in x/y and magnified sections depict Delta positive GFP+ cells (identified by arrowheads, GFP channel removed to facilitate Delta observation). Graph (C) shows quantification of the total number of GFP+ Delta+ cells per posterior midgut. Mean ± SEM plotted. Graph (D) depicts the average percentage of GFP+ cells with Delta expression per posterior midgut. Data was analysed by Student's t-test and statistical significance set at $P < 0.05$. Mean ± SEM plotted; $^*P < 0.05$; WT n = 3; Gtp-bp RNAi n = 3.

4.2.5 *Gtp-bp* is required for ISC self-renewal and maintenance

To further examine the role of *Gtp-bp* in stem cell maintenance and differentiation, the inducible esg-FLPout system was employed (Section 2.2.2.4 – The FLPout System). Using this system, every progenitor cell and its new progeny would express UAS-GFP in addition to the UAS-Gtp-bp RNAi, allowing study of the effect of *Gtp-bp* knockdown on ISC proliferation and the differentiation of subsequent progeny.

Normally, the posterior midgut epithelium renews itself within about 14 days (Ohlstein and Spradling, 2006; Jiang et al., 2009). As such, at 19 days, when the midguts were imaged, large portions of control midgut epithelia was replaced by GFP+ clones. However, following Gtp-bp RNAi expression, the growth of GFP-marked clones was greatly decreased and instead, mainly GFP+ single cells were observed, indicating major defects in gut epithelial renewal in the posterior midgut (Figure 4.7).

Epithelial turnover is therefore effectively blocked in flies expressing Gtp-bp RNAi, suggestive of defective differentiation. However, due to the observation of a small number of GFP+ EC-like cells in the Gtp-bp RNAi midguts, it appears that some differentiation towards the EC cell fate does still occur upon *Gtp-bp* knockdown. However, it is possible that this could be due to the use of RNAi as a method to silence gene expression. The depletion of target, homologous mRNA takes time and other factors such as protein stability, turnover and the efficiency of the RNAi itself all dictate the effectiveness of target gene knockdown. Nevertheless, these results clearly demonstrate that proper Gtp-bp function is required for tissue self-renewal and ISC maintenance in the *Drosophila* midgut and again suggests a potential involvement of *Gtp-bp* in progenitor differentiation.

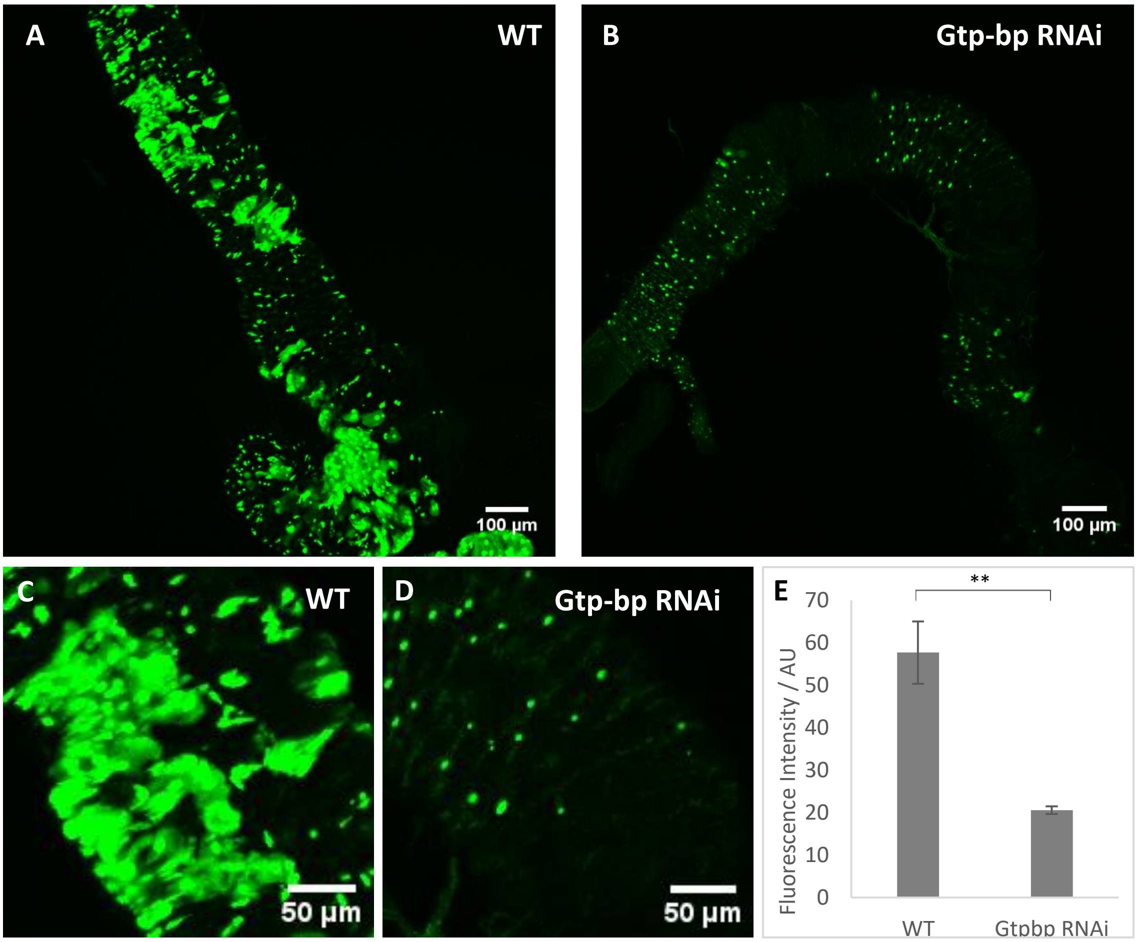

Figure 4.7 *Gtp-bp* knockdown inhibits proper midgut renewal.

The FLPout system was used to both drive the expression of GFP (A and C) and GFP with a Gtp-bp RNAi transgene (B and D) within midgut progenitors and mark their progeny. Following transfer to 29°C, flies were aged a further 19 days and posterior midguts dissected and imaged. Images are maximum intensity z-projections of all z-sections in x/y. The graph in (E) shows quantification of the mean GFP intensity per PM. Data was analysed by Student's t-test and statistical significance set at $P < 0.05$. WT n = 3; Gtp-bp RNAi n = 3; P**<0.01, mean ± SEM plotted.

4.2.6 Loss of Gtp-bp activity in an oncogenic *Ras* tumour model induces regional specific hyper-proliferation

In order to further examine whether the ISC loss phenotype observed is due to defective proliferation within the ISC community, the effect of *Gtp-bp* LOF in an oncogenic *Ras* tumour model was explored. In the posterior midgut, EGFR signalling is known to activate ISC growth and division via the Ras/Raf/MAPK pathway and accordingly, a number of papers have demonstrated ISC hyper-proliferation upon expression of activated *Ras* (*RasV12*) (Xu et al., 2011; Jin et al., 2015). To this end, the esg-Gal4 system was used to express UAS-*RasV12* (activated *Ras*) and UAS-Gtp-bp RNAi specifically within the ISC/EB populations.

Notably, co-expression of both *RasV12* and Gtp-bp RNAi within the ISCs of the posterior midgut results in their hyper-proliferation at all three time points analysed (Figure 4.8 A-B''). Thus, the loss of ISC phenotype previously observed upon *Gtp-bp* knockdown at 19 days (Figure 4.6) was completely inverted upon expression of an enabling *Ras* mutation, displaying that given stimulation, ISCs lacking proper Gtp-bp function are still capable of proliferation.

However, differential GFP intensity was observed between compartments (Figure 1.5). A significant increase in intensity was detected in *RasV12* + Gtp-bp RNAi expressing midguts between the P1 compartment and other compartments of this genotype at the 3 day time point (Figure 4.8 B). Interestingly, this regional-specific increase in intensity was not detected in the P1 sub-region of posterior midguts expressing *RasV12* or Gtp-bp RNAi alone (Figure 4.8 C). This finding indicates particular sensitivity in the P1 compartment to loss of *Gtp-bp* in combination with

RasV12. Correspondingly, closer analysis of the upper epithelial monolayer consistently displayed a visible increase in cell density within the plane of the epithelium in this sub-region compared with the same sub-region in midguts expressing *RasV12* alone (Figure 4.9).

A significant increase in intensity was also detected in *RasV12* expressing midguts between the P1 compartment and other sub-regions of this genotype at the 8 day time point, however this increase in intensity was not as dramatic as that observed in the *RasV12* + Gtp-bp RNAi midguts at 3 days. Contrastingly, at all other time points GFP intensity remained relatively constant between sub-regions and no significant changes were detected.

These results suggest that, with stimulation (at least by active Ras), Gtp-bp-depleted ISCs are capable of proliferating. However, it must be considered that in this system, *RasV12* and Gtp-bp RNAi expression are switched on simultaneously, but for reasons previously described, RNAi may take longer to have an effect. For this reason, it is possible that *RasV12* could stimulate ISC proliferation before the RNAi can effectively deplete Gtp-bp mRNA. Unexpectedly, in young flies, the hyper-proliferation induced in Gtp-bp RNAi expressing ISCs upon RasV12 expression appears to be heightened in the P1 sub-region, perhaps due to conditions existing in this particular compartment at the 3 day time point that are more conducive to hyper-proliferation. These results suggest that, at least under some circumstances, loss of Gtp-bp may promote oncogenic *Ras*-mediated hyper-proliferation.

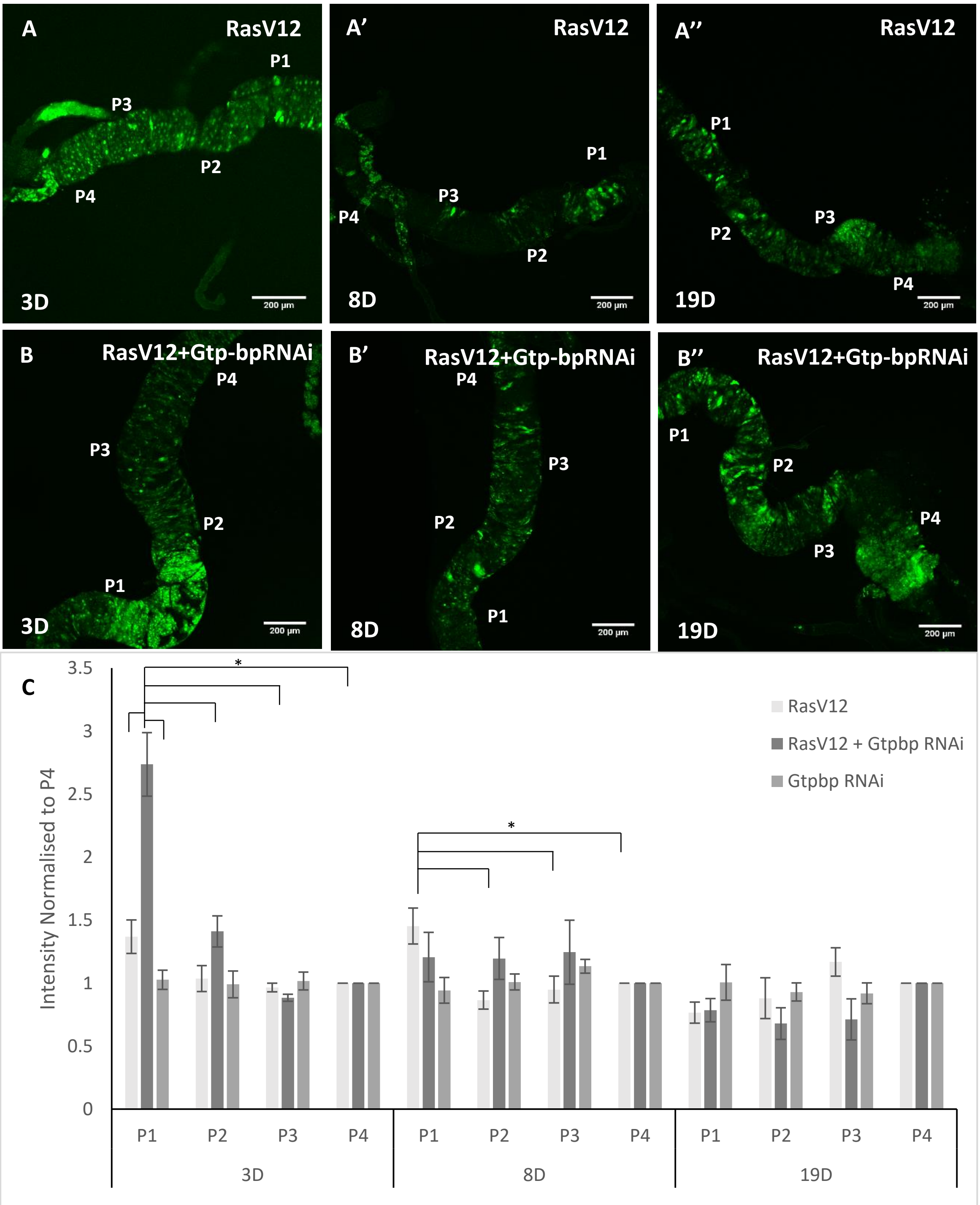

Figure 4.8. *Gtp-bp* knockdown in a *Ras* tumour model results in a regional-specific increase in GFP intensity.

Esg-Gal4 was used to drive the expression of GFP and either overactive *Ras* (*RasV12*) alone (A-A''), *RasV12* plus a Gtp-bp RNAi transgene (B-B'') or Gtp-bp RNAi alone (Figure 4.5) within ISCs/EBs. Following transfer to 29^{o}C, flies were aged a further 3 (A and B), 8 (A' and B') and 19 (A'' and B'') days and posterior midguts dissected and imaged. Images are maximum intensity z-projections of all z-sections in x/y. Posterior regions P1-4 are indicated, with P4 being the posterior-most end. Graph C shows quantification of the relative fluorescence intensity of GFP in posterior midgut regions P1-4, normalised to intensity in region P4. Data was analysed by Student's t-test and statistical significance set at $P < 0.05$. Mean ± SEM plotted; *P = <0.05; *RasV12* 3d n = 13, *RasV12* 8d n = 11, *RasV12* 19d n = 8; *RasV12*+Gtp-bp RNAi 3d n = 13, *RasV12*+Gtp-bp RNAi 8d n = 9, *RasV12*+Gtp-bp RNAi 19d n = 8; Gtp-bp RNAi 3d n = 10, Gtp-bp RNAi 8d n = 7; Gtp-bp RNAi 19d n = 8.

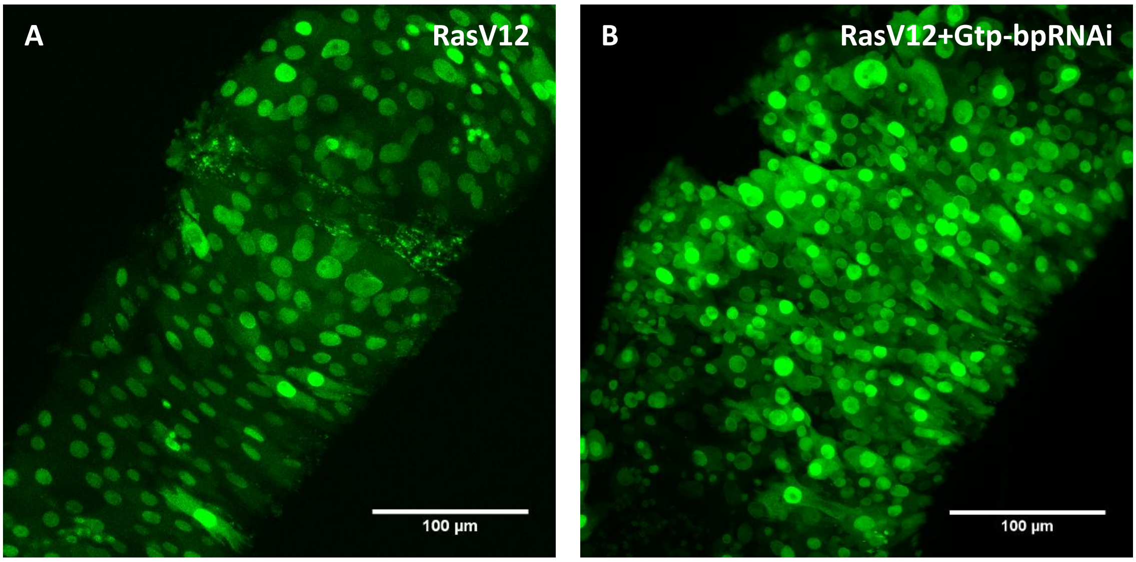

Figure 4.9. Loss of Gtp-bp may promote *Ras*-induced ISC proliferation in the P1 sub-region of posterior midgut.

Three days post RNAi induction, posterior midguts of flies expressing esg-Gal4 driven GFP and either constitutively active *Ras* (*RasV12*) alone (A), or RasV12 plus Gtp-bp RNAi (B) were dissected and imaged. ISC and EB cells are marked with GFP. Hyper-proliferation of P1 region can be observed in (A) and (B), displayed as multiple z-sections in x/y.

4.2.6.1 *RasV12* expression alters ISC/EB morphology

Along with hyper-proliferation, the expression of activated *Ras* resulted in the formation of rounded, large and abnormally-shaped ISC and EB cells, as previously reported (Tauc et al., 2017). Interestingly, this change in cell morphology was still observed in the presence of Gtp-bp RNAi. The cell shape observed upon *RasV12* expression was in stark contrast to WT control or Gtp-bp RNAi expressing progenitors, in which cells appeared small, well-structured and possessed protrusions (Figure 4.10). This suggests that *Ras* activation influences ISC morphology as well as proliferation in the *Drosophila* midgut independently of Gtp-bp.

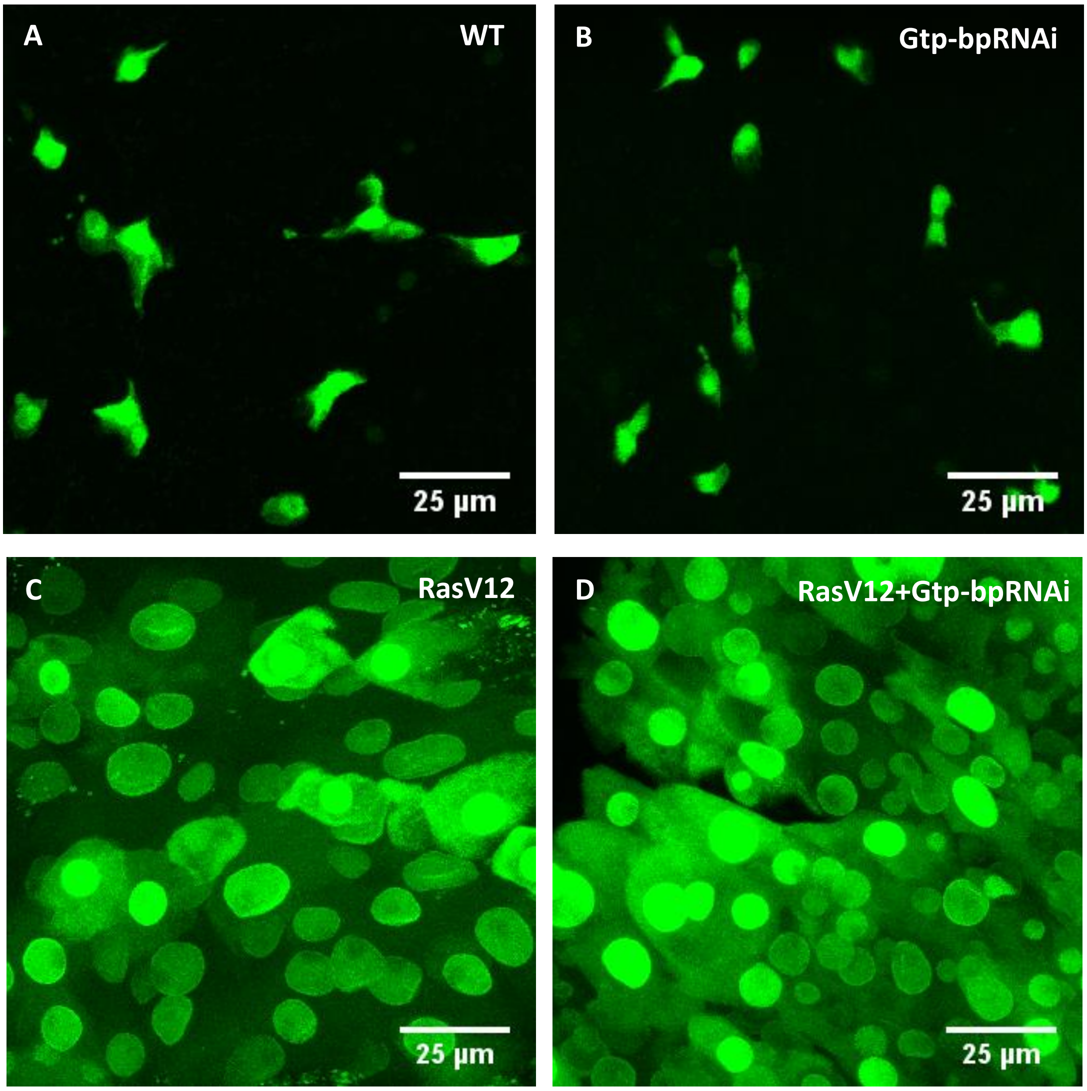

Figure 4.10. *RasV12* expression in ISC/EB cells results in rounded and abnormal cell morphology. Esg-Gal4 was used to drive the expression of GFP (A) and either Gtp-bp RNAi alone (B), *RasV12* alone (C), or *RasV12* + Gtp-bp RNAi (D) within both ISC and EB cells. Following transfer to 29ºC, flies were aged up to 3 days and posterior midguts dissected and imaged. Images are maximum intensity z-projections of multiple z-sections in x/y.

4.2.7 Loss of Gtp-bp function restricts *RasV12*-induced multi-layering within the midgut epithelium

To see whether *Gtp-bp* knockdown had a further effect on any oncogenic *Ras*-induced phenotypes, the extent of multi-layering – a key aspect of tumour progression and a pre-requisite for invasion – within the midgut epithelium, was analysed.

On account of the apparent hyper-proliferation detected in the P1 sub-region upon co-expression of *RasV12* and Gtp-bp RNAi at 3 days, multi-layering was analysed in this region and time point. As knockdown of *Gtp-bp* in the *RasV12* model results in increased GFP intensity in this region, it was anticipated that the epithelium would also exhibit a high degree of multi-layering. Surprisingly no evidence for this was found. Although multi-layering was clearly present in both genotypes, the additional expression of Gtp-bp RNAi actually appeared to reduce the thickness of multi-layered tissue in this region when compared with *RasV12* alone (Figure 4.11).

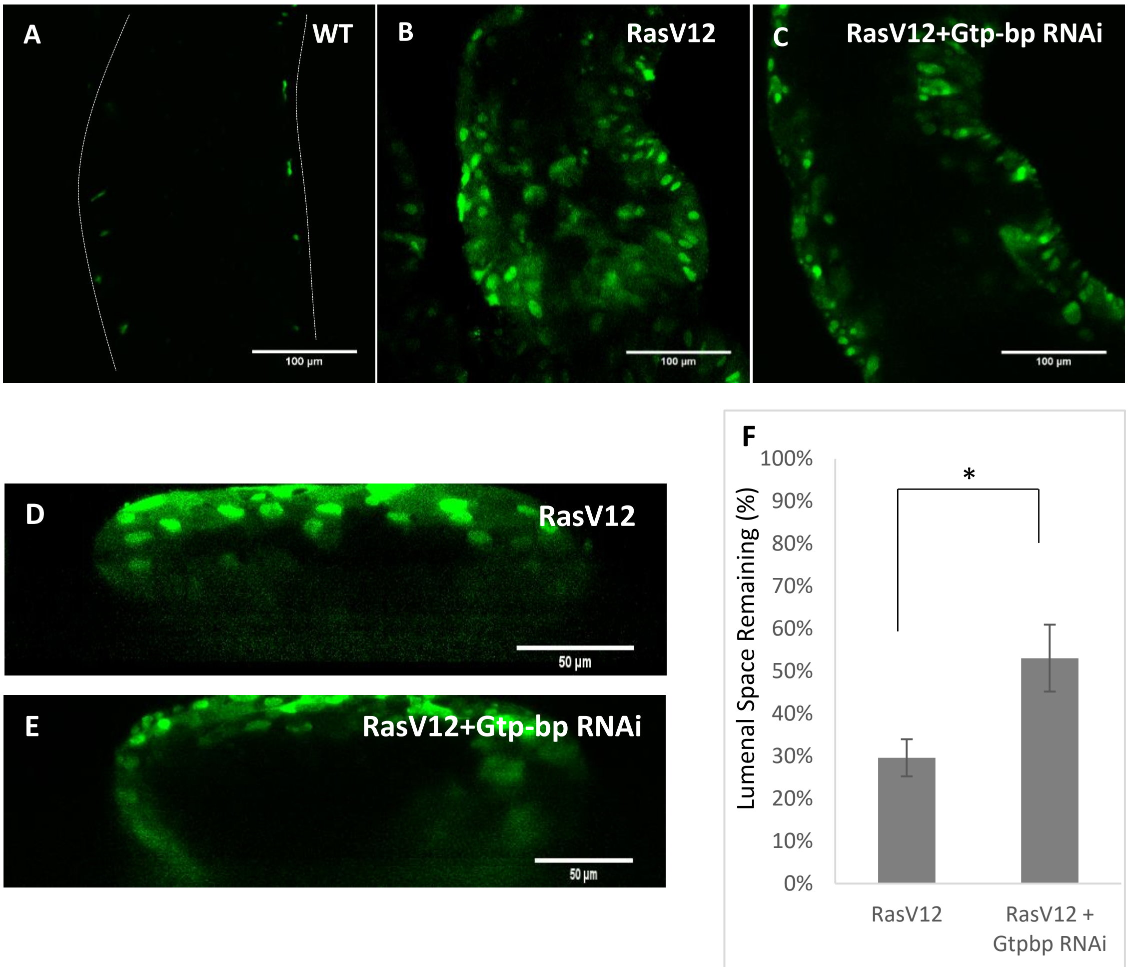

Figure 4.11. *Gtp-bp* knockdown lessens the multi-layering phenotype induced by overactive *Ras*. Three days post RNAi induction, posterior midguts of flies expressing esg-Gal4 driven GFP (A) and either overactive *Ras* (*RasV12*) alone (B and D), or *RasV12* plus a Gtp-bp RNAi transgene (C and E) were dissected and imaged. ISC and EB cells are marked with GFP. Clear evidence of multi-layering can be observed in (B) and (C), displayed as single z-sections in x/y. White dotted lines in (A) aid midgut visualisation. (D) and (E) are reconstructions of all z-sections in y/z. The graph in (F) shows the % of lumenal space remaining at the point of most intense multi-layering at the midpoint of each gut. Three separate measurements were taken per gut and an average calculated for each. Data was analysed by Student's t-test and statistical significance set at $P < 0.05$. Mean ± SEM plotted; *$P < 0.05$; *RasV12* n = 4, *RasV12* + Gtp-bp RNAi n = 4.

Chapter 5

Discussion

5.1 *In vitro* invasion assays using the U87 glioblastoma cell line.

5.1.1 *SRPRA* and *HCN2* knockdown has little effect on the invasiveness of U87 glioblastoma cells

Depletion of *SRPRA* and *HCN2* did not affect the invasive capabilities of U87 glioblastoma cells. Although this is at variance with the genetic screen, where depletion of *Gtp-bp* and *Ih* appears to promote invasion in the *Drosophila* notum, it is important to note that these two systems represent different cancer models; an *in vivo Drosophila* model of epithelial cancer and an *in vitro* model of human malignant brain cancer. In recent years it has become increasingly evident that there are tissue- and cell-type specific differences in tumourigenesis and the organisation of oncogenic signalling pathways (Schneider et al., 2017) and hence, although the genetic screen was used to identify interesting genes, it was not anticipated that the same results would necessarily be seen in both systems.

Invasion in epithelial cancer is largely reliant on the EMT (Section 1.3.2 – the EMT), which controls the switch between cancer proliferation and metastasis. In contrast, glioblastomas derive from immature astrocytes, not epithelial cells and seldom metastasise and therefore, until recently, the EMT had not been linked to glioblastoma progression. The transition of glioma cells from a proliferative to an invasive phenotype is highly dependent on local micro-environmental cues that prompt tumour cells to egress from the primary tumour mass. Most notable are signals activated by a hypoxic tumour environment, such as hypoxia inducible factor-1 (HIF-1), which promotes the expression of genes implicated in glioma cell invasion such as MMPs. Interestingly, a recent body of evidence has suggested that EMT-like traits may also play a role in the invasive phenotype of gliomas. For example hepatocyte growth factor and TGF-β are strong stimulators of glioblastoma invasion and also essential for EMT (Xie et al., 2014; Noh et al, 2017; Hoelzinger et al., 2007). Nevertheless, genes that promote invasion in an epithelial model of cancer will not necessarily mediate invasion in a model of glioblastoma, as the cell types and molecular mechanisms that govern invasion in each vary. Furthermore, the genetic screen used a cancer model that is only moderately invasive to begin with, whereas the U87 cells utilised in this project represent a highly invasive cell line. Thus, if *SRPRA* and *HCN2* are implicated in the acquisition of an invasive phenotype, rather than its maintenance, then their depletion may not have an effect in an invasive system that has already undergone this process.

In addition, it is important to note that there was variability between independent invasion assay repeats which may have influenced results. This was particularly evident upon *SRPRA* knockdown in which especially high variation between individual experiments was detected. This indicates that at present, the assay is running at sub-optimal conditions. Further optimisation of the assay will therefore be required to improve the reliability of results. Accordingly, control experiments testing a range of different U87 cell densities and matrix concentrations will be valuable to ensure that the density of cells seeded and the ECM-like barrier through which they must invade are optimal. By repeating the invasion assays for all four genes in the optimised system, it will be possible to generate more reliable results.

Furthermore, it is now known that for many the pro-invasive hits from the screen, the delaminated phenotype observed is not solely due to increased invasion and a proportion of the delaminating cells are actually apoptotic. To this end, gene knockdown promotes apoptosis in some of the transformed cells, which then delaminate from the epithelium; yet remain GFP+ for long enough to be detected, mimicking invading cells (Cornhill, 2016). A proportion of the detected delaminated cells do not however, show signs of apoptosis and appear to be truly invasive. It is currently unclear as to how many genes originally identified as invasive are also apoptotic when knocked down, or indeed the extent of apoptosis between different invasive hits.

The results obtained here indicate that depletion of *HCN2* and *SRPRA* may not alter cellular invasion in a metastatic brain cancer. However, further investigation into the roles of these genes in the acquisition of an invasive phenotype may be warranted. It would be interesting to analyse their effects on a pre-metastatic brain cancer and indeed in other cancer types. In fact, by using cBioPortal to analyse expression and mutation data from large scale cancer genomics projects (Cerami et al., 2012), it appears that both of these genes are frequently amplified, mutated and deleted in a number of cancer data sets, especially in prostate and breast cancers (Eirew et al., 2015; Beltran et al., 2016). Consequently, it would also be of interest to repeat the invasion assays using human epithelial cancer cell lines, which are also likely to be more representative of the epithelial model used in the screen. The MCF-7 cell line, a well-studied human non-invasive epithelial cancer cell line derived from breast adenocarcinoma, would be a good candidate for such experiments.

5.1.2 Loss of *JAG1* and *TSNAX* may suppress glioblastoma cell invasion

JAG1, is one of the canonical ligands for Notch receptors and as such, plays a critical role in multiple signalling pathways (Section 3.1.2 – *Ser* and *JAG1*). Knockdown of *JAG1* in *in vitro* invasion assays resulted in a significant reduction in the invasive capabilities of the U87 glioblastoma-derived cell line, suggesting that this gene may have a potential role in mediating cellular invasion in glioblastoma. Although at variance with data previously collected in the *Drosophila* screen, it is important to note that the role of Notch signalling in cancer is complex (Section 1.7 – The Notch Pathway) and can have both oncogenic and tumour-suppressive effects depending on cellular context (Leong and Karsan, 2006).

Indeed, the decrease in invasion observed is supported by a range of evidence linking the Notch pathway and its ligands to various aspects of tumour biology. High expression of *JAG1* is associated with increased tumour progression, metastatic potential and poor overall survival in a range of cancers including colorectal cancer, lung cancer, breast cancer and glioblastoma (Sugiyama et al., 2010; Chang et al., 2016; Berdanz-Knoll et al., 2016; Qiu et al., 2015). Furthermore, loss of *JAG1* expression in colon and lung cancer cell lines has been shown to decrease the invasive and migratory capabilities of cancer cells (Chang et al., 2016; Dai et al., 2014). In glioblastoma, the majority of research on Notch signalling to date has focused on its role in tumour development and proliferation. Notably, *Notch-1* has been linked to EGF signalling, the major proliferative pathway in glioblastoma, via up-regulation of EGFR transcription through its regulation of p53, an activator of the EGFR promoter (Purow et al., 2008). Further to this, knockdown of both *JAG1* and

Notch-1 in glioblastoma cell lines slows cell growth (Purow et al., 2005). Less research has been undertaken regarding the role of Notch signalling in glioma invasion, however siRNA-mediated down-regulation of *Notch-1* has been shown to attenuate the invasive capabilities of malignant glioma cells (Xu et al., 2010).

The results obtained here imply that *JAG1* may influence cellular invasion in glioblastoma, as in other solid malignancies, suggesting a function for *JAG1* in cancer cell invasion in different cancer types. However, these results will need to be validated upon invasion assay optimisation, as due to the aforementioned variation detected in some of the genes tested in this study, the results obtained should be considered as unreliable at present. Following this, further research will be useful in order to understand how loss of *JAG1* might suppress invasion in this system. *JAG1* loss in colon cancer cell lines has been associated with decreased expression of MMP2 and MMP9 (Dai et al., 2014). Both MMP2 and 9 are proteases commonly up-regulated in glioblastoma and implicated in disease progression. For this reason, it would be interesting to analyse the effect of *JAG1* knockdown on their expression in glioblastoma cells by way of immunohistochemistry, qPCR or western blot.

TSNAX has been implicated in a number of cellular processes with its binding partner *Transilin* (Section 3.1.4 – *Trax* and *TSNAX*), including DNA repair and RNA processing. Upon siRNA mediated knockdown of *TSNAX* in U87 glioblastoma cells, a significant decrease in invasion was observed, indicating that *TSNAX* may have a role in the regulation of cellular invasion in glioblastoma. As *TSNAX* has not previously been implicated in glioblastoma or cancer invasion before, this is an interesting observation worthy of further analysis. In order to validate this novel finding, further research will be required. The use of a more sophisticated system, such as a 3D cell culture model or primary cell line isolated from glioblastoma tissue, would represent a more physiologically relevant option in which to investigate the potential role of *TSNAX* in glioblastoma invasion.

It would also be interesting to see whether *TSNAX* expression levels are commonly altered in glioblastoma, for example by immunohistochemistry of a glioblastoma tissue microarray (TMA). As a starting point of such analysis, cBioPortal was utilised to analyse expression data from large-scale cancer data sets (Cerami et al., 2012). No genetic alterations in *TSNAX* were recorded in any of the brain cancer data sets present on the database. However, *TSNAX* was found to be frequently amplified in a range of epithelial cancers. This was particularly evident in a number of invasive breast cancer and prostate cancer studies (Pereira et al, 2016). On account of such findings, repeating the invasion assays using breast cancer and prostate cancer epithelial cell lines would also be of interest.

Interestingly, a role for *TSNAX* has recently been uncovered independent from *Transilin* in ataxia telangiectasia mutated (ATM)-mediated DNA repair (Wang et al., 2016). It was demonstrated that TSNAX facilitates the activation of ATM and optimises the MRN (Mre11-Rad50-Nbs1) complex – ATM – H2AX repair machinery. Furthermore, *TSNAX* down-regulation was shown to result in the failure of ATM activation, impairing DNA repair and causing eventual stress-induced apoptosis in mouse fibroblasts. On account of recent evidence regarding the effect of apoptosis on delamination in the screen system, it is tempting to postulate that the increase in invasion recorded upon *Trax* knockdown in the genetic screen could also be linked, at least in part, to an increase in DNA damage-induced apoptosis. If so, the knockdown of *Trax* could increase susceptibility of transformed cells to apoptosis, hence resulting in an increased number of delaminated apoptotic cells. This is, however, just speculation and further analysis of apoptosis in the *Drosophila* screen system, for example by way of apoliner live constructs (Bardet at al., 2008) or TUNEL assay (Arama and Steller, 2006), would be required to confirm this.

5.2 The further characterisation of pro-invasive hit *Gtp-bp*

5.2.1 Loss of Gtp-bp represses ISC proliferation and renewal

Prior to this study, previous research showed that loss of Gtp-bp function in the *Drosophila* notum both promotes epithelial cell delamination and reduces clonal tissue size.

As in the notum, *Gtp-bp*^{B} negatively marked clones generated in the midgut were substantially smaller than WT clones. The consistent observation of this phenotype between different systems is convincing evidence that loss of proper Gtp-bp activity inhibits clonal expansion. This was accompanied by a not significant but noteworthy reduction in the number of clones detected per posterior midgut upon loss of Gtp-bp activity, supported by preliminary MARCM data where *Gtp-bp*^{B} clones were significantly less abundant than WT clones. As the aforementioned clones are mitotic, emanating from the only dividing cells in the gut - the ISCs - they can be used as a measure of ISC proliferation and number (Apidianakis and Rahme, 2011). Therefore, collectively, this data indicates that loss of Gtp-bp function may impact the proliferative capacity of ISCs, hence suggesting a role for *Gtp-bp* in the regulation of ISC proliferation and/or maintenance.

The dramatic and significant decrease in ISCs and EBs upon expression of Gtp-bp RNAi further supports this. Although little change in progenitor number was observed in young flies, at later time points, after the epithelium should have undergone extensive renewal, ISC and EB populations expressing Gtp-bp RNAi were greatly reduced. Moreover, the expression of Gtp-bp RNAi resulted in a major block in gut epithelial turnover, indicating that proper Gtp-bp function is a requirement for ISC self-renewal and subsequent differentiation. Such findings are again suggestive of impaired ISC proliferation upon loss of proper Gtp-bp activity, although apoptosis should also be considered.

Interestingly, a role for this gene in proliferation has been recorded. Knockdown of *Srpr* in mouse keratinocytes and *S.cerevisiae* has been shown to inhibit cell proliferation. *Srpr* was shown to regulate cell growth by promoting G_1 to S-phase cell cycle progression and hence knockdown resulted in cell cycle arrest at G_0/G_1 and a concurrent reduction of cells in S-phase. Notably, no increase in apoptosis was observed (Kim et al., 2016; Ogg et al., 1992). On account of the high conservation of the SRPR between organisms, it is possible that this role in cell cycle progression is also applicable to *Drosophila.*

Taken together, these results suggest that loss of Gtp-bp function may disrupt ISC proliferation thus suppressing both midgut epithelial renewal and clonal growth. To further explore this, experiments should include phosphohistone H3 (PH3) staining to assess ISC mitotic responses, or assays for BrdU incorporation – a marker of progression through S-phase of the cell cycle – to monitor the proliferation rate of ISCs upon *Gtp-bp* knockdown. Moreover, staining for apoptosis markers, such as cleaved-caspase 3, will also be important to study whether apoptosis plays a role in the ISC-loss phenotype observed.

The expression of activated *Ras* in the midgut is known to cause hyper-proliferation of ISCs via activation of the EGFR/Ras/MAPK pathway (Jin et al., 2015). In this study, co-expression of *Gtp-bp* RNAi and *RasV12* was also shown to induce such hyper-proliferation in ISCs, even at late time points, suggesting that ISCs lacking Gtp-bp are indeed capable of proliferation, yet under normal conditions this ability is suppressed. However, these results must be interpreted with caution. For reasons previously discussed (Section 4.2.5), RNAi-mediated knockdown of *Gtp-bp* may take longer to have an effect than the expression of a mutant, constitutively active Ras. Consequently, it is possible that *RasV12* expression stimulates hyper-proliferation within the ISC population of the midgut before *Gtp-bp* has been effectively knocked down. In order to validate these results, an important further experiment will therefore be to utilise the MARCM system to generate *Gtp-bp*^{B} mutant clones that simultaneously express *RasV12.*

The phenotypic effects observed upon loss of Gtp-bp activity may also be attributable to a disruption in the positive feedback loops which exist in the midgut to stimulate ISC proliferation upon alterations in midgut homeostasis. When damaged or aged cells are lost from the epithelium, both they and the underlying visceral muscle release pro-mitotic EGFR and Unpaired ligands which activate EGFR and JAK-STAT pathways respectively in ISCs, promoting growth, division and epithelial regeneration. Moreover, EGFR signalling is also vital for ISC proliferation itself (Lucchetta and Ohlstein, 2012; Jiang et al., 2009). If a component of one of these pathways was disrupted upon Gtp-bp loss, perhaps as a result of defective protein targeting, it is possible that the activation of ISC proliferation and subsequent epithelial renewal would be impaired. However, the expression of constitutively active *Ras* (as in this study) within affected ISCs could potentially bypass such a block in the feedback system and activate the EGFR/Ras/MAPK pathway further downstream, thus restoring ISC division. In order to explore whether ISCs deficient for Gtp-bp are capable of responding to damage-induced proliferation cues released by dying EC cells, it would be interesting to induce artificial damage in guts expressing Gtp-bp RNAi and monitor the ISC proliferative response by way of Dextran Sodium Sulphate (DSS) feeding experiments.

Due to the presence of positive feedback loops in the midgut, it is difficult to ascertain what the primary effect of Gtp-bp LOF is. For example, if loss of Gtp-bp activity disrupts midgut feedback loops, ISC proliferation and subsequent differentiation may be affected. However, if differentiation itself is defective (discussed in detail below) resulting in the loss of differentiated cell types, then this could influence the effectiveness of the positive feedback loops themselves and hence affect ISC proliferation downstream. As such, it is possible that a number of different aspects are disrupted upon Gtp-bp LOF in this system.

5.2.2 *Gtp-bp* may be required for specification of the EC cell fate

Research carried out prior to this project involving the SOP cells of the *Drosophila* notum has suggested that *Gtp-bp* may play a role in cell fate decisions, likely by involvement in Delta/Notch (Dl/N) signalling.

Loss of Gtp-bp activity in the posterior midgut resulted in a severe disruption in midgut homeostasis. Analysis of differentiated cell type abundance in negatively marked mitotic clones revealed an apparent reduction in the EC population, an observation supported by preliminary MARCM data and suggestive of a potential differentiation defect upon loss of Gtp-bp activity. Staining midguts for Pdm-1 – a POU domain TF that marks the large polyploid nuclei of ECs – will be useful to further validate this. Interestingly, despite a decrease in EC-containing clones, there was no significant change in the number of EE-containing clones upon loss of Gtp-bp. This could suggest that, rather than inhibiting EB differentiation completely, Gtp-bp loss may instead cause a lineage-specific differentiation defect and affect EC cell fate specification only.

Differentiation in the ISC lineage is controlled by Dl/N signalling. As previously described (Section 1.6.1 – The role of the Notch pathway in ISC maintenance and differentiation), ISCs express Dl which activates N signalling in daughter EBs. The cell fate decision between EE or EC cells is regulated by the intensity of the Dl signal, with high levels of Dl in the parent ISC promoting high levels N activity in the EB daughter resulting in differentiation toward the EC cell fate and low levels of Dl specifying EE differentiation (Ohlstein and Spradling, 2006; Micchelli and Perrimon, 2006; Jiang and Edgar, 2011). Accordingly, it has been recorded that when Dl/N is suppressed, either by RNAi or clonal deletion, EC cell formation is blocked (Kapuria at al., 2012; Ohlstein and Spradling, 2007). On account of such research, the findings observed here could suggest that, as in the nota, loss of Gtp-bp disrupts Dl/N signalling, hence restricting EC differentiation. In the above-mentioned literature, low levels of Delta or N also afforded EE cell accumulation and growing clusters of ISC cells. These so-called "EE pools" were not observed within *Gtp-bp*^{B} clones in this study; however there was substantial variation in the number of Pros+ cells detected per posterior midgut and hence a larger sample size may yield different results. Furthermore, driving Gtp-bp RNAi in the ISC/EB populations by way of Esg-Gal4 and staining for Prospero would also be useful to gauge the effect of loss of Gtp-bp function on EE abundance. In addition, Delta staining of Gtp-bp LOF clones will be required to see if multiple ISCs make up the Pros- EC- cells within *Gtp-bp*^{B} multi-cell clones. This analysis was in fact attempted, however, issues with the consistency of the Delta antibody meant that reliable results were not obtained.

As a result of previous work in the nota and evidence gathered here, it is tempting to hypothesise that loss of Gtp-bp may disrupt Dl/N signalling, resulting in inadequate Notch pathway activation in EBs and thus suppressing differentiation towards the EC cell fate. In order to examine if this is indeed the case, a key experiment will involve the analysis of the difference in the Delta expression levels between WT ISCs and ISCs expressing Gtp-bp RNAi by immunostaining for Delta and measuring the intensity of Delta expression. It may also be of interest to explore the effect of Gtp-bp loss on ISC and EB populations separately. As EC cells were observed in a small proportion of both *Gtp-bp*^{B} negatively marked clones and FLPout clones, it is possible that the effect on differentiation afforded upon *Gtp-bp* knockdown is cell-type specific. By using two recently developed Gal4 lines – Delta-Gal4 and Su(H)GBE-Gal4 (Zeng et al., 2010) – it would be possible to express Gtp-bp RNAi specifically in the ISC or EB populations respectively and hence examine this further.

5.2.3 Loss of Gtp-bp function alters oncogenic *Ras*-induced phenotypes

In addition to providing further insight into its role in proliferation, analysis of *Gtp-bp* knockdown in an overactive *RasV12* model also allowed study of this gene in a tumour context. Surprisingly, upon co-expression of Gtp-bp RNAi and *RasV12*, significantly increased GFP intensity was consistently recorded in the anterior-most region (P1) of the posterior midgut in young flies, compared to other sub-regions. This apparent increase in proliferation is in stark contrast to the decreased clone sizes previously recorded upon Gtp-bp LOF, both in the notum and in the midgut, which were suggestive of impaired proliferation, alluding perhaps to context-dependent functions for the gene. Nevertheless, this finding implies that *Gtp-bp* knockdown promotes Ras-induced hyper-proliferation at this time point, hence exerting an oncogenic effect, however interestingly only in this specific posterior midgut region.

This observation is perhaps related to the complex regionalisation displayed by the *Drosophila* midgut. Recent studies have shown the midgut to comprise 10 sub-regions, each with variations in cell behaviour and gene expression. Gene expression is highly specific and each sub-region expresses 50 - 150 genes 10 times higher than any other (Marianes and Spradling, 2013). Regionalisation is largely maintained by populations of ISCs which display high levels of transcriptional variation; differing in the levels of effectors and targets of key signalling pathways including EGFR/Ras/MAPK and JAK/STAT (Dutta et al., 2015).

If the regionally specific hyper-proliferation observed in this study is indeed due to differences between midgut sub-compartments, it appears to also be dependent on age, as older flies displayed more consistent levels of hyper-proliferation across midgut sub-regions. Indeed, midgut gene expression, compartmentalisation and ISC number and activity have been shown to alter with age (Choi et al., 2008; Buchon et al., 2013). However, most ageing research utilises very old flies, usually in the range of 30-60 days and hence it is difficult to know whether, at the time points utilised in this study, aging would have any impact on regional gene expression.

Notably, regional epigenetic differences also affect the development of midgut tumours. Tumours generated by knockdown of Notch signalling in ISC/EBs by way of the esg-Gal4 driver have been shown to preferentially arise in the P1 region, where tumours were found to be earliest onset and largest, a finding attributed to pre-existing variation in Dl/N signalling in this compartment (Marianes and Spradling, 2013). Thus, this data could further support the claim that Dl/N signalling is perturbed upon Gtp-bp loss in the midgut, causing rapid ISC proliferation preferentially in this compartment. To explore this further, experiments could include driving Notch RNAi expression within ISC/EB populations in the *RasV12* model and seeing whether a similar phenotype is observed.

Further analysis of the P1 region also demonstrated that loss of Gtp-bp function appears to reduce Ras-induced multi-layering. Due to the high GFP intensity detected in this region, this result is unexpected and suggests that although cells proliferate abundantly, loss of Gtp-bp function may promote proper cell-cell adhesion (Section 1.3.1 – Epithelial Polarity) and organisation of the epithelial monolayer when in combination with overactive Ras*.* These results are at variance with previous experiments undertaken in the nota prior to this project which recorded that *Gtp-bp* knockdown stimulates the delamination of invasive cells (Data not shown), as multi-layering typically precedes invasion. Reasons for these findings are unclear, however could again suggest that *Gtp-bp* has both biphasic and context-dependent roles in tumourigenesis.

Conversely, it is perhaps possible that the reduction in multi-layering observed upon Gtp-bp depletion could in fact indicate invasion in this system. If loss of proper Gtp-bp activity heightened the invasive capacity of cells in the midgut as it does in the notum, cells might invade more extensively from multi-layered tissue, hence resulting in a concurrent reduction in tissue thickness upon Gtp-bp loss. Unfortunately, on account of midgut structure, delaminated cells would likely then enter the lumen and be lost and hence it would be difficult to accurately quantify the levels of invading cells in this system.

5.2.4 Expression of oncogenic Ras perturbs ISC and EB morphology

In addition to promoting hyper-proliferation, expression of oncogenic Ras within the ISC/EB populations of the *Drosophila* posterior midgut also appeared to disrupt ISC and EB morphology. Interestingly, this change was still evident in the presence of Gtp-bp RNAi expression. Cells expressing *RasV12* were large and rounded, lacking the triangular shape characteristic of ISCs and the membrane protrusions frequently observed in EBs.

Similar observations in cell morphology upon *RasV12* expression have previously been recorded in both the midgut (Tauc et al., 2017) and *Drosophila* wing disc (Prober and Edgar, 2000), however reasons for this cell shape change have not been researched. In recent years, it has emerged that extensive cross-talk exists between Ras and Rho-GTPase families (Popoff and Geny, 2009; Sagi and Hall, 2000). Rho-GTPases have a pivotal role in actin cytoskeleton regulation (Etienne-Manneville and Hall, 2002) and the organisation of actin-based cell protrusions (Georgiou and Baum, 2010). Conjointly, the rounded morphology characteristic of amoeboid movement in cancer cell invasion is attributed to high Rho-GTPase activity which drives increased actomyosin contractility (Parri and Chiarugi, 2010). It therefore could be hypothesised that the abnormal ISC/EB cell morphology observed upon the expression of oncogenic *Ras* is attributable to changes in the actin cytoskeleton, potentially by alterations in Rho-GTPase activity mediated by Ras over-activation.

5.3 Concluding Statements

In this study, four genes identified as presenting pro-invasive phenotypes in a loss-of-function genetic screen undertaken in the *Drosophila* epithelium – *Gtp-bp, Ser, Ih* and *Trax* – were further researched. First, human homologs of these genes were studied in *in vitro* invasion assays using the adult U87 glioblastoma cell line. The results obtained provide evidence that both *JAG1* and *TSNAX* may mediate cellular invasion in U87 glioblastoma cells and hence could play a role in invasion in glioblastoma, although further experiments will be required to confirm this. In the case of *TSNAX* this result is particularly interesting, as the gene has not been linked to cancer progression before.

The study of *Gtp-bp* in the *Drosophila* midgut acted to further contribute to the characterisation of this gene. Loss of Gtp-bp activity in the posterior midgut was shown to both suppress clonal expansion and inhibit ISC self-renewal, indicating a potential role for Gtp-bp in the regulation of ISC proliferation. Moreover, analysis of the differentiated cell types in the midgut upon Gtp-bp loss of function showed a reduction in the enterocyte population, suggesting that Gtp-bp may be required for lineage-specific differentiation towards the enterocyte cell fate. Thus, like in the nota, loss of Gtp-bp activity in the posterior midgut may impair proper differentiation.

Finally, the examination of the effect of RNAi-mediated, Gtp-bp depletion in an oncogenic *Ras* tumour model provided some evidence that in certain circumstances, loss of proper Gtp-bp function may promote Ras-induced proliferation, suggestive of context-dependent roles for this gene in tumourigenesis.

In conclusion, this project has begun the characterisation of a number of pro-invasive genes identified from a large-scale, loss-of-function genetic screen in *Drosophila melanogaster* and in doing so, has identified two potential targets for further glioblastoma research. Furthermore, the study of *Gtp-bp* in the posterior midgut has suggested potential functions for this gene in both proliferation and differentiation, supporting prior research carried out in the lab and providing further evidence for novel roles of SRP-dependent co-translational protein targeting in cell fate decisions, tissue homeostasis and potentially tumourigenesis.

Chapter 6. Bibliography

Chapter 6. Bibliography

Adams, M. D., Celniker, S. E., Holt, R. A., Evans, C. A., Gocayne, J. D., Amanatides, P. G., . . . Venter, J. C. (2000). The genome sequence of Drosophila melanogaster. *Science, 287*(5461), 2185-2195.

Adamson, C., Kanu, O. O., Mehta, A. I., Di, C., Lin, N., Mattox, A. K., & Bigner, D. D. (2009). Glioblastoma multiforme: a review of where we have been and where we are going. *Expert Opin Investig Drugs, 18*(8), 1061-1083. doi:10.1517/13543780903052764

Akopian, D., Shen, K., Zhang, X., & Shan, S. O. (2013). Signal recognition particle: an essential protein-targeting machine. *Annu Rev Biochem, 82*, 693-721. doi:10.1146/annurev-biochem-072711-164732

Andersson, E. R., Sandberg, R., & Lendahl, U. (2011). Notch signaling: simplicity in design, versatility in function. doi:10.1242/dev.063610

Andersson, E. R., Sandberg, R., & Lendahl, U. (2011). Notch signaling: simplicity in design, versatility in function. *Development, 138*, 3593-3612. doi:10.1242/dev.063610

Aoki, K., Suzuki, K., Sugano, T., Tasaka, T., Nakahara, K., Kuge, O., . . . Kasai, M. (1995). A novel gene, Translin, encodes a recombination hotspot binding protein associated with chromosomal translocations. *Nat Genet, 10*(2), 167-174. doi:10.1038/ng0695-167

Apidianakis, Y., & Rahme, L. G. (2011). Drosophila melanogaster as a model for human intestinal infection and pathology. *Dis Model Mech, 4*(1), 21-30. doi:10.1242/dmm.003970

Arama, E., & Steller, H. (2006). Detection of apoptosis by terminal deoxynucleotidyl transferase-mediated dUTP nick-end labeling and acridine orange in Drosophila embryos and adult male gonads. *Nat Protoc, 1*(4), 1725-1731. doi:10.1038/nprot.2006.235

Aranda, V., Nolan, M. E., & Muthuswamy, S. K. (2008). Par complex in cancer: a regulator of normal cell polarity joins the dark side. *Oncogene, 27*(55), 6878-6887. doi:10.1038/onc.2008.340

Artavanis-Tsakonas, S., Rand, M. D., & Lake, R. J. (1999). Notch Signaling: Cell Fate Control and Signal Integration in Development. *Science, 284*(5415), 770-776. doi:10.1126/science.284.5415.770

Bardet, P. L., Kolahgar, G., Mynett, A., Miguel-Aliaga, I., Briscoe, J., Meier, P., & Vincent, J. P. (2008). A fluorescent reporter of caspase activity for live imaging. *Proc Natl Acad Sci U S A, 105*(37), 13901-13905. doi:10.1073/pnas.0806983105

Bardin, A. J., Perdigoto, C. N., Southall, T. D., Brand, A. H., & Schweisguth, F. (2010). Transcriptional control of stem cell maintenance in the Drosophila intestine. *Development, 137*(5), 705-714. doi:10.1242/dev.039404

Bar-Sagi, D., & Hall, A. (2000). Ras and Rho GTPases: a family reunion. *Cell, 103*(2), 227-238.

Beadle, C., Assanah, M., Monzo, P., Vallee, R., Rosenfeld, S., & Canoll, P. (2008). The role of myosin II in glioma invasion of the brain. *Molecular Biology of the Cell, 19*(8), 3357-3368.

Beauchesne, P. (2011). Extra-Neural Metastases of Malignant Gliomas: Myth or Reality? *Cancers (Basel), 3*(1), 461-477.

Bednarz-Knoll, N., Efstathiou, A., Gotzhein, F., Wikman, H., Mueller, V., Kang, Y., & Pantel, K. (2016). Potential Involvement of Jagged1 in Metastatic Progression of Human Breast Carcinomas. *Clin Chem, 62*(2), 378-386. doi:10.1373/clinchem.2015.246686

Bedogni, B., Warneke, J. A., Nickoloff, B. J., Giaccia, A. J., & Powell, M. B. (2008). Notch1 is an effector of Akt and hypoxia in melanoma development. *J Clin Invest, 118*(11), 3660-3670. doi:10.1172/JCI36157

Beltran, H., Prandi, D., Mosquera, J. M., Benelli, M., Puca, L., Cyrta, J., . . . Demichelis, F. (2016). Divergent clonal evolution of castration-resistant neuroendocrine prostate cancer. *Nat Med, 22*(3), 298-305. doi:10.1038/nm.4045

Bergers, G., & Benjamin, L. (2003). Angiogenesis: Tumorigenesis and the angiogenic switch. *Nature Reviews Cancer, 3*(401-410).

Betschinger, J., Mechtler, K., & Knoblich, J. A. (2003). The Par complex directs asymmetric cell division by phosphorylating the cytoskeletal protein Lgl. *Nature, 422*(6929), 326-330. doi:10.1038/nature01486

Bilder, D., & Perrimon, N. (2000) Localization of apical epithelial determinants by the basolateral PDZ. *Nature, 403*(6770), 676-680. doi:10.1038/35001108

Bilder, D., & Perrimon, N. (2000). Cooperative Regulation of Cell Polarity and Growth by *Drosophila* Tumor Suppressors. *Science, 289*(5476), 113-116.

Blair, S. S. (2003). Genetic mosaic techniques for studying Drosophila development. doi:10.1242/dev.00774

Bray, S. J. (2016). Notch signalling in context. *Nature Reviews Molecular Cell Biology, 17*, 722-735. doi:doi:10.1038/nrm.2016.94

Brumby, A., & Richardson, H. (2003). *Scribble* mutants cooperate with oncogenic Ras or Notch to cause neoplastic overgrowth in *Drosophila*. *The EMBO Journal, 22*, 5769–5779.

Buchon, N., Osman, D., David, F. P., Fang, H. Y., Boquete, J. P., Deplancke, B., & Lemaitre, B. (2013). Morphological and molecular characterization of adult midgut compartmentalization in Drosophila. *Cell Rep, 3*(5), 1725-1738. doi:10.1016/j.celrep.2013.04.001

Bulgakova, N. A., & Knust, E. (2009). The Crumbs complex: from epithelial-cell polarity to retinal degeneration. *J Cell Sci, 122*(Pt 15), 2587-2596. doi:10.1242/jcs.023648

Carpenter, A., Jones, T., Lamprecht, M., Clarke, C., Kang, I., Friman, O., Guertin, D., et al. (2006) CellProfiler: image analysis software for identifying and quantifying cell phenotypes. *Genome Biol*., *7*(10), 100.

Cavallaro, U., & Christofori, G. (2004). Cell adhesion and signalling by cadherins and Ig-CAMs in cancer. *Nature Reviews Cancer, 4*(2), 118-132.

Cell Motility in Cancer Invasion and Metastasis. (2006). (A. Wells Ed. Illustrated ed. Vol. Volume 8 of Cancer Metastasis): Springer Science and Business Media.

Cerami, E., Gao, J., Dogrusoz, U., Gross, B. E., Sumer, S. O., Aksoy, B. A., . . . Schultz, N. (2012). The cBio cancer genomics portal: an open platform for exploring multidimensional cancer genomics data. *Cancer Discov, 2*(5), 401-404. doi:10.1158/2159-8290.CD-12-0095

Chang, W. H., Ho, B. C., Hsiao, Y. J., Chen, J. S., Yeh, C. H., Chen, H. Y., . . . Yu, S. L. (2016). JAG1 Is Associated with Poor Survival through Inducing Metastasis in Lung Cancer. *PLoS One, 11*(3), e0150355. doi:10.1371/journal.pone.0150355

Chen, J., & Zhang, M. (2013). The Par3/Par6/aPKC complex and epithelial cell polarity. *Exp Cell Res, 319*(10), 1357-1364. doi:10.1016/j.yexcr.2013.03.021

Chen, Z., & Wang, Z. (2012). Functional study of hyperpolarization activated channel (Ih) in Drosophila behavior. *Sci China Life Sci, 55*(1), 2-7. doi:10.1007/s11427-012-4270-6

Cheresh, D., & Weis, S. (2011). Tumor angiogenesis: molecular pathways and therapeutic targets. *Nature Medicine, 17*(11), 1359-1370.

Chiang, S. P., Cabrera, R. M., & Segall, J. E. (2016). Tumor cell intravasation. *Am J Physiol Cell Physiol, 311*(1), C1-C14. doi:10.1152/ajpcell.00238.2015

Chiaruttini, C., Vicario, A., Li, Z., Baj, G., Braiuca, P., Wu, Y., . . . Tongiorgi, E. (2009). Dendritic trafficking of BDNF mRNA is mediated by translin and blocked by the G196A (Val66Met) mutation. *Proc Natl Acad Sci U S A, 106*(38), 16481-16486. doi:10.1073/pnas.0902833106

Choi, Y. J., Hwang, M. S., Park, J. S., Bae, S. K., Kim, Y. S., & Yoo, M. A. (2008). Age-related upregulation of Drosophila caudal gene via NF-kappaB in the adult posterior midgut. *Biochim Biophys Acta, 1780*(10), 1093-1100. doi:10.1016/j.bbagen.2008.06.008

Christofori, G., & Semb, H. (1999). The role of the cell-adhesion molecule E-cadherin as a tumour-suppressor gene. *Trends Biochem Sci, 24*(2), 73-76.

Claussen, M., Koch, R., Jin, Z. Y., & Suter, B. (2006). Functional characterization of Drosophila Translin and Trax. *Genetics, 174*(3), 1337-1347. doi:10.1534/genetics.106.063016

Cloughesy, T. F., Cavenee, W. K., & Mischel, P. S. (2014). Glioblastoma: From Molecular Pathology to Targeted Treatment. *http://dx.doi.org/10.1146/annurev-pathol-011110-130324*. doi:10.1146/annurev-pathol-011110-130324

Cordle, J., Johnson, S., Tay, J. Z., Roversi, P., Wilkin, M. B., de Madrid, B. H., . . . Handford, P. A. (2008). A conserved face of the Jagged/Serrate DSL domain is involved in Notch trans-activation and cis-inhibition. *Nat Struct Mol Biol, 15*(8), 849-857. doi:10.1038/nsmb.1457

Cornhill, Z. (2016). *An RNAi-mediated genetic screen identifies genes that promote tumour progression in a living epithelium.* (PhD), University of Nottingham, Nottingham, UK.

Cuddapah, V. A., Robel, S., & Sontheimer, H. (2014). A neurocentric perspective on glioma invasion. *Nature Reviews Neuroscience, 17*(7), 455-465.

Dahmann, C. (2008). *Drosophila* (C. Dahmann Ed. 1 ed.): Humana Press.

Dai, Y., Wilson, G., Huang, B., Peng, M., Teng, G., Zhang, D., . . . Qiao, L. (2014). Silencing of Jagged1 inhibits cell growth and invasion in colorectal cancer. *Cell Death Dis, 5*, e1170. doi:10.1038/cddis.2014.137

Dang, T. P., Gazdar, A. F., Virmani, A. K., Sepetavec, T., Hande, K. R., Minna, J. D., . . . Carbone, D. P. (2000). Chromosome 19 translocation, overexpression of Notch3, and human lung cancer. *J Natl Cancer Inst, 92*(16), 1355-1357.

Deepa, P., Akshaya, A., & Solomon, P. (2009). WONDER ANIMAL MODEL FOR GENETIC STUDIES - Drosophila Melanogaster –ITS LIFE CYCLE AND BREEDING METHODS – A REVIEW. *Sri Ramachandra Journal of Medicine, 2*(2), 33-38.

Deryugina, E. I., & Quigley, J. P. (2015). Tumor angiogenesis: MMP-mediated induction of intravasation- and metastasis-sustaining neovasculature. *Matrix Biol, 44-46*, 94-112. doi:10.1016/j.matbio.2015.04.004

Duffy, J. (2002). GAL4 system in *drosophila*: A fly geneticist's swiss army knife. *Genesis, 34*(1-2), 1-15.

Dutta, D., Dobson, A. J., Houtz, P. L., Gläßer, C., Revah, J., Korzelius, J., . . . Buchon, N. (2015). Regional Cell-Specific Transcriptome Mapping Reveals Regulatory Complexity in the Adult Drosophila Midgut. *Cell Rep, 12*(2), 346-358. doi:10.1016/j.celrep.2015.06.009

Eirew, P., Steif, A., Khattra, J., Ha, G., Yap, D., Farahani, H., . . . Aparicio, S. (2015). Dynamics of genomic clones in breast cancer patient xenografts at single-cell resolution. *Nature, 518*(7539), 422-426. doi:10.1038/nature13952

Ellisen, L. W., Bird, J., West, D. C., Soreng, A. L., Reynolds, T. C., Smith, S. D., & Sklar, J. (1991). TAN-1, the human homolog of the Drosophila notch gene, is broken by chromosomal translocations in T lymphoblastic neoplasms. *Cell, 66*(4), 649-661.

Emery, E. C., Young, G. T., Berrocoso, E. M., Chen, L., & McNaughton, P. A. (2011). HCN2 ion channels play a central role in inflammatory and neuropathic pain. *Science, 333*(6048), 1462-1466. doi:10.1126/science.1206243

Etienne-Manneville, S., & Hall, A. (2002). Rho GTPases in cell biology. *Nature, 420*(6916), 629-635. doi:10.1038/nature01148

Gardiol D. , Zacchi A. , Petrera F. , Stanta G. , & L., B. (2006). Human discs large and scrib are localized at the same regions in colon mucosa and changes in their expression patterns are correlated with loss of tissue architecture during malignant progression . *Internation Journal of Cancer, 119*, 1285-1290.

Georgiou, M., & Baum, B. (2010). Polarity proteins and Rho GTPases cooperate to spatially organise epithelial actin-based protrusions. *J Cell Sci, 123*(Pt 7), 1089-1098. doi:10.1242/jcs.060772

Gonzalo-Gomez, A., Turiegano, E., León, Y., Molina, I., Torroja, L., & Canal, I. (2012). Ih current is necessary to maintain normal dopamine fluctuations and sleep consolidation in Drosophila. *PLoS One, 7*(5), e36477. doi:10.1371/journal.pone.0036477

Greenwald, I. (1998). LIN-12/Notch signaling: lessons from worms and flies. *Genes and Development, 12*, 1751-1762. doi:10.1101/gad.12.12.1751

Grivennikov, S. I., Greten, F. R., & Karin, M. (2010). Immunity, Inflammation, and Cancer. *Cell, 140*(6), 883-899. doi:10.1016/j.cell.2010.01.025

Grochowski, C. M., Loomes, K. M., & Spinner, N. B. (2016). Jagged1 (JAG1): Structure, expression, and disease associations. *Gene, 576*(1 Pt 3), 381-384. doi:10.1016/j.gene.2015.10.065

Gu, Y., Hukriede, N. A., & Fleming, R. J. (1995). Serrate expression can functionally replace Delta activity during neuroblast segregation in the Drosophila embryo. *Development, 121*, 855-865.

Hallahan, A. R., Pritchard, J. I., Hansen, S., Benson, M., Stoeck, J., Hatton, B. A., . . . Olson, J. M. (2004). The SmoA1 mouse model reveals that notch signaling is critical for the growth and survival of sonic hedgehog-induced medulloblastomas. *Cancer Res, 64*(21), 7794-7800. doi:10.1158/0008-5472.CAN-04-1813

Hanahan, D. & W., Robert. (2000). The Hallmarks of Cancer. *Cell, 100*(7), 57-70. doi:10.1016/S0092-8674(00)81683-9

Hanahan, D. & W., Robert. (2011). Hallmarks of Cancer: The Next Generation. *Cell, 144*(5), 646-674. doi:10.1016/j.cell.2011.02.013

Heiden, M. G. V., Cantley, L. C., & Thompson, C. B. (2009). Understanding the Warburg Effect: The Metabolic Requirements of Cell Proliferation. doi:10.1126/science.1160809

Hoelzinger, D. B., Demuth, T., & Berens, M. E. (2007). Autocrine factors that sustain glioma invasion and paracrine biology in the brain microenvironment. *J Natl Cancer Inst, 99*(21), 1583-1593. doi:10.1093/jnci/djm187

Holland, E. C. (2000). Glioblastoma multiforme: The terminator *Proc Natl Acad Sci U S A* (Vol. 97, pp. 6242-6244).

Hosaka, T., Kanoe, H., Nakayama, T., Murakami, H., Yamamoto, H., Nakamata, T., . . . Toguchida, J. (2000). Translin binds to the sequences adjacent to the breakpoints of the TLS and CHOP genes in liposarcomas with translocation t(12;6). *Oncogene, 19*(50), 5821-5825. doi:10.1038/sj.onc.1203943

Hou, L., Veeravagu, A., Hsu, A., & Tse, V. (2006). Recurrent glioblastoma multiforme: a review of natural history and management options. *Neurosurgical Focus, 20*(5).

Houtz, P. L., & Buchon, N. (2014). Methods to assess intestinal stem cell activity in response to microbes in Drosophila melanogaster. *Methods Mol Biol, 1213*, 171-182. doi:10.1007/978-1-4939-1453-1_14

Huang, R. Y., Guilford, P., & Thiery, J. P. (2012). Early events in cell adhesion and polarity during epithelial-mesenchymal transition. *J Cell Sci, 125*(Pt 19), 4417-4422. doi:10.1242/jcs.099697

Human Genome Sequencing, C. (2004). Finishing the euchromatic sequence of the human genome. *Nature, 431*(7011), 931-945.

Humbert, P. O., Grzeschik, N. A., Brumby, A. M., Galea, R., Elsum, I., & Richardson, H. E. (2008). Control of tumourigenesis by the Scribble/Dlg/Lgl polarity module. *Oncogene, 27*(55), 6888-6907. doi:10.1038/onc.2008.341

Jadhav, B., McKenna, M., Johnson, N., High, S., Sinning, I., & Pool, M. R. (2015). Mammalian SRP receptor switches the Sec61 translocase from Sec62 to SRP-dependent translocation. *Nat Commun, 6*, 10133. doi:10.1038/ncomms10133

Jeon, H. M., Kim, S. H., Jin, X., Park, J. B., Joshi, K., Nakano, I., & Kim, H. (2014). Crosstalk between glioma-initiating cells and endothelial cells drives tumor progression. *Cancer Res, 74*(16), 4482-4492. doi:10.1158/0008-5472.CAN-13-1597

Jiang, H., & Edgar, B. A. (2011). Intestinal stem cells in the adult Drosophila midgut. *Exp Cell Res, 317*(19), 2780-2788. doi:10.1016/j.yexcr.2011.07.020

Jiang, H., Patel, P. H., Kohlmaier, A., Grenley, M. O., McEwen, D. G., & Edgar, B. A. (2009). Cytokine/Jak/Stat signaling mediates regeneration and homeostasis in the Drosophila midgut. *Cell, 137*(7), 1343-1355. doi:10.1016/j.cell.2009.05.014

Jin, Y., Ha, N., Forés, M., Xiang, J., Gläßer, C., Maldera, J., . . . Edgar, B. A. (2015). EGFR/Ras Signaling Controls Drosophila Intestinal Stem Cell Proliferation via Capicua-Regulated Genes. *PLoS Genet, 11*(12), e1005634. doi:10.1371/journal.pgen.1005634

Kapuria, S., Karpac, J., Biteau, B., Hwangbo, D., & Jasper, H. (2012). Notch-mediated suppression of TSC2 expression regulates cell differentiation in the Drosophila intestinal stem cell lineage. *PLoS Genet, 8*(11), e1003045. doi:10.1371/journal.pgen.1003045

Karim, F. D., & Rubin, G. M. (1998). Ectopic expression of activated Ras1 induces hyperplastic growth and increased cell death in Drosophila imaginal tissues. *Development, 125*(1), 1-9.

Kasai, M., Matsuzaki, T., Katayanagi, K., Omori, A., Maziarz, R. T., Strominger, J. L., . . . Suzuki, K. (1997). The translin ring specifically recognizes DNA ends at recombination hot spots in the human genome. *J Biol Chem, 272*(17), 11402-11407.

Kim, B. K., Yoo, H. I., Choi, K., Lee, A. R., & Yoon, S. K. (2016). Regulation of Srpr Expression by miR-330-5p Controls Proliferation of Mouse Epidermal Keratinocyte. *PLoS One, 11*(10), e0164896. doi:10.1371/journal.pone.0164896

Kuraishi, T., Binggeli, O., Opota, O., Buchon, N., & Lemaitre, B. (2011). Genetic evidence for a protective role of the peritrophic matrix against intestinal bacterial infection in Drosophila melanogaster. *Proc Natl Acad Sci U S A, 108*(38), 15966-15971. doi:10.1073/pnas.1105994108

Lakkaraju, A., Mary, C., Scherrer, A., Johnson, A., & Strub, K. (2008). SRP Keeps Polypeptides Translocation-Competent by Slowing Translation to Match Limiting ER-Targeting Sites. *Cell, 133*(3), 440-451. http://dx.doi.org/10.1016/j.cell.2008.02.049

Lamouille, S., Xu, J., & Derynck, R. (2014). Molecular mechanisms of epithelial-mesenchymal transition. *Nat Rev Mol Cell Biol, 15*(3), 178-196. doi:10.1038/nrm3758

Laprise, P., & al, e. (2009). Yurt, Coracle, Neurexin IV and the Na^{+},K+-ATPase form a novel group of epithelial polarity proteins. *Nature, 459*, 1141-1145.

Laprise, P., & Tepass, U. (2011). Novel insights into epithelial polarity proteins in Drosophila. *Trends in Cell Biology, 21*(7), 401-408, doi:http://dx.doi.org/10.1016/j.tcb.2011.03.005

Lee, T., & Luo, L. (1999). Mosaic Analysis with a Repressible Cell Marker for Studies of Gene Function in Neuronal Morphogenesis. *Neuron, 22*, 451-461.

Lee, T., & Luo, L. (2001). Mosaic analysis with a repressible cell marker (MARCM) for Drosophila neural development. *TRENDS In Neuroscience, 24*(5), 251-254.

Lemaitre, B., & Miguel-Aliaga, I. (2013). The digestive tract of Drosophila melanogaster. *Annu Rev Genet, 47*, 377-404. doi:10.1146/annurev-genet-111212-133343

Leong, K. G., & Karsan, A. (2006). Recent insights into the role of Notch signaling in tumorigenesis. *Blood, 107*(6), 2223-2233. doi:10.1182/blood-2005-08-3329

Leong, K. G., Niessen, K., Kulic, I., Raouf, A., Eaves, C., Pollet, I., & Karsan, A. (2007). Jagged1-mediated Notch activation induces epithelial-to-mesenchymal transition through Slug-induced repression of E-cadherin. *J Exp Med, 204*(12), 2935-2948. doi:10.1084/jem.20071082

Lewis, A. S., & Chetkovich, D. M. (2011). HCN channels in behavior and neurological disease: too hyper or not active enough? *Mol Cell Neurosci, 46*(2), 357-367. doi:10.1016/j.mcn.2010.11.007

Li, D., Masiero, M., Banham, A. H., & Harris, A. L. (2014). The notch ligand JAGGED1 as a target for anti-tumor therapy. *Front Oncol, 4*, 254. doi:10.3389/fonc.2014.00254

Lindsell, C. E., Shawber, C. J., Boulter, J., & Weinmaster, G. (1995). Jagged: a mammalian ligand that activates Notch1. *Cell, 80*(6), 909-917.

Lino, M. M., Merlo, A., & Boulay, J. L. (2010). Notch signaling in glioblastoma: a developmental drug target? *BMC Med, 8*, 72. doi:10.1186/1741-7015-8-72

Lisovsky, M., Dresser, K., Baker, S., Fisher, A., Woda, B., Banner, B., & Lauwers, G. Y. (2009). Cell polarity protein Lgl2 is lost or aberrantly localized in gastric dysplasia and adenocarcinoma: an immunohistochemical study . *Modern Pathology, 22*, 977-984.

Lodish, H., Berk, A., & Zipursky, S. L. (2000). *Molecular Cell Biology* (4th Edition ed.). New York: W. H. Freeman.

Lucchetta, E. M., & Ohlstein, B. (2012). The Drosophila midgut: a model for stem cell driven tissue regeneration. *Wiley Interdiscip Rev Dev Biol, 1*(5), 781-788. doi:10.1002/wdev.51

Mack, G., & Marshall, A. (2010). Lost in migration. *Nature Biotechnology., 28*(3), 214-229.

Maeda, K., Takemura, M., Umemori, M., & Adachi-Yamada, T. (2008). E-cadherin prolongs the moment for interaction between intestinal stem cell and its progenitor cell to ensure Notch signaling in adult Drosophila midgut. *Genes Cells, 13*(12), 1219-1227. doi:10.1111/j.1365-2443.2008.01239.x

Marianes, A., & Spradling, A. C. (2013). Physiological and stem cell compartmentalization within the Drosophila midgut. *Elife, 2*, e00886. doi:10.7554/eLife.00886

Martin TA, Ye L, Sanders AJ, et al. Cancer Invasion and Metastasis: Molecular and Cellular Perspective. In: Madame Curie Bioscience Database [Internet]. Austin (TX): Landes Bioscience; 2000-2013. Available from: https://www.ncbi.nlm.nih.gov/books/NBK164700/

Martin-Belmonte, F., & Perez-Moreno, M. (2011). Epithelial cell polarity, stem cells and cancer. *Nat Rev Cancer, 12*(1), 23-38. doi:10.1038/nrc3169

McGuire, S. E., Mao, Z., & Davis, R. L. (2004). Spatiotemporal gene expression targeting with the TARGET and gene-switch systems in Drosophila. *Sci STKE, 2004*(220), pl6. doi:10.1126/stke.2202004pl6

Mehlen, P., & Puisieux, A. (2006). Metastasis: a question of life or death. *Nat Rev Cancer, 6*(6), 449-458. doi:10.1038/nrc1886

Mentlein, R., Hattermann, K., & Held-Feindt, J. (2012). Lost in disruption: role of proteases in glioma invasion and progression. *Biochimica et Biophysica Acta, 1825*(2), 178-185.

Micchelli, C. A., & Perrimon, N. (2005). Evidence that stem cells reside in the adult Drosophila midgut epithelium. *Nature, 439*(7075), 475-479. doi:doi:10.1038/nature04371

Miles, W. O., Dyson, N. J., & Walker, J. A. (2011). Modeling tumor invasion and metastasis in Drosophila. *Dis Model Mech, 4*(6), 753-761. doi:10.1242/dmm.006908

Montana, V., & Sontheimer, H. (2011). Bradykinin promotes the chemotactic invasion of primary brain tumours. *The Journal of Neuroscience., 31*(13), 4858-4867.

Munro, E. M. (2006). PAR proteins and the cytoskeleton: a marriage of equals. *Curr Opin Cell Biol, 18*(1), 86-94. doi:10.1016/j.ceb.2005.12.007

Nance, J., Munro, E. M., & Priess, J. R. (2003). C. elegans PAR-3 and PAR-6 are required for apicobasal asymmetries associated with cell adhesion and gastrulation. *Development, 130*(22), 5339-5350. doi:10.1242/dev.00735

Nguyen, D., Bos, P., & Massague, J. (2009). Metastasis: from dissemination to organ-specific colonization. *Nature Reviews Cancer, 9*, 274-284.

Noh, M. G., Oh, S. J., Ahn, E. J., Kim, Y. J., Jung, T. Y., Jung, S., . . . Moon, K. S. (2017). Prognostic significance of E-cadherin and N-cadherin expression in Gliomas. *BMC Cancer, 17*(1), 583. doi:10.1186/s12885-017-3591-z

Ogg, S. C., Poritz, M. A., & Walter, P. (1992). Signal recognition particle receptor is important for cell growth and protein secretion in Saccharomyces cerevisiae. *Mol Biol Cell, 3*(8), 895-911.

Ohlstein, B., & Spradling, A. (2005). The adult Drosophila posterior midgut is maintained by pluripotent stem cells. *Nature, 439*(7075), 470-474. doi:doi:10.1038/nature04333

Ohlstein, B., & Spradling, A. (2007). Multipotent Drosophila Intestinal Stem Cells Specify Daughter Cell Fates by Differential Notch Signaling. *Science, 315*(5814), 988-992. doi:10.1126/science.1136606

Okuda, A., Kishi, T., Okochi, T., Ikeda, M., Kitajima, T., Tsunoka, T., . . . Iwata, N. (2010). Translin-associated factor X gene (TSNAX) may be associated with female major depressive disorder in the Japanese population. *Neuromolecular Med, 12*(1), 78-85. doi:10.1007/s12017-009-8090-1

Pagès, F., Galon, J., Dieu-Nosjean, M.-C., Tartour, E., Sautès-Fridman, C., & Fridman, W.-H. (2009). Immune infiltration in human tumors: a prognostic factor that should not be ignored. *Oncogene, 29*(8), 1093-1102. doi:doi:10.1038/onc.2009.416

Paget, S. (1989). The distribution of secondary growths in cancer of the breast. 1889. *Cancer Metastasis Rev, 8*(2), 98-101.

Pandey, U. B., & Nichols, C. D. (2011). Human Disease Models in Drosophila melanogaster and the Role of the Fly in Therapeutic Drug Discovery. *Pharmacol Rev, 63*(2), 411-436. doi:10.1124/pr.110.003293

Parri, M., & Chiarugi, P. (2010). Rac and Rho GTPases in cancer cell motility control. *Cell Commun Signal, 8*, 23. doi:10.1186/1478-811X-8-23

Parvathi, D., Amritha, A., & Solomon, P. (2009) Wonder animal model for genetic studies - *Drosophila Melanogaster* – its life cycle and breeding methods – a review, *Sri Ramachandra Journal of Medicine*, *2*, 33-38

Paw, I., Carpenter, R. C., Watabe, K., Debinski, W., & Lo, H. W. (2015). Mechanisms regulating glioma invasion. *Cancer Lett, 362*(1), 1-7. doi:10.1016/j.canlet.2015.03.015

Pearson H.B. , Perez-Mancera P.A. , Dow L.E. , Ryan A. , Tennstedt P. , Bogani D. , . . . P.O., H. (2011). *expression is deregulated in human prostate cancer, and its deficiency in mice promotes prostate neoplasia*. *Journal of Clinical Investigation, 121*, 4257 – 4267.

Pereira, B., Chin, S. F., Rueda, O. M., Vollan, H. K., Provenzano, E., Bardwell, H. A., . . . Caldas, C. (2016). The somatic mutation profiles of 2,433 breast cancers refines their genomic and transcriptomic landscapes. *Nat Commun, 7*, 11479. doi:10.1038/ncomms11479

Popoff, M. R., & Geny, B. (2009). Multifaceted role of Rho, Rac, Cdc42 and Ras in intercellular junctions, lessons from toxins. *Biochim Biophys Acta, 1788*(4), 797-812. doi:10.1016/j.bbamem.2009.01.011

Prober, D. A., & Edgar, B. A. (2000). Ras1 promotes cellular growth in the Drosophila wing. *Cell, 100*(4), 435-446.

Purow, B. W., Haque, R. M., Noel, M. W., Su, Q., Burdick, M. J., Lee, J., . . . Fine, H. A. (2005). Expression of Notch-1 and its ligands, Delta-like-1 and Jagged-1, is critical for glioma cell survival and proliferation. *Cancer Res, 65*(6), 2353-2363. doi:10.1158/0008-5472.CAN-04-1890

Purow, B. W., Sundaresan, T. K., Burdick, M. J., Kefas, B. A., Comeau, L. D., Hawkinson, M. P., . . . Fine, H. A. (2008). Notch-1 regulates transcription of the epidermal growth factor receptor through p53. *Carcinogenesis, 29*(5), 918-925. doi:10.1093/carcin/bgn079

Purow, B. W., Sundaresan, T. K., Burdick, M. J., Kefas, B. A., Comeau, L. D., Hawkinson, M. P., . . . Fine, H. A. (2008). Notch-1 regulates transcription of the epidermal growth factor receptor through p53. *Carcinogenesis, 29*(5), 918-925. doi:10.1093/carcin/bgn079

Qiu, X. X., Wang, C. H., You, N., Chen, B. J., Wang, X. F., Chen, Y. P., & Lin, Z. X. (2015). High Jagged1 expression is associated with poor outcome in primary glioblastoma. *Med Oncol, 32*(1), 341. doi:10.1007/s12032-014-0341-9

Radtke, F., Wilson, A., Stark, G., Bauer, M., van Meerwijk, J., MacDonald, H. R., & Aguet, M. (1999). Deficient T cell fate specification in mice with an induced inactivation of Notch1. *Immunity, 10*(5), 547-558.

Raftopoulou, M., & Hall, A. (2004). Cell Migration: Rho GTPases lead the way. *Developmental Biology, 265*(1), 23-32.

Rao, J. S. (2003). Molecular mechanisms of glioma invasiveness: the role of proteases. *Nature Reviews Cancer, 3*, 489-501.

Reedijk, M., Odorcic, S., Chang, L., Zhang, H., Miller, N., McCready, D. R., Egan, S. E. (2005). High-level coexpression of JAG1 and NOTCH1 is observed in human breast cancer and is associated with poor overall survival. *Cancer Res, 65*(18), 8530-8537. doi:10.1158/0008-5472.CAN-05-1069

Reiter, L. T., Potocki, L., Chien, S., Gribskov, M., & Bier, E. (2001). A Systematic Analysis of Human Disease-Associated Gene Sequences In Drosophila melanogaster. *Genome Res, 11*(6), 1114-1125. doi:10.1101/gr.169101

Reymond, N., Borda d'Agua, B., & Ridley, A. (2009) Metastasis: from dissemination to organ-specific colonization. *Nat Rev Can, 9*(4), 274-284, doi:10.1038/nrc2622.

Reymond, N., d'Água, B. B., & Ridley, A. J. (2013). Crossing the endothelial barrier during metastasis. *Nat Rev Cancer, 13*(12), 858-870. doi:10.1038/nrc3628

Roote, J., & Prokop, A. (2013). How to Design a Genetic Mating Scheme: A Basic Training Package for Drosophila Genetics. *G3*. doi:10.1534/g3.112.004820

Royer, C., & Lu, X. (2011). Epithelial cell polarity: a major gatekeeper against cancer? *Cell Death Differ, 18*(9), 1470-1477. doi:10.1038/cdd.2011.60

Saraogi, I., & Shan, S. O. (2011). Molecular mechanism of co-translational protein targeting by the signal recognition particle. *Traffic, 12*(5), 535-542. doi:10.1111/j.1600-0854.2011.01171.x

Schneider, G., Schmidt-Supprian, M., Rad, R., & Saur, D. (2017). Tissue-specific tumorigenesis: context matters. *Nat Rev Cancer, 17*(4), 239-253. doi:10.1038/nrc.2017.5

Schultz, J., Milpetz, F., Bork, P., & Ponting, C. (1998). SMART, a simple modular architecture research tool: Identification of signaling domains. *PNAS*, *95*(11), 5857-5864. http://dx.doi.org/10.1073/pnas.95.11.5857

Sethi, N., & Kang, Y. (2011). Notch signalling in cancer progression and bone metastasis. *Br J Cancer, 105*(12), 1805-1810. doi:10.1038/bjc.2011.497

Shan, S.-O., Schmid, S., & Zhang, X. (2009). Signal recognition particle (SRP) and SRP receptor: A new paradigm for multi-state regulatory GTPases. *Biochemistry, 48*(29), 6696-6704.

Shibue, T., & Weinberg, R. (2011). Metastatic colonization: Settlement, adaptation and propagation of tumor cells in a foreign tissue environment. *Seminars in Cancer Biology, 21*(2), 99-106.

South, A., Cho, R. & Aster, J. (2012). The double-edged sword of Notch signaling in cancer. *Sem Cell Dev Biol, 23*(4), 458-464, https://doi.org/10.1016/j.semcdb.2012.01.017

Speicher, S. A., Thomas, U., Hinz, U., & Knust, E. (1994). The Serrate locus of Drosophila and its role in morphogenesis of the wing imaginal discs: control of cell proliferation. *Development, 120*(3), 535-544.

Stocker, H., & Gallant, P. (2008). Getting started : an overview on raising and handling Drosophila. *Methods Mol Biol, 420*, 27-44. doi:10.1007/978-1-59745-583-1_2

Strand, M., & Micchelli, C. A. (2011). Quiescent gastric stem cells maintain the adult Drosophila stomach. *Proc Natl Acad Sci U S A, 108*(43), 17696-17701. doi:10.1073/pnas.1109794108

Sugiyama, M., Oki, E., Nakaji, Y., Tsutsumi, S., Ono, N., Nakanishi, R., . . . Maehara, Y. (2016). High expression of the Notch ligand Jagged-1 is associated with poor prognosis after surgery for colorectal cancer. *Cancer Sci, 107*(11), 1705-1716. doi:10.1111/cas.13075

Takashima, S., & Hartenstein, V. (2012). Genetic control of intestinal stem cell specification and development: a comparative view. *Stem Cell Rev, 8*(2), 597-608. doi:10.1007/s12015-012-9351-1

Tania, M., Khan, M. A., & Fu, J. (2014). Epithelial to mesenchymal transition inducing transcription factors and metastatic cancer. *Tumour Biol, 35*(8), 7335-7342. doi:10.1007/s13277-014-2163-y

Tauc, H. M., Tasdogan, A., Meyer, P., & Pandur, P. (2017). Nipped-A regulates intestinal stem cell proliferation in Drosophila. *Development, 144*(4), 612-623. doi:10.1242/dev.142703

Theodosiou, N. X., Tian. (1998). Use of FLP/FRT System to StudyDrosophilaDevelopment - ScienceDirect. *METHODS: A Comparison to Methods in Enzymology, 14*, 355-365.

Vaira, V., Faversani, A., Dohi, T., Maggioni, M., Nosotti, M., Tosi, D., . . . Bosari, S. (2011). Aberrant overexpression of the cell polarity module scribble in human cancer . . *American Journal of Pathology, 178*, 2478 – 2483.

Vinay, D. S., Ryan, E. P., Pawelec, G., Talib, W. H., Stagg, J., Elkord, E., . . . Kwon, B. S. (2015). Immune evasion in cancer: Mechanistic basis and therapeutic strategies. *Seminars in Cancer Biology, 35, Supplement*, S185-S198. doi:http://dx.doi.org/10.1016/j.semcancer.2015.03.004

Vogelmann, R., & Nelson, W. J. (2005). Fractionation of the epithelial apical junctional complex: reassessment of protein distributions in different substructures. *Mol Biol Cell, 16*(2), 701-716. doi:10.1091/mbc.E04-09-0827

Vogelstein, B., & Kinzler, K. W. (2004). Cancer genes and the pathways they control. *Nature Medicine, 10*(8), 789-799. doi:doi:10.1038/nm1087

Wang, J. Y., Chen, S. Y., Sun, C. N., Chien, T., & Chern, Y. (2016). A central role of TRAX in the ATM-mediated DNA repair. *Oncogene, 35*(13), 1657-1670. doi:10.1038/onc.2015.228

Wang, M., Wang, T., Liu, S., Yoshida, D., & Teramoto, A. (2003). The expression of matrix metalloproteinase-2 and -9 in human gliomas of different pathological grades. *Brain Tumor Pathol, 20*(2), 65-72.

Wang, N. J. et al. (2011). Loss-of-function mutations in Notch receptors in cutaneous and lung squamous cell carcinoma. *PNAS, 108*(43), 17761–17766, doi: 10.1073/pnas.1114669108

Wang, Z., Banerjee, S., Li, Y., Rahman, K. M., Zhang, Y., & Sarkar, F. H. (2006). Down-regulation of notch-1 inhibits invasion by inactivation of nuclear factor-kappaB, vascular endothelial growth factor, and matrix metalloproteinase-9 in pancreatic cancer cells. *Cancer Res, 66*(5), 2778-2784. doi:10.1158/0008-5472.CAN-05-4281

Wanninger, A. (2017). *Evolutionary Developmental Biology of Invertebrates 5* (A. Wanninger Ed. Vol. 5). New York: Springer.

Watkins, S., & Sontheimer, H. (2011). Hydrodynamic cellular volume changes enable glioma invasion. *Journal of Neuroscience, 31*(47), 17250-17259.

Weinberg, R. (2014). *The Biology of Cancer* (2nd ed.). New York, USA.: Garland Science, Taylor & Francis Group.

Xie, Q., Mittal, S., & Berens, M. E. (2014). Targeting adaptive glioblastoma: an overview of proliferation and invasion. *Neuro Oncol, 16*(12), 1575-1584. doi:10.1093/neuonc/nou147

Xu, P., Qiu, M., Zhang, Z., Kang, C., Jiang, R., Jia, Z., . . . Pu, P. (2010). The oncogenic roles of Notch1 in astrocytic gliomas in vitro and in vivo. *J Neurooncol, 97*(1), 41-51. doi:10.1007/s11060-009-0007-1

Yang, S., Cho, Y. S., Chennathukuzhi, V. M., Underkoffler, L. A., Loomes, K., & Hecht, N. B. (2004). Translin-associated factor X is post-transcriptionally regulated by its partner protein TB-RBP, and both are essential for normal cell proliferation. *J Biol Chem, 279*(13), 12605-12614. doi:10.1074/jbc.M313133200

Yang, S., Cho, Y. S., Chennathukuzhi, V. M., Underkoffler, L. A., Loomes, K., & Hecht, N. B. (2004). Translin-associated factor X is post-transcriptionally regulated by its partner protein TB-RBP, and both are essential for normal cell proliferation. *J Biol Chem, 279*(13), 12605-12614. doi:10.1074/jbc.M313133200

Yang, S., & Hecht, N. B. (2004). Translin associated protein X is essential for cellular proliferation. *FEBS Lett, 576*(1-2), 221-225. doi:10.1016/j.febslet.2004.08.082

Yilmaz, M., & Christofori, G. (2009). EMT, the cytoskeleton, and cancer cell invasion. *Cancer Metastasis Rev, 28*(1-2), 15-33. doi:10.1007/s10555-008-9169-0

Zavadil, J., Cermak, L., Soto-Nieves, N., & Böttinger, E. P. (2004). Integration of TGF-beta/Smad and Jagged1/Notch signalling in epithelial-to-mesenchymal transition. *EMBO J, 23*(5), 1155-1165. doi:10.1038/sj.emboj.7600069

Zeng, X., Chauhan, C., & Hou, S. X. (2010). Characterization of midgut stem cell- and enteroblast-specific Gal4 lines in drosophila. *Genesis, 48*(10), 607-611. doi:10.1002/dvg.20661

Zhan L. , Rosenberg A. , Bergami K.C. , Yu M. , Xuan Z. , Jaffe A.B. , . . . S.K., M. (2008). Deregulation of scribble promotes mammary tumorigenesis and reveals a role for cell polarity in carcinoma. *Cell, 135*, 865 – 878.

Zhang, X., Schaffitzel, C., Ban, N., & Shan, S. O. (2009). Multiple conformational switches in a GTPase complex control co-translational protein targeting. *Proc Natl Acad Sci U S A, 106*(6), 1754-1759. doi:10.1073/pnas.0808573106

Chapter 7. Appendix

Chapter 7. Appendix

Appendix A. Temperature gradient optimisation of *SRPRA* and *JAG1* primers

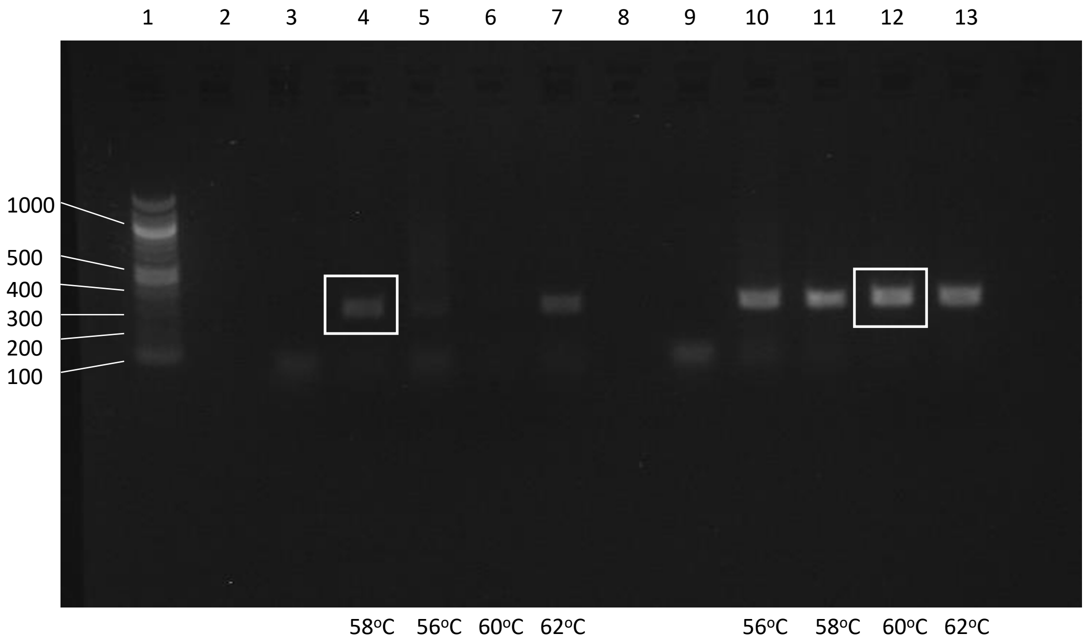

Temperature gradient optimisation of *SRPR* and *JAG1* primers. All reactions were evaluated in a single run. Lane 1 contains the DNA ladder; lanes 3 and 9 are negative controls; lanes 4-7 are *SRPRA* PCR products at the temperatures indicated; lanes 10-13 are *JAG1* PCR products at the temperatures indicated. U87 cDNA was used in all reactions. Lower bands represent unwanted PCR products such as primer dimers. White box indicates the optimal primer annealing temperature.

Appendix B. Temperature gradient optimisation of *HCN2* and *TSNAX* primers

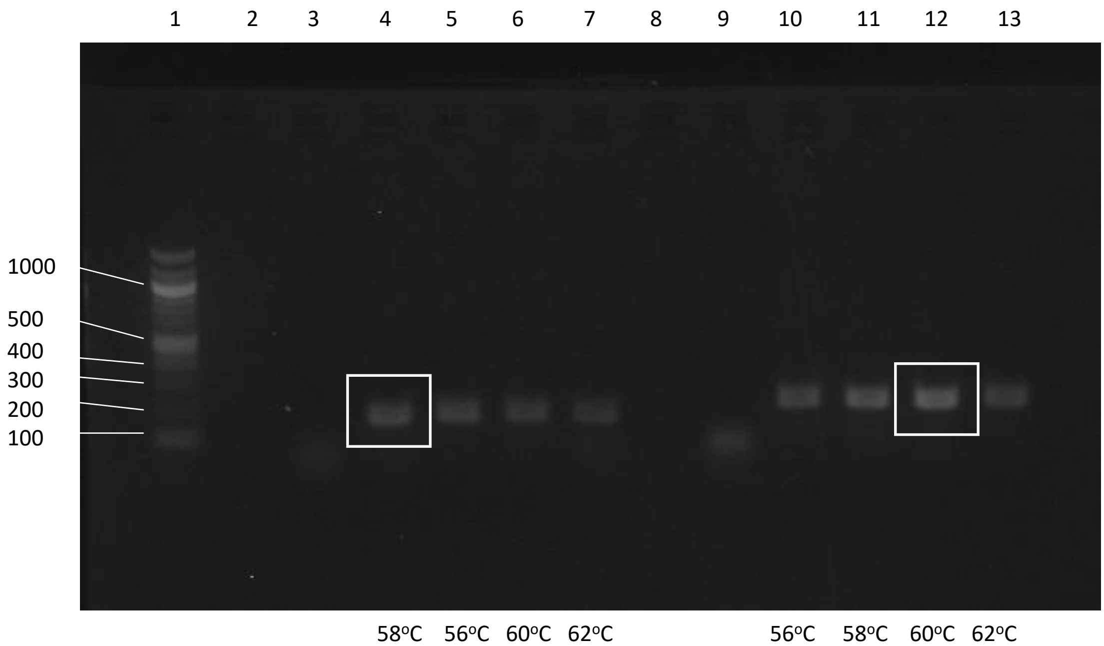

Temperature gradient optimisation of *HCN2* and *TSNAX* primers. All reactions were evaluated in a single run. Lane 1 contains the DNA ladder; lanes 3 and 9 are negative controls; lanes 4-7 are *HCN2* PCR products at the temperatures indicated; lanes 10-13 are *TSNAX* PCR products at the temperatures indicated. U87 cDNA was used in all reactions. Lower bands represent unwanted PCR products such as primer dimers. White box indicates the optimal primer annealing temperature.

Appendix C. Expression levels of *SRPRA* in U87 cells.

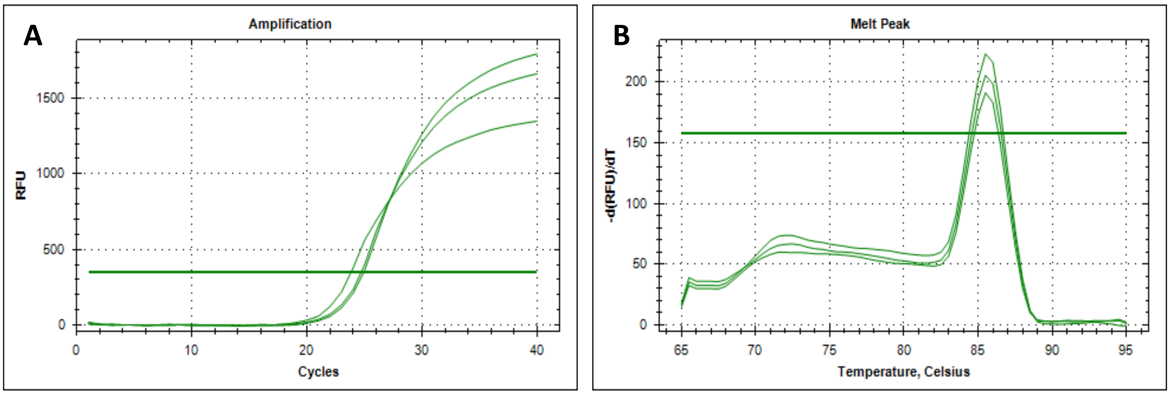

RT-PCR amplification curve (A) and melt curve (B) using cDNA harvested from the U87 cell line using *SRPRA*-specific primers to validate *SRPRA* expression in this cell line prior to knockdown.

Appendix D. Expression levels of *JAG1* in U87 cells.

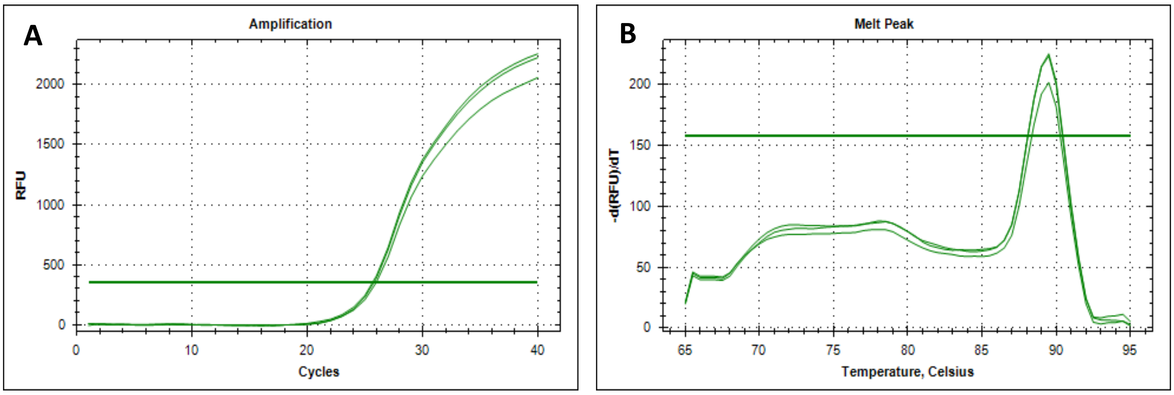

RT-PCR amplification curve (A) and melt curve (B) using cDNA harvested from the U87 cell line using *JAG1*-specific primers to validate *JAG1* expression in this cell line prior to knockdown.

Appendix E. Expression levels of *HCN2* in U87 cells.

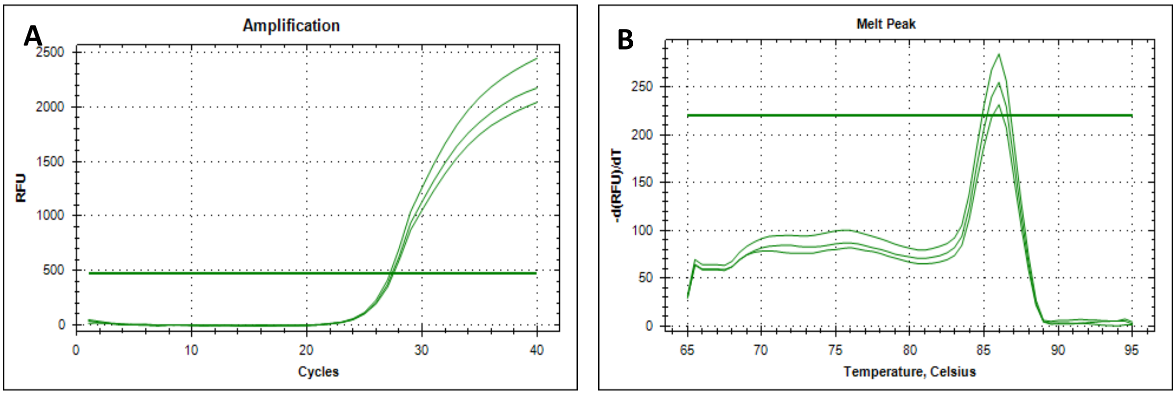

RT-PCR amplification curve (A) and melt curve (B) using cDNA harvested from the U87 cell line using *HCN2*-specific primers to validate *HCN2* expression in this cell line prior to knockdown.

Appendix F. Expression levels of *TSNAX* in U87 cells.

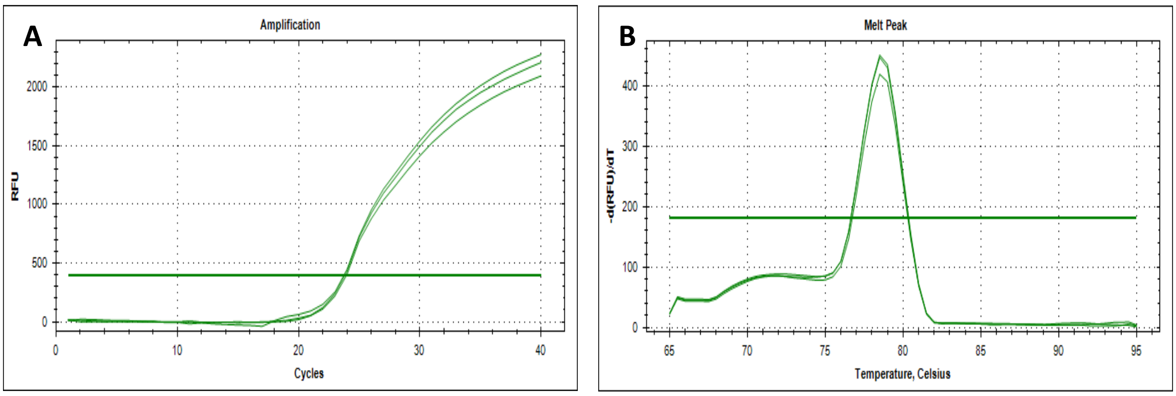

RT-PCR amplification curve (A) and melt curve (B) using cDNA harvested from the U87 cell line using *TSANX*-specific primers to validate *TSNAX* expression in this cell line prior to knockdown.

Appendix G. Expression levels of *SRPRA* post-siRNA transfection

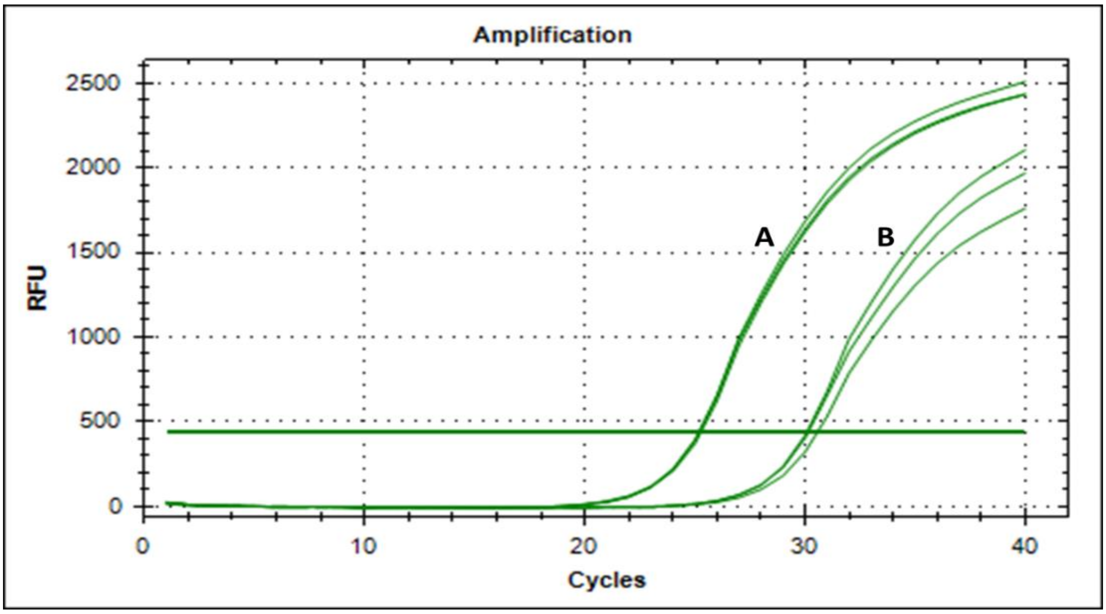

RT-PCR to analyse SRPRA expression. In order to assess effectiveness of SRPRA siRNA knockdown, U87 Glioblastoma cells were transfected with A) non-targeting control siRNA and B) SRPRA siRNA. Following a 48 hour transfection period, RT-PCR was carried out using extracted cDNA using SRPRA-specific primers (shown) as well as GAPDH-specific primers (for ΔΔCT calculation). RT-PCR was carried out in triplicate and repeated twice to ensure knockdown was consistent.

Appendix H. Expression levels of *JAG1* post-siRNA transfection

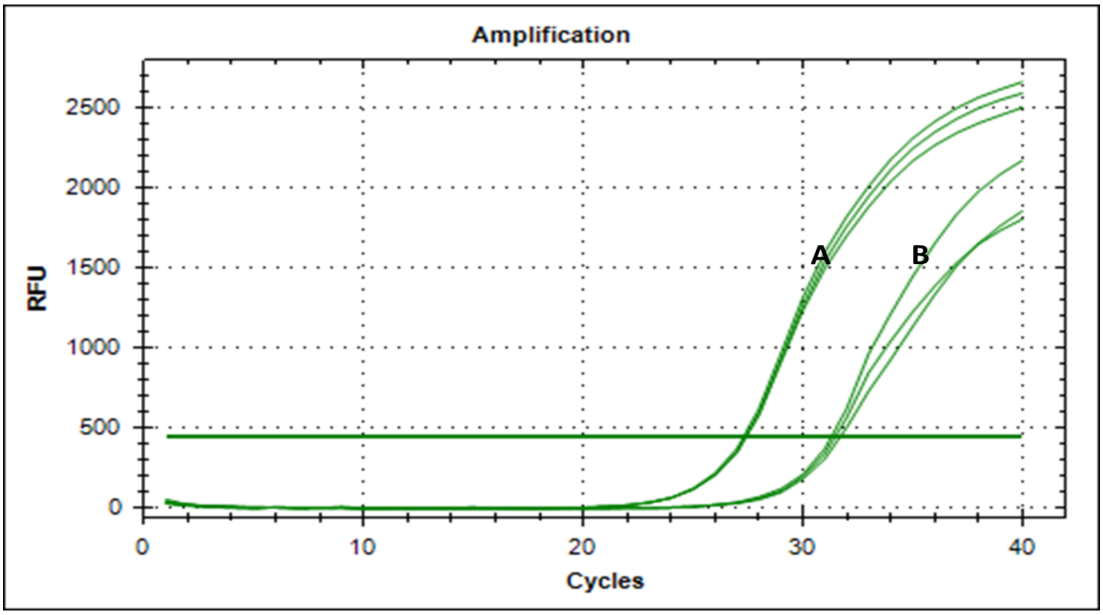

RT-PCR to analyse JAG1 expression. In order to assess effectiveness of JAG1 siRNA knockdown, U87 Glioblastoma cells were transfected with A) non-targeting control siRNA and B) JAG1 siRNA. Following a 48 hour transfection period, RT-PCR was carried out using extracted cDNA using JAG1-specific primers (shown) as well as GAPDH-specific primers (for ΔΔCT calculation). RT-PCR was carried out in triplicate and repeated twice to ensure knockdown was consistent.

Appendix I. Expression levels of *HCN2* post-siRNA transfection

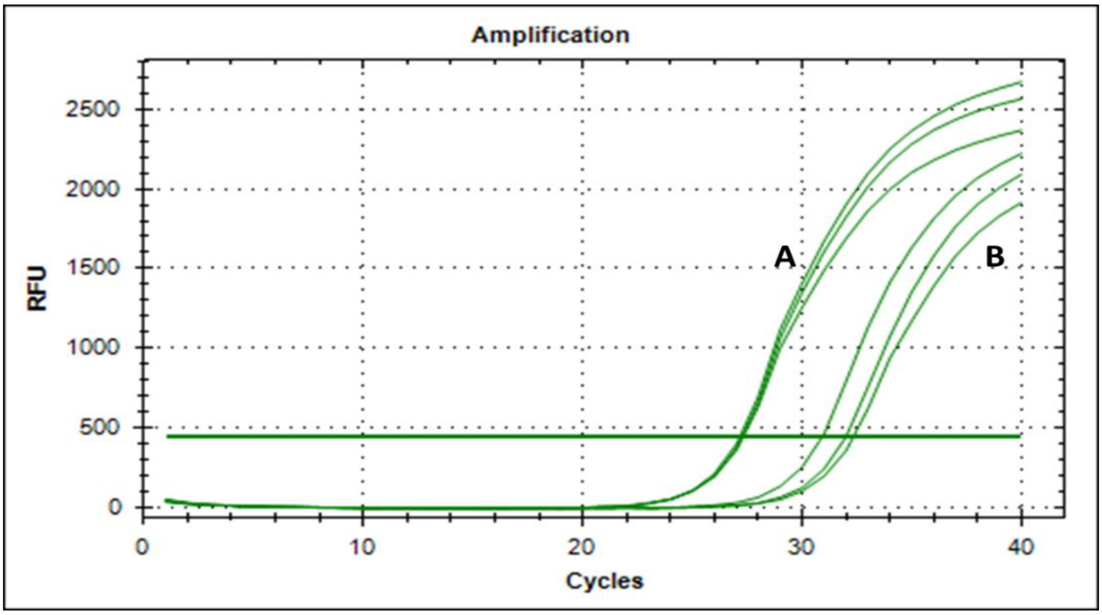

RT-PCR to analyse HCN2 expression. In order to assess effectiveness of HCN2 siRNA knockdown, U87 Glioblastoma cells were transfected with A) non-targeting control siRNA and B) HCN2 siRNA. Following a 48 hour transfection period, RT-PCR was carried out using extracted cDNA using HCN2-specific primers (shown) as well as GAPDH-specific primers (for ΔΔCT calculation). RT-PCR was carried out in triplicate and repeated twice to ensure knockdown was consistent.

Appendix J. Expression levels of *TSNAX* post-siRNA transfection

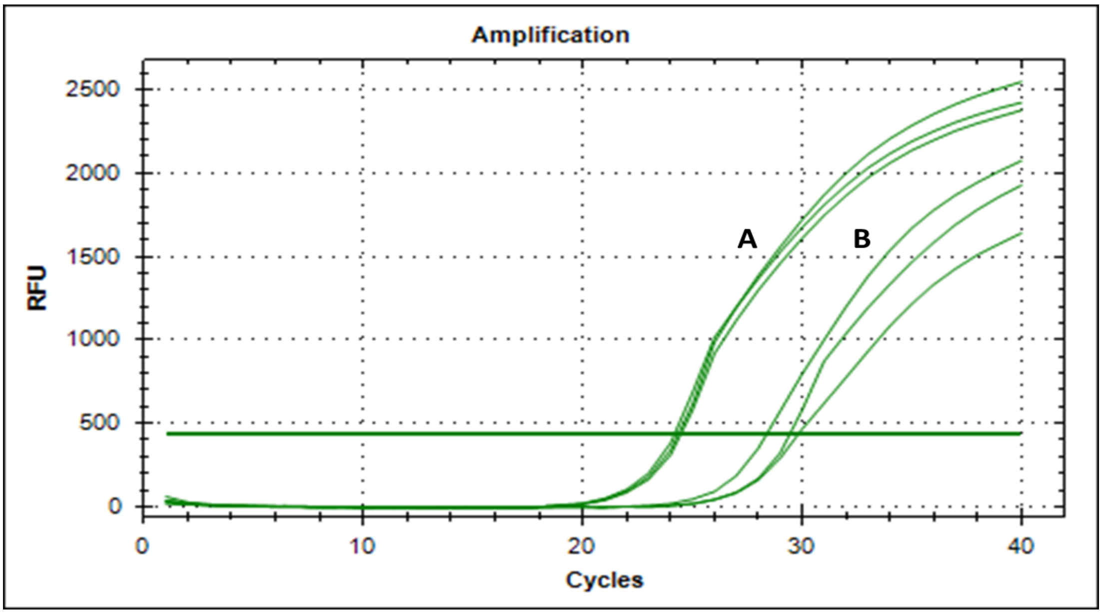

RT-PCR to analyse TSNAX expression. In order to assess effectiveness of TSNAX siRNA knockdown, U87 Glioblastoma cells were transfected with A) non-targeting control siRNA and B) TSNAX siRNA. Following a 48 hour transfection period, RT-PCR was carried out using extracted cDNA using TSNAX-specific primers (shown) as well as GAPDH-specific primers (for ΔΔCT calculation). RT-PCR was carried out in triplicate and repeated twice to ensure knockdown was consistent.

Appendix K. Scoring system utilised in the genetic screen

	Category			
Score	**Clonal Tissue**	**Invading Cells**	**Dividing Cells**	**Multi-layering**
2	50% +	Extensive	Extensive	50% +
1	35-50% +	Lots	Lots	15-50%
0	15-35%	Medium	Medium	0-15%
-1	5-15%	Few	Few	None
-2	0-5%	None	None	/

A description of the scoring system used in the screen, where 0 describes the phenotype common of the lgl -/- mutant genotype. In each case five animals were independently quantified by two scientists and results averaged. Clonal tissue size was quantified as the percentage of the imaged notum covered by mutant cones and multi-layering as the percentage of total clonal tissue exhibiting multi-layering.